

**NASA
Technical
Paper
2813**

1988

Static Performance
of Nonaxisymmetric
Nozzles With Yaw
Thrust-Vectoring Vanes

Mary L. Mason and
Bobby L. Berrier

*Langley Research Center
Hampton, Virginia*

NASA

National Aeronautics
and Space Administration

Scientific and Technical
Information Division

Summary

A static (wind-off) test has been conducted in the static test facility of the Langley 16-Foot Transonic Tunnel to evaluate the effects of post-exit vane yaw vectoring on nonaxisymmetric nozzles. Three baseline nozzles were tested: an unvectored two-dimensional convergent nozzle, an unvectored two-dimensional convergent-divergent nozzle, and a pitch-vectorred two-dimensional convergent-divergent nozzle. Each nozzle geometry was tested with three exit aspect ratios (ratio of nozzle width to height at exit) of 1.5, 2.5, and 4.0. Two post-exit yaw vanes were externally mounted on the nozzle sidewalls at the nozzle exit to generate yaw thrust vectoring. Vane deflection angle (0° , -20° , and -30°), vane planform, and vane curvature were varied during the test. Results indicate that the post-exit vane concept produced resultant yaw vector angles which were always smaller than the geometric yaw vector angle. Losses in resultant thrust ratio increased with the magnitude of resultant yaw vector angle. The widest post-exit vane produced the largest degree of flow turning, but vane curvature had little effect on thrust vectoring. Pitch thrust vectoring was independent of yaw thrust vectoring.

Introduction

The next generation of fighter aircraft will be a versatile and specialized class of vehicles designed for operation over a wide range of flight and combat conditions. Future fighter aircraft requirements will probably include transonic and supersonic cruise capability, short take-off and landing (STOL) features, high turn rates, and supersonic maneuverability at conventional and high angles of attack. Studies of "supermaneuverability" indicate that advanced fighters will require aircraft control beyond the stall limit (post-stall maneuverability). (See refs. 1 through 5.) Increased aircraft control power may be achieved by modifying the fighter propulsion system. Addition of multiaxis thrust-vectoring capability to the engine exhaust system can result in powered-control moments for extended maneuverability which are independent of airframe aerodynamics and aircraft angle of attack (refs. 2 through 8).

Thrust vectoring is a powered-controls concept which uses the exhaust nozzle to direct the thrust force vector (by directing the exhaust jet) away from the nominal axial direction. Incorporating thrust vectoring into the propulsion system improves overall performance by expanding the aircraft flight envelope and adding a STOL capability (refs. 4 through

16). Multiaxis thrust vectoring is effective at flight conditions where control power from conventional aerodynamic control surfaces is degraded, such as very low speeds or very high angles of attack. Use of thrust vectoring to augment aircraft control could allow the designer to reduce the size of conventional control surfaces; thus, weight and drag are reduced and the aircraft operational envelope is expanded to include post-stall flight conditions.

The variable-geometry nonaxisymmetric nozzle is a highly integrable propulsion exhaust system. Investigations have shown that nonaxisymmetric nozzle systems meet isolated and installed performance requirements and integrate well into the airframe for low installed drag (refs. 15 through 21). The geometry of nonaxisymmetric nozzle designs can be easily modified to include multiaxis thrust vectoring and thrust reversing. A number of investigations, conducted at both static (wind-off) and wind-on test conditions, have verified the effectiveness of nonaxisymmetric nozzles for pitch thrust vectoring (refs. 14 through 24). Several recent studies evaluated static and wind-on effects of lateral or yaw thrust vectoring on nonaxisymmetric nozzle performance (refs. 7 and 24 through 26).

To continue the development of yaw thrust-vectoring nonaxisymmetric nozzles, a wind-off test has been conducted in the static test facility of the Langley 16-Foot Transonic Tunnel. High-pressure air was used to simulate the exhaust jet. Two generic nonaxisymmetric nozzle concepts were investigated: a two-dimensional (2-D) convergent nozzle and a two-dimensional convergent-divergent (2-D C-D) nozzle. A pitch-vectorred two-dimensional convergent-divergent nozzle configuration was also tested. Each of these three nozzle configurations was tested with nozzle exit aspect ratios (ratio of nozzle width to height at exit) of 1.5, 2.5, and 4.0. Yaw thrust vectoring was implemented on each nozzle configuration by two externally mounted vanes (one on each sidewall) which hinged at the nozzle exit. This thrust-vectoring concept is referred to as "post-exit yaw vane." The vane geometric parameters investigated were vane planform, vane curvature, and vane deflection angle. The test nozzle pressure ratios ranged from 1.6 to 6.0. The results of this investigation are presented as basic nozzle performance data (discharge coefficient, internal thrust ratio, and resultant thrust ratio) and nozzle-vane flow-turning capability (resultant thrust-vector angles).

During another phase of this investigation, the post-exit vane thrust-vectoring concept was applied to an axisymmetric nozzle configuration. In this case, the post-exit vanes were used for both pitch and yaw thrust vectoring. The results of this study

are presented in reference 27. Selected results on both nonaxisymmetric and axisymmetric nozzles are presented in reference 28.

Symbols

All forces (except resultant gross thrust) and all resultant vector angles are referred to the model body axis (measured from the model centerline). A detailed discussion of the data reduction and calibration procedures and definitions of forces, angles, and propulsion relations used in this report are presented in reference 29.

AR	nozzle exit aspect ratio (ratio of nozzle width to height, measured at nozzle exit)
A_e	nozzle exit area, in ²
A_e/A_t	nozzle expansion ratio
A_t	measured nozzle throat area, in ²
A_v	individual yaw vane planform area, in ²
A_v/A_e	ratio of vane planform area to nozzle exit area
C_d	nozzle discharge coefficient, w_p/w_i
F	measured thrust along body axis, positive in forward direction, lbf
F_i	ideal isentropic gross thrust, $w_p \sqrt{\frac{R_j T_{t,j}}{g^2} \frac{2\gamma}{\gamma-1} \left[1 - \left(\frac{p_a}{p_{t,j}} \right)^{(\gamma-1)/\gamma} \right]}$, lbf
F_N	measured normal force, lbf
F_T	resultant gross thrust, $\sqrt{F^2 + F_N^2 + F_S^2}$, lbf
F_S	measured side force, lbf
g	acceleration due to gravity, 32.174 ft/sec ²
NPR	nozzle pressure ratio, $p_{t,j}/p_a$
(NPR) _d	design nozzle pressure ratio (NPR for fully expanded flow at nozzle exit)
p_a	ambient pressure, psi
$p_{t,j}$	jet total pressure, psi
R_j	gas constant, 1716 ft ² /sec ² -°R for air
$T_{t,j}$	jet total temperature, °R

w	width of nozzle measured at exit, in.
w_i	ideal weight-flow rate, lbf/sec
w_p	measured weight-flow rate, lbf/sec
γ	ratio of specific heats, 1.3997 for air
δ_p	resultant pitch thrust-vector angle, $\tan^{-1} \frac{F_N}{F}$, deg
δ_s	resultant splay thrust-vector angle, positive in clockwise direction from nozzle top, $\tan^{-1} \frac{F_S}{F_N}$, deg
δ_y	resultant yaw thrust-vector angle, $\tan^{-1} \frac{F_S}{F}$, deg
$\delta_{v,p}$	geometric pitch vector angle measured from model centerline, positive deflection angle produces positive normal force, deg
$\delta_{v,y}$	geometric yaw vector angle measured from model centerline, positive deflection angle produces a positive side force, deg

Abbreviations:

C-D	convergent-divergent
Sta.	model station, in.
V1-V4	flat yaw vane configuration designations
V5	curved yaw vane configuration designation
2-D	two-dimensional

Apparatus and Methods

Static Test Facility

This investigation was conducted in the static test facility of the Langley 16-Foot Transonic Tunnel. The static test facility has been used extensively in the development and testing of nonaxisymmetric nozzle concepts for evaluating nozzle internal performance (ref. 24). Nozzle testing is conducted with a single-engine propulsion simulation system which generates a compressed-air jet that exhausts to the atmosphere. This facility uses the same filtered dry air supply as the 16-Foot Transonic Tunnel and has a similar air control system which includes a heat exchanger for maintaining a constant stagnation temperature in the exhaust jet (ref. 30).

Single-Engine Propulsion Simulation System

A sketch of the single-engine air-powered nacelle model on which the test nozzles were installed is

presented in figure 1. The propulsion simulation system is shown with a convergent nozzle and a set of yaw vanes installed.

An external high-pressure air system provided a continuous flow of clean dry air at a controlled temperature of about 530°R. The air pressure was varied during jet simulation from atmospheric pressure (jet off) up to about 90 psi in the nozzle. The high-pressure air was brought through a dolly-mounted support strut by six tubes which connect to a high-pressure plenum chamber. As shown in figure 1, the air was then discharged perpendicularly into the model low-pressure plenum through eight multiple-hole nozzles equally spaced around the high-pressure plenum. This method was designed to minimize the forces imposed by the transfer of axial momentum as the air is passed from the nonmetric high-pressure plenum to the metric (mounted to the force balance) low-pressure plenum. Two flexible metal bellows were used to seal the air system and compensate for axial forces caused by pressurization of the low-pressure plenum.

The air then passed from the low-pressure plenum through a transition section, a choke plate, and an instrumentation section. The transition section provided a smooth flow path from the circular low-pressure plenum to the rectangular choke plate and instrumentation section. The instrumentation section had a flow-path width-to-height ratio of 1.437. From the instrumentation section, the airflow entered an adapter (installed at model station 41.13) which was used to vary the nozzle aspect ratio by varying the width of the flow path. All nozzles were installed to the aspect ratio adapter at model station 44.63.

Nozzle and Post-Exit Vane Designs

Detailed sketches of the aspect ratio adapter section and the test nozzles are presented in figure 2. Geometric parameters and sketches of the post-exit yaw vector vanes are presented in figure 3. Photographs of typical test nozzle installations with and without yaw vanes are shown in figures 4 through 6.

Nozzles. Two generic nonaxisymmetric nozzle concepts were investigated: a two-dimensional (2-D) convergent nozzle and a two-dimensional convergent-divergent (2-D C-D) nozzle. The 2-D C-D nozzle type was tested with and without pitch thrust vectoring ($\delta_{v,p} = -11.7^\circ$ and 0°). These three nozzle configurations were tested as baselines (without yaw vanes) and with post-exit yaw vanes installed.

The unvectored 2-D C-D nozzle was formed from the 2-D convergent nozzle by installing triangular-shaped duct inserts to the upper and lower nozzle flaps. (See fig. 2(b).) The inserts introduced conver-

gence and divergence to the internal flow path and reduced the nozzle throat area. The pitch-vectorred 2-D C-D nozzle was formed by a single duct insert to the lower flap of the 2-D convergent nozzle. (See fig. 2(b).) Since only the lower flap was modified for pitch thrust vectoring, the nozzle throat was translated upward above the model centerline. The nozzle exit remained fixed in the same location as the exit of the unvectored 2-D C-D nozzle. Each of the three basic nozzle configurations was tested with three different exit aspect ratios (exit width divided by exit height) of 1.5, 2.5, and 4.0. A separate set of 2-D convergent flaps and duct inserts was built for each exit aspect ratio tested. The nozzle exit aspect ratio was varied by using the aspect ratio adapter section to adjust the width of the flow path and then by installing the appropriate set of nozzle flaps with or without duct inserts. The height at the exit was held nominally constant (at 1 in.) for all test configurations. Thus, nozzle throat and exit areas decreased with decreasing exit aspect ratio. All nozzles used the same sidewalls regardless of nozzle type or exit aspect ratio. Design parametrics (A_e/A_t , $(NPR)_d$) for each test nozzle are given in figure 2. The variation of nozzle geometry with exit aspect ratio is clearly seen in the photographs of figures 4 through 6.

Post-exit vanes. The post-exit vanes were mounted to the nozzle sidewalls with the vane hinge line located at the nozzle exit. (See fig. 1.) The vanes were equally deflected laterally to turn the exhaust jet in the yaw plane. Four different flat vane planforms were tested. (See fig. 3(a).) Vane V1 served as the baseline flat vane and had a height of 1.0 in. (identical to the height of the nozzle exit) and a length of 1.625 in. Vanes V2 and V3 also had heights of 1.0 in. but had lengths of 2.125 in. (longer than V1) and 1.125 in. (shorter than V1), respectively. Vane V4 had the same length as the baseline V1 (1.625 in.) but had a larger height of 1.5 in. To investigate the effect of vane curvature, the baseline V1 flat vane planform was modified with a radius of curvature of 3.0 in. and a trailing-edge terminal angle of 10° . The curved vane, designated V5, still kept the same height and length as V1. (See fig. 3(b).) For a given post-exit vane planform area A_v , the ratio of vane area to nozzle exit area A_v/A_e increased with decreasing exit aspect ratio. The values of A_v/A_e for each combination of vane and aspect ratio are given in figure 3. All five post-exit vanes were tested with the unvectored 2-D convergent and unvectored 2-D C-D nozzle configurations. Only the baseline flat vane V1 was tested with the pitch-vectorred 2-D C-D nozzle configuration.

Figure

Basic data plots:

Effect of vane installation and deflection for—	
2-D convergent nozzle with AR = 1.5 and $\delta_{v,p} = 0^\circ$	7
2-D C-D nozzle with AR = 1.5 and $\delta_{v,p} = 0^\circ$	8
2-D C-D nozzle with AR = 1.5 and $\delta_{v,p} = -11.7^\circ$	9
2-D convergent nozzle with AR = 2.5 and $\delta_{v,p} = 0^\circ$	10
2-D C-D nozzle with AR = 2.5 and $\delta_{v,p} = 0^\circ$	11
2-D C-D nozzle with AR = 2.5 and $\delta_{v,p} = -11.7^\circ$	12
2-D convergent nozzle with AR = 4.0 and $\delta_{v,p} = 0^\circ$	13
2-D C-D nozzle with AR = 4.0 and $\delta_{v,p} = 0^\circ$	14
2-D C-D nozzle with AR = 4.0 and $\delta_{v,p} = -11.7^\circ$	15

Summary data plots:

Effect of nozzle exit aspect ratio with vanes off	16
Effect of exit aspect ratio with vane V1 and $\delta_{v,y} = -30^\circ$	17
Effect of nozzle type with vanes off	18
Effect of nozzle type with vane V1 and $\delta_{v,y} = -30^\circ$	19
Effect of flat vane planform for 2-D convergent nozzle with $\delta_{v,p} = 0^\circ$ and $\delta_{v,y} = -30^\circ$	20
Effect of flat vane planform for 2-D C-D nozzle with $\delta_{v,p} = 0^\circ$ and $\delta_{v,y} = -30^\circ$	21
Effect of vane curvature for 2-D convergent nozzle with $\delta_{v,p} = 0^\circ$ and $\delta_{v,y} = -30^\circ$	22
Effect of vane curvature for 2-D C-D nozzle with $\delta_{v,p} = 0^\circ$ and $\delta_{v,y} = -30^\circ$	23

Results and Discussion

Basic Data

The basic data figures present the effects of post-exit vane installation ($\delta_{v,y} = 0^\circ$) and deflection on nozzle performance. Specific effects of nozzle type, exit aspect ratio, vane geometry, and vane curvature are discussed in detail later. In general, the trends

in nozzle performance for the baseline nozzle configurations without yaw vectoring are consistent with earlier studies of nonaxisymmetric nozzles (refs. 17 through 21, 24, and 26).

Regardless of nozzle geometry, the post-exit vane yaw vectoring concept always produced resultant yaw vector angles which were smaller than the geometric yaw vector angle of the vanes. Other investigations of thrust-vectoring concepts (refs. 16, 26, and 27) indicated that low values of resultant thrust-vector angle can result from turning supersonic exhaust flow. Vectoring supersonic flow at the nozzle exit is less efficient in turning than vectoring lower velocity flow in the vicinity of the nozzle throat. Thrust-vectoring concepts which initiate flow turning inside the nozzle at subsonic or slightly supersonic conditions tend to result in thrust-vector angles which are equal to or, in some cases, greater than the geometric vector angle.

For the post-exit vanes, the largest values of δ_y were generated by the nozzles with the smallest exit aspect ratio of 1.5 (compare fig. 7 with figs. 10 and 13). For all test nozzle-vane configurations, the maximum value of δ_y was -22° for the 2-D C-D nozzle with vane V4 and AR = 1.5, $\delta_{v,p} = 0^\circ$, $\delta_{v,y} = -30^\circ$, and NPR = 6.0. Increasing the exit aspect ratio had an adverse effect on δ_y . Depending on vane geometry and/or exit aspect ratio, δ_y either remained nearly constant over the tested NPR range or increased slightly with increasing NPR.

Trends in nozzle discharge coefficient C_d depended on the nozzle type, 2-D C-D or 2-D convergent. For the baseline 2-D C-D nozzles (without post-exit vanes) with and without pitch vectoring, C_d remained relatively constant with increasing NPR for NPR > 2.0. (See figs. 8, 11, and 14 for 2-D C-D nozzles without pitch vectoring and figs. 9, 12, and 15 for pitch-vectoring 2-D C-D nozzles.) When post-exit vanes were installed ($\delta_{v,y} = 0^\circ$) and deflected, there was no effect of yaw vectoring on C_d levels for any of the 2-D C-D nozzle-vane configurations. However, the baseline 2-D convergent nozzles (without post-exit vanes) produced an effect of NPR on C_d . (See figs. 7, 10, and 13.) For NPR > 2.0, C_d increased with increasing NPR, indicating a variation in effective throat area with NPR. This effect of NPR on C_d continued when the post-exit vanes were installed and deflected. In addition, use of the post-exit vanes on the 2-D convergent nozzles resulted in a variation of C_d with vane angle. Post-exit vane installation alone (without deflection, $\delta_{v,y} = 0^\circ$) slightly decreased C_d over the NPR range tested. Deflections of the yaw vanes further diminished C_d levels to 3 to 5 percent below the baseline results. As nozzle exit aspect ratio increased, this effect of post-exit

vane installation and deflection on C_d decreased in magnitude.

The measured geometric throat area of each nozzle configuration was used in computing the ideal weight-flow rate (w_i) term of C_d , even when the post-exit vanes were installed and deployed. The geometric throat area was determined by measurements of nozzle throat height and nozzle throat width, which varied with exit aspect ratio. For the 2-D C-D nozzles, the throat location is well upstream of the nozzle exit and, as a result, deflection of the post-exit vanes at the exit would not affect the magnitude of either the geometric throat area or the effective throat area. However, the throat of a 2-D convergent nozzle is coincident with the nozzle exit. Installation and deflection of post-exit vanes at the exit of a convergent nozzle could change the effective throat area either by changing the actual throat geometry or by introducing a different flow condition at the nozzle geometric throat (exit) for each vane deflection angle. When the post-exit vanes are installed at some deflection angle, the minimum distance between the vanes is inclined to the model axis such that the actual width of the flow path between the vanes is smaller than the measured minimum width of the convergent nozzle. The minimum distance between the vanes decreases with increasing vane deflection angle. Thus, for the convergent nozzles with deflected post-exit vanes, it is probable that the effective throat area moves out of the nozzle exit on one side of the nozzle and onto the post-exit vane which deflects into the exhaust jet. The effective throat area thus becomes inclined across the flow path between the post-exit vanes and is reduced by increasing the vane deflection angle. This reduction in effective throat area with increasing vane deflection angle would explain the trends in C_d measured for the convergent nozzles.

For the 2-D convergent nozzle configurations, increasing the exit aspect ratio of the nozzle does not change this effect of vane deflection on effective throat area (figs. 7, 10, and 13). The coefficient C_d decreased with increasing vane deflection angle. However, as mentioned earlier, increasing AR decreased the magnitude of the trends in C_d . Since geometric throat area increased with increasing AR, the relative influence of the post-exit vanes on effective throat area (and, thus, on discharge coefficient) is reduced with increasing AR. (For example, compare fig. 7(a) with fig. 13(a).) The effects of AR on performance are discussed in more detail later.

The small reduction in C_d which occurs when the post-exit vanes are installed undeflected ($\delta_{v,y} = 0^\circ$) probably results from additional nozzle boundary-layer growth along the surface of the vanes. Increasing the boundary layer would move the effective

throat area slightly downstream of the nozzle exit. As a result, the effective throat width (and effective throat area) would decrease slightly, producing a decrease in C_d from the baseline (vanes off) levels.

For all baseline nozzles without post-exit vanes, peak values of internal and resultant thrust ratios occurred near the value of design nozzle pressure ratio $(NPR)_d$. (See fig. 21(b).) Both F/F_i and F_r/F_i increased to a peak at the design condition $(NPR = (NPR)_d)$, then leveled off and decreased as NPR rose above $(NPR)_d$. Such trends are common for most nozzle types. Typically, thrust ratio data are reduced by overexpansion losses at values of NPR below design and by underexpansion losses at values of NPR above design. Installation and deflection of the post-exit vanes caused the NPR at which peak performance occurred to vary from the design nozzle pressure ratio $(NPR)_d$. This effect is most obvious for the nozzles with exit aspect ratio of 1.5. (See figs. 7 through 9.) Design nozzle pressure ratio is a function of geometric nozzle expansion ratio A_e/A_t . As discussed earlier, vane installation and deflection may change the effective exit area and/or the effective throat area, resulting in a new value of effective expansion ratio and, thus, effective $(NPR)_d$ for the yaw-vector configurations. For the 2-D convergent nozzle configurations, the post-exit vanes change the effective throat area from the baseline, as indicated by the variation of C_d with vane installation and deflection angle which was discussed earlier.

For the 2-D C-D nozzle configurations, effective A_e was probably affected by the post-exit vanes instead of effective A_t . The throat of each 2-D C-D nozzle was far enough upstream of the exit to be unaffected by the post-exit vanes. In addition, C_d showed no variation with vane installation and deflection; this indicates that, for the 2-D C-D nozzles, A_t remained independent of the vanes and any variation in A_e/A_t could only result from changes in effective A_e .

For most configurations, adding the post-exit vanes at $\delta_{v,y} = 0^\circ$ caused a small decrease (of 1 percent or less) in the internal and resultant thrust ratios. Both thrust ratios, F/F_i and F_r/F_i , also decreased with increasing geometric deflection angle $\delta_{v,y}$ and with subsequently increasing resultant yaw vector angle δ_y . The most significant thrust losses occurred for the nozzles with AR = 1.5, which had the largest resultant yaw vector angles. For example, in figure 7(d), vane V4 on the 2-D convergent nozzle with AR = 1.5 resulted in $\delta_y = -22^\circ$, a 13-percent loss in F_r/F_i and a 19-percent loss in F/F_i at NPR = 6.0. The losses in F/F_i were always equal to or greater than losses in F_r/F_i . Recall that losses in F/F_i reflect a decrease in axial thrust along the

body axis. Internal thrust ratio F/F_i decreases as δ_y increases because a larger part of the gross thrust is diverted from the body axis to the thrust-vectoring plane. Internal thrust ratio F/F_i is also reduced by a decrease in nozzle efficiency (caused by increased friction drag, shock losses, expansion losses, etc.). Losses in resultant thrust ratio F_r/F_i , however, do not include any losses due to resultant vector angle (see section "Data Reduction") but reflect an actual performance penalty in gross thrust resulting from a decreased nozzle efficiency. An earlier investigation of thrust vectoring (ref. 16) reported that thrust vectoring a supersonic jet (vectoring downstream of the nozzle throat) can produce large losses in resultant thrust ratio. A reduction in F_r/F_i may result from friction or pressure drag on the post-exit vanes. The installation penalty (at $\delta_{v,y} = 0^\circ$) probably results from combined friction and pressure drag. Additional thrust losses during vane deflection ($\delta_{v,y} > 0^\circ$) may result from exhaust flow separation on the right post-exit vane which extended out of the jet to act as an expansion surface. A simple oil-flow study of the flow field on the expansion vane showed a reverse-flow pattern during yaw thrust vectoring which is indicative of jet flow separation. The left post-exit vane acted as a compression surface and probably had a more significant effect on flow turning than the expansion vane. In fact, results shown in reference 27 on a post-exit vane concept installed on an axisymmetric nozzle indicated that a post-exit vane deflected away from the exhaust stream produced a negligible amount of flow turning.

Yaw thrust vectoring had no effect on resultant pitch vector angle δ_p , regardless of nozzle exit aspect ratio or post-exit vane deflection angle. This result is shown in figures 9, 12, and 15. Pitch vectoring was initiated at the nozzle throat, well upstream of the exit, so that the exhaust jet was probably fully deflected in pitch before it reached the post-exit vanes.

Pitch thrust vectoring had no effect on yaw thrust vectoring at values of NPR above design. In fact, δ_y showed the same variation with NPR whether pitch vectoring was implemented or not. This independence of pitch thrust-vector angle and yaw thrust-vector angle at and above the nozzle design condition is an important result of the post-exit vane thrust-vectoring concept. A highly desirable feature of a multiaxis thrust-vectoring system is that thrust vectoring about one axis does not degrade thrust-vectoring performance about the other axis. The post-exit vane concept can successfully provide usable uncoupled pitch and yaw vectoring, although flow turning in the yaw plane did result in significant thrust losses.

Resultant splay vector angle δ_s was not presented for any of the unvectored nozzle configurations since splay vector angle is undefined for pure axial (unvectored) exhaust flow (see section "Symbols"). For a pure negative pitch-vector nozzle configuration, δ_s equals -180° . The basic δ_s data are generally within 5° of this defined level. The pitch-vector configurations with and without the $\delta_{v,y} = 0^\circ$ vanes resulted in values of δ_s near -180° . When the post-exit vanes were deflected and $\delta_{v,p} = 0^\circ$ (no pitch vectoring), values of δ_s near -90° resulted. Configurations with combined pitch and yaw vectoring ($\delta_{v,p} = -11.7^\circ$ and $\delta_{v,y} < 0^\circ$) produced values of δ_s which fell between -180° and -90° , depending on the value of δ_y and NPR. As expected, when δ_y was greater than δ_p , the value δ_s was closer to -90° ; when δ_p was greater than δ_y , δ_s was closer to -180° . Equal amounts of negative pitch and yaw thrust vectoring ($\delta_y = \delta_p$) would produce a value of resultant splay angle equal to -135° .

Summary Data

Effect of exit aspect ratio. The effects of nozzle exit aspect ratio on nozzle performance are summarized in figure 16 for the baseline nozzles without post-exit vanes and in figure 17 for the baseline nozzles with vane V1 installed at $\delta_{v,y} = -30^\circ$. Performance parameters are plotted as functions of exit aspect ratio for fixed NPR values of 2.5, 4.0, and 6.0. These values of NPR are representative of choked flow conditions. Exit aspect ratio had only small effects on baseline nozzle performance. The magnitude of C_d , F/F_i , and F_r/F_i each varied only 1.5 percent or less with AR, and there was no effect of AR on δ_p for the baseline pitch-vector nozzle. (See fig. 16 (c).)

The yaw-vector configurations (fig. 17) showed a larger effect of AR on nozzle performance than the baseline configurations. For vane V1 at $\delta_{v,y} = -30^\circ$, resultant yaw vector angle decreased in magnitude (that is, became less negative) with increasing aspect ratio. Internal and resultant thrust ratios increased with increasing AR. The largest values of δ_y were generated by the nozzle configurations with AR = 1.5. At NPR = 6.0, the magnitude of δ_y decreased from 18.5° to 7° as AR increased from 1.5 to 4.0. This effect of exit aspect ratio on δ_y probably results from two geometric design characteristics: the physical distance between the post-exit vanes (nozzle width) and the sizing of the post-exit vanes. It is not possible to determine from the data which of these two factors had the greater effect on nozzle performance.

Nozzle exit aspect ratio was varied by holding the exit height constant and changing the width of the exit. Thus, nozzle exit area A_e decreased

with decreasing AR. As the exit width, AR, and A_e decreased, the sidewalls and sidewall-mounted post-exit vanes moved closer together so that a larger percentage of the exhaust flow periphery was directly affected by the yaw vanes. Since decreasing AR physically decreased the distance between the post-exit vanes, it was expected that the jet exhaust core (center portion of exhaust flow) would be more efficiently turned by vanes installed on nozzles with low AR than by vanes installed on nozzles with higher AR. In fact, the nozzles with AR = 1.5 and post-exit vanes, the configurations which physically contacted the largest percentage of the exhaust flow periphery, provided the largest values of δ_y measured during this investigation. As AR and A_e increased, the proximity of the sidewalls decreased, the vanes affected a smaller percentage of the exhaust flow periphery, and smaller values of δ_y resulted.

Post-exit vane planform and area were not varied with AR. The same post-exit vanes were tested with each nozzle configuration regardless of nozzle geometry or exit aspect ratio. As AR increased, the ratio of vane area to exit area A_v/A_e decreased and, thus, the relative size of the post-exit vanes decreased. This effect of AR on the relative vane size probably contributes to the decrease in δ_y with increasing AR. For example, vane V1 with the nozzles with AR = 1.5 results in $A_v/A_e = 1.083$, with the nozzles with AR = 2.5 results in $A_v/A_e = 0.65$, and with the nozzles with AR = 4.0 results in $A_v/A_e = 0.406$. (See fig. 3(a).) If the size of the post-exit vanes had been increased with increasing AR to keep the ratio A_v/A_e at a constant value independent of AR, then larger values of δ_y would probably have resulted for the nozzles with AR = 2.5 and AR = 4.0. Other effects of vane planform are discussed later.

Effect of nozzle type. The effects of 2-D nozzle type on nozzle internal performance are presented in figure 18 for nozzle configurations without thrust vectoring and in figure 19 for the nozzle-vane configurations with vane V1 installed and $\delta_{v,y} = -30^\circ$. Nozzle internal performance parameters C_d , F/F_i , F_r/F_i , and δ_y (fig. 19) are presented as functions of nozzle exit aspect ratio at three fixed NPR values: 2.5, 4.0, and 6.0. The performance data for the unvectored baseline nozzle show almost no effect of nozzle type on C_d . The effect of nozzle type on the thrust ratio data varies with NPR. At NPR = 2.5, there is little effect of nozzle type on either F/F_i or F_r/F_i . However, at NPR = 4.0 (fig. 18(b)) and 6.0 (fig. 18(c)), the thrust ratios for the 2-D convergent nozzles were lower than those for the 2-D C-D nozzles, regardless of AR. This difference in thrust ratios due to nozzle type increased as NPR increased. The thrust ratio

data reflect the different design parameters (A_e/A_t , $(NPR)_d$) of the two nozzle types. The 2-D C-D nozzles had a higher value of $(NPR)_d$ than the 2-D convergent nozzles. (See fig. 2(b).) At NPR = 4.0 and 6.0, the 2-D C-D nozzles were operating closer to design conditions than the convergent nozzles. Consequently, at these particular values of NPR, under-expansion losses decreased the thrust ratios of the convergent nozzles to produce the differences in thrust levels between the two nozzle types.

The effect of nozzle type on the thrust-ratio performance data of the yaw-vectoring configurations (fig. 19) was similar to the results for the unvectored nozzles. At NPR = 2.5, there was little effect of nozzle type on F/F_i or F_r/F_i . At NPR = 4.0 and 6.0, the 2-D C-D configurations produced slightly (1 percent or less) higher thrust ratios than the 2-D convergent nozzle-vane configurations. Similarly, nozzle type had only a small effect (about 1 percent or less) on resultant yaw vector angle δ_y . However, nozzle type had a large effect on C_d data for the nozzle-vane configurations. The 2-D convergent configurations had significantly lower C_d levels than the 2-D C-D configurations for $\delta_{v,y} = -30^\circ$. This effect of nozzle type on C_d results from the effective throat area variation with vane deflection angle which occurred for the convergent nozzles with deflected post-exit vanes and was discussed earlier in the section "Basic Data."

Effect of flat post-exit vane planform. The effects of flat vane planform on nozzle performance are summarized in figure 20 for the 2-D convergent nozzles, $\delta_{v,y} = -30^\circ$, and in figure 21 for the 2-D C-D nozzles, $\delta_{v,p} = 0^\circ$ and $\delta_{v,y} = -30^\circ$. The performance parameters F/F_i , F_r/F_i , and δ_y are presented as functions of the vane area ratio A_v/A_e (ratio of single vane area to nozzle exit area). Results are presented for the vane deflection $\delta_{v,y}$ of -30° at three values of NPR (NPR = 2.5, 4.0, and 6.0) for each nozzle exit aspect ratio.

With the exception of vane V2 ($A_v/A_e = 1.417$) installed on the nozzles with AR = 1.5 and operating at NPR = 6.0, increasing vane planform area resulted in significant increases (i.e., larger negative values) in resultant yaw vector angle δ_y , regardless of NPR, nozzle aspect ratio, or nozzle type. However, this beneficial effect on δ_y was accompanied by large adverse effects on F/F_i and F_r/F_i . For each AR tested, the largest negative values of δ_y resulted from the $\delta_{v,y} = -30^\circ$ deflection of vane V4, which also had the largest value of A_v/A_e tested. The V4 vane geometry had the same length as the baseline vane V1 but was wider. The smallest negative values of δ_y resulted from vane V3, which had the smallest value of A_v/A_e tested. Vane V3 had the baseline

width but was shorter in length than baseline vane V1. Vane V2, which had the baseline width but was longer than vane V1, had an inconsistent (with AR) effect on δ_y . When AR = 1.5 and NPR = 6.0, δ_y results for the V2 configurations were smaller in magnitude than δ_y results for the V1 configurations. However, at other combinations of AR and NPR, values of δ_y for vane V2 were larger in magnitude than values for vane V1. (Recall that A_v/A_e for vane V2 was always greater than A_v/A_e for vane V1, regardless of AR.)

Increasing vane width consistently increased δ_y more effectively than increasing vane length. This result was independent of nozzle type. If the V4 vane data in figures 20 and 21 are ignored, the remaining data indicate the performance trends due to vane length only. In general, the V1, V2, and V3 data indicate that the beneficial effect of increasing vane length on δ_y reached a maximum (for vane V1) and then diminished as vane length increased (vane V3). An optimum vane length for generating a maximum δ_y probably exists for each nozzle geometry and operating condition.

Effect of post-exit vane curvature. The effects of post-exit vane curvature on nozzle internal performance are presented in figure 22 for the 2-D convergent nozzle configurations and in figure 23 for the 2-D C-D nozzle configurations. Performance parameters F/F_i , F_r/F_i , and δ_y are plotted as functions of AR for three values of NPR (NPR = 2.5, 4.0, and 6.0). Results are presented for $\delta_{v,y} = -30^\circ$ only.

The effects of vane curvature on nozzle performance were generally small. At NPR = 2.5, vane curvature increased the magnitude of δ_y by as much as 2° , depending on AR and nozzle type. However, by NPR = 6.0, there was almost no effect of vane curvature on δ_y . Increases in δ_y due to vane curvature were paralleled by decreases in the thrust ratios. The thrust losses associated with vane curvature were possibly the result of increased pressure drag on the curved vanes. Overall, performance gains due to vane curvature were minimal. For a realistic operational aircraft, the extra fabrication costs of a curved vane instead of a flat vane would probably cancel out any small improvements in flow turning which result from vane curvature.

Conclusions

A static (wind-off) experiment has been conducted in the static test facility of the Langley 16-Foot Transonic Tunnel to investigate the effects of yaw thrust vectoring by post-exit vanes on non-axisymmetric nozzle performance. Two types of non-axisymmetric nozzles were tested: a two-dimensional

convergent nozzle and a two-dimensional convergent-divergent nozzle. The two-dimensional convergent-divergent nozzle was tested with and without pitch thrust vectoring. The three basic nozzle configurations were tested as baselines (without yaw vanes) and with post-exit vanes installed. Each nozzle configuration was tested with three different nozzle exit aspect ratios (ratio of nozzle width to height at the exit) of 1.5, 2.5, and 4.0. Post-exit vanes for yaw thrust vectoring were externally mounted at the nozzle exit and extended downstream behind the nozzle. The effects of vane deflection angle, vane planform, and vane curvature were examined. The test was conducted at nozzle pressure ratios from 1.6 to 6.0. The results of this investigation can be summarized as follows:

1. Resultant yaw vector angles were always smaller than the geometric yaw vector angles.
2. Installing the post-exit vanes without vane deflection produced a small loss in resultant gross thrust. Vane deflection for yaw thrust vectoring produced significant additional resultant thrust losses.
3. Pitch thrust-vectoring performance was independent of yaw thrust-vectoring operation. Pitch thrust vectoring had little effect on resultant yaw vector angle.
4. The magnitude of resultant yaw vector angle decreased with increasing nozzle exit aspect ratio.
5. There was very little effect of nozzle type (two-dimensional convergent or convergent-divergent) on resultant yaw vector angle.
6. Increasing post-exit vane planform area generally produced large increases in resultant yaw vector angle, regardless of other nozzle geometric or exhaust flow parameters. However, larger yaw vector angles were accompanied by large adverse effects on thrust. For the range of variables tested, increasing vane width was more beneficial than increasing vane length.
7. Vane curvature had only a small effect on resultant yaw vector angle or resultant thrust ratio.

References

1. Herbst, W. B.: Future Fighter Technologies. *J. Aircr.*, vol. 17, no. 8, Aug. 1980, pp. 561-566.
2. Herbst, W. B.: Supermaneuverability. *Workshop on Unsteady Separated Flow*, Michael S. Francis and Marvin W. Luttgies, eds., AFOSR-TR-84-0911, U.S. Air Force, May 1984, pp. 1-9. (Available from DTIC as AD P004 153.)
3. Gallaway, C. R.; and Osborn, R. F.: Aerodynamics Perspective of Supermaneuverability. AIAA Paper 85-4068, Oct. 1985.
4. Hienz, Egon; and Vedova, Ralph: Requirements, Definition and Preliminary Design for an Axisymmetric Vectoring Nozzle, To Enhance Aircraft Maneuverability. AIAA Paper 84-1212, June 1984.
5. Herrick, Paul W.: Propulsion Influences on Air Combat. AIAA Paper 85-1457, July 1985.
6. Miller, L. Earl: *Post Stall Maneuvers and Thrust Vectoring Performance Analysis*. AFWAL-TR-84-3109, U.S. Air Force, July 1984. (Available from DTIC as AD A158 100.)
7. Capone, Francis J.; and Mason, Mary L.: *Multiaxis Aircraft Control Power From Thrust Vectoring at High Angles of Attack*. NASA TM-87741, 1986.
8. Kraus, W.; Przibilla, H.; and Haux, U.: Stability and Control for High Angle of Attack Maneuvering. *Criteria for Handling Qualities of Military Aircraft*, AGARD-CP-333, June 1982, pp. 15-1-15-11.
9. Mello, J. F.; and Kotansky, D. R.: Aero/Propulsion Technology for STOL and Maneuver. AIAA Paper 85-4013, Oct. 1985.
10. White, S. N.: *Feasibility Study for Integrating Thrust Vectoring as Primary Flight Control System*. NASA CR-165758, 1981.
11. Lacey, David W.: Air Combat Advantages From Reaction Control Systems. SAE Tech. Paper Ser. 801177, Oct. 1980.
12. Richey, G. K.; Surber, L. E.; and Berrier, B. L.: Airframe-Propulsion Integration for Fighter Aircraft. AIAA Paper 83-0084, Jan. 1983.
13. Nelson, B. D.; and Nicolai, L. M.: Application of Multi-Function Nozzles to Advanced Fighters. AIAA Paper 81-2618, Dec. 1981.
14. Lander, J. A.; and Palcza, J. Lawrence: Exhaust Nozzle Deflector Systems for V/STOL Fighter Aircraft. AIAA Paper 74-1169, Oct. 1974.
15. Capone, Francis J.: Summary of Propulsive-Lift Research in the Langley 16-Ft. Transonic Tunnel. *J. Aircr.*, vol. 13, no. 10, Oct. 1976, pp. 803-808.
16. Berrier, B. L.; and Re, R. J.: A Review of Thrust-Vectoring Schemes for Fighter Aircraft. AIAA Paper 78-1023, July 1978.
17. Capone, Francis J.: The Nonaxisymmetric Nozzle—It Is for Real. AIAA Paper 79-1810, Aug. 1979.
18. Berrier, Bobby L.; Palcza, J. Lawrence; and Richey, G. Keith: Nonaxisymmetric Nozzle Technology Program—An Overview. AIAA Paper 77-1225, Aug. 1977.
19. Hiley, P. E.; Wallace, H. W.; and Booz, D. E.: Study of Non-Axisymmetric Nozzles Installed in Advanced Fighter Aircraft. AIAA Paper 75-1316, Sept.-Oct. 1975.
20. Capone, Francis J.; and Berrier, Bobby L.: *Investigation of Axisymmetric and Nonaxisymmetric Nozzles Installed on a 0.10-Scale F-18 Prototype Airplane Model*. NASA TP-1638, 1980.
21. *F-15 2-D Nozzle System Integration Study. Volume I—Technical Report*. NASA CR-145295, 1978.
22. Capone, Francis J.; and Maiden, Donald L.: *Performance of Twin Two-Dimensional Wedge Nozzles Including Thrust Vectoring and Reversing Effects at Speeds up to Mach 2.20*. NASA TN D-8449, 1977.
23. Wasson, H. R.; Hall, G. R.; and Palcza, J. L.: Results of a Feasibility Study To Add Canards and ADEN Nozzle to the YF-17. AIAA Paper 77-1227, Aug. 1977.
24. Leavitt, Laurence D.: Summary of Nonaxisymmetric Nozzle Internal Performance From the NASA Langley Static Test Facility. AIAA Paper 85-1347, July 1985.
25. Lacey, David W.; and Murphy, Richard D.: *Jet Engine Thrust Turning by the Use of Small Externally Mounted Vanes*. DTNSRDC-82/080, U.S. Navy, Jan. 1983. (Available from DTIC as AD B070 970L.)
26. Mason, Mary L.; and Berrier, Bobby L.: *Static Investigation of Several Yaw Vectoring Concepts on Nonaxisymmetric Nozzles*. NASA TP-2432, 1985.
27. Berrier, Bobby L.; and Mason, Mary L.: *Static Performance on an Axisymmetric Nozzle With Post-Exit Vanes for Multiaxis Thrust Vectoring*. NASA TP-2800, 1988.
28. Berrier, Bobby L.; and Mason, Mary L.: Static Investigation of Post-Exit Vanes for Multiaxis Thrust Vectoring. AIAA Paper 87-1834, June-July 1987.
29. Capone, Francis J.: *Static Performance of Five Twin-Engine Nonaxisymmetric Nozzles With Vectoring and Reversing Capability*. NASA TP-1224, 1978.
30. Peddrew, Kathryn H., compiler: *A User's Guide to the Langley 16-Foot Transonic Tunnel*. NASA TM-83186, 1981.
31. Berrier, Bobby L.; Leavitt, Laurence D.; and Bangert, Linda S.: *Operating Characteristics of the Multiple Critical Venturi System and Secondary Calibration Nozzles Used for Weight-Flow Measurements in the Langley 16-Foot Transonic Tunnel*. NASA TM-86405, 1985.
32. Mercer, Charles E.; Berrier, Bobby L.; Capone, Francis J.; Grayston, Alan M.; and Sherman, C. D.: *Computations for the 16-Foot Transonic Tunnel—NASA, Langley Research Center. Revision 1*. NASA TM-86319, 1987.
33. Shapiro, Ascher H.: *The Dynamics and Thermodynamics of Compressible Fluid Flow, Volume I*. Ronald Press Co., c.1953.

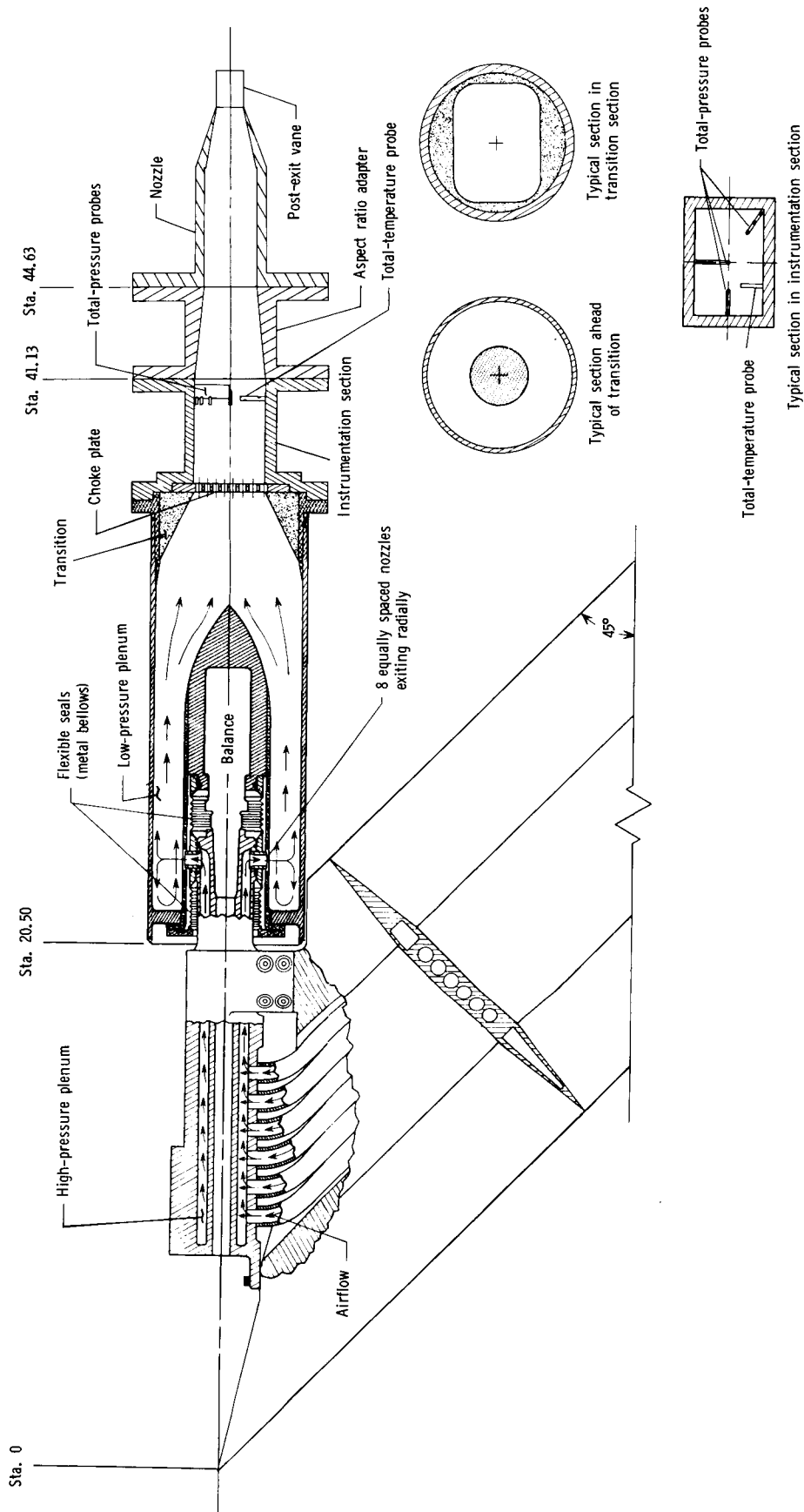
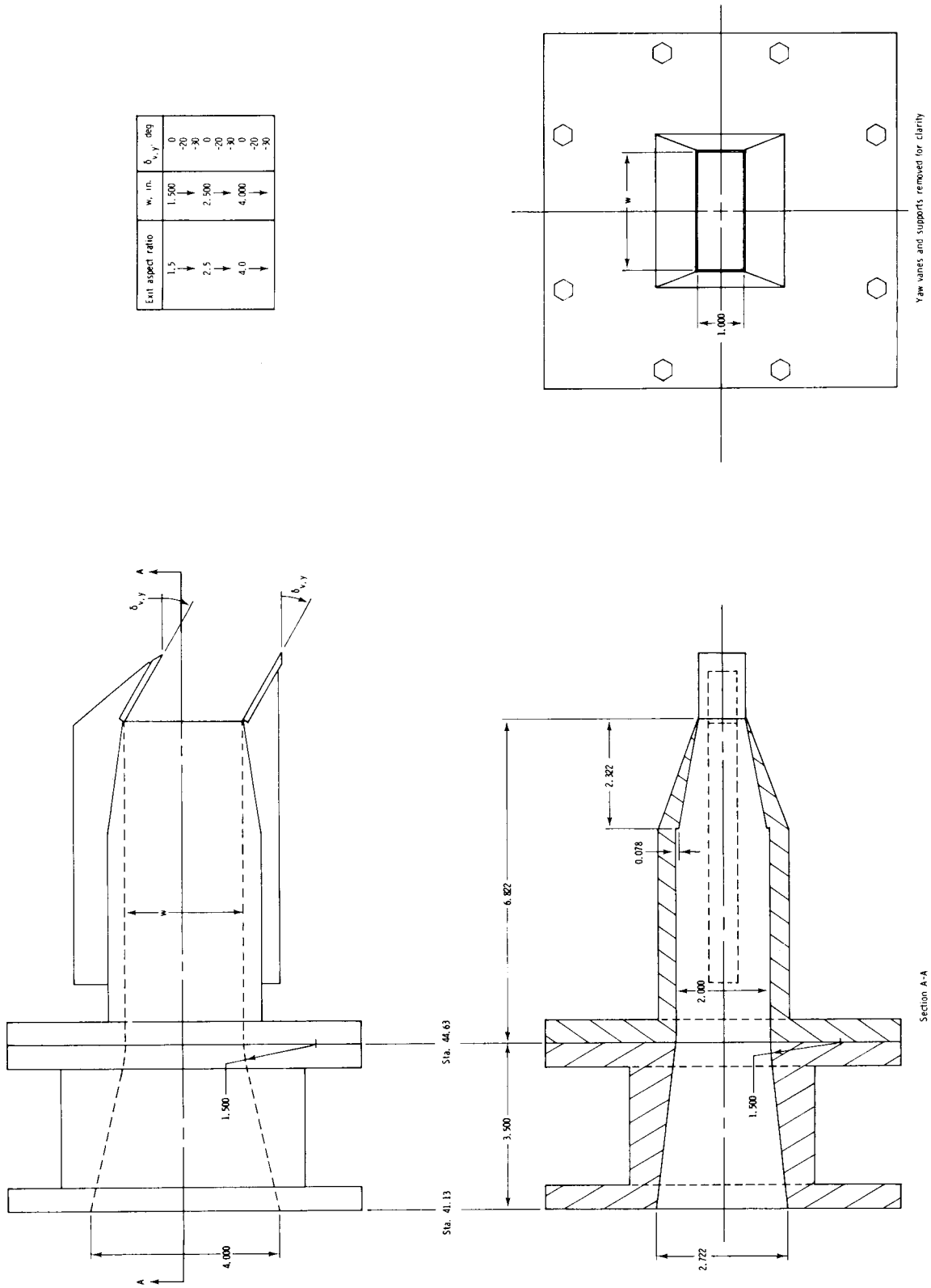


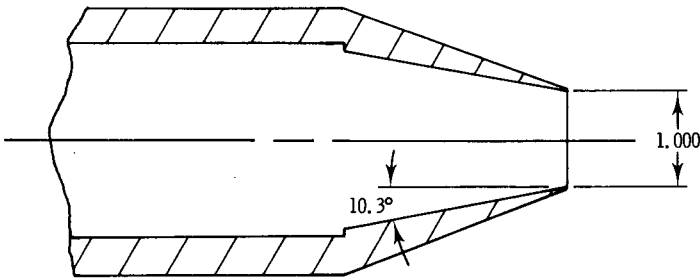
Figure 1. Sketch of air-powered nacelle model with typical nonaxisymmetric nozzle installed. Linear dimensions are in inches.



(a) Adapter and nozzle with post-exit vanes installed.

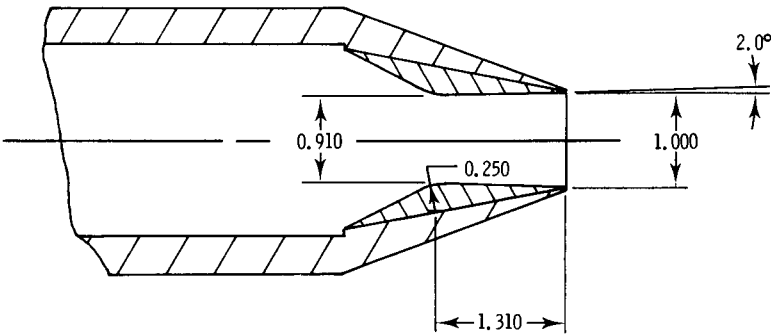
Figure 2. Sketches showing geometry of adapter and nozzles. Nozzle with exit aspect ratio of 2.5 shown. Linear dimensions are in inches.

Nonaxisymmetric convergent nozzle



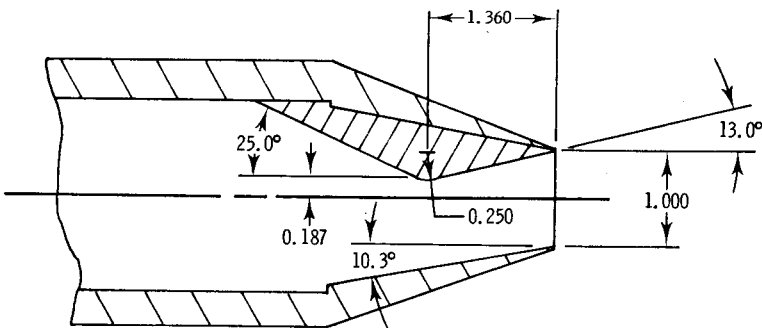
Exit aspect ratio	$\delta_{v,p}$, deg	A_t , in ²	A_e/A_t	$(NPR)_d$
1.5	0	1.522	1.00	1.89
2.5	↓	2.519	↓	↓
4.0	↓	3.985	↓	↓

Nonaxisymmetric convergent-divergent nozzle



Exit aspect ratio	$\delta_{v,p}$, deg	A_t , in ²	A_e/A_t	$(NPR)_d$
1.5	0	1.301	1.09	2.97
2.5	↓	2.345	1.05	2.63
4.0	↓	3.508	1.08	2.89

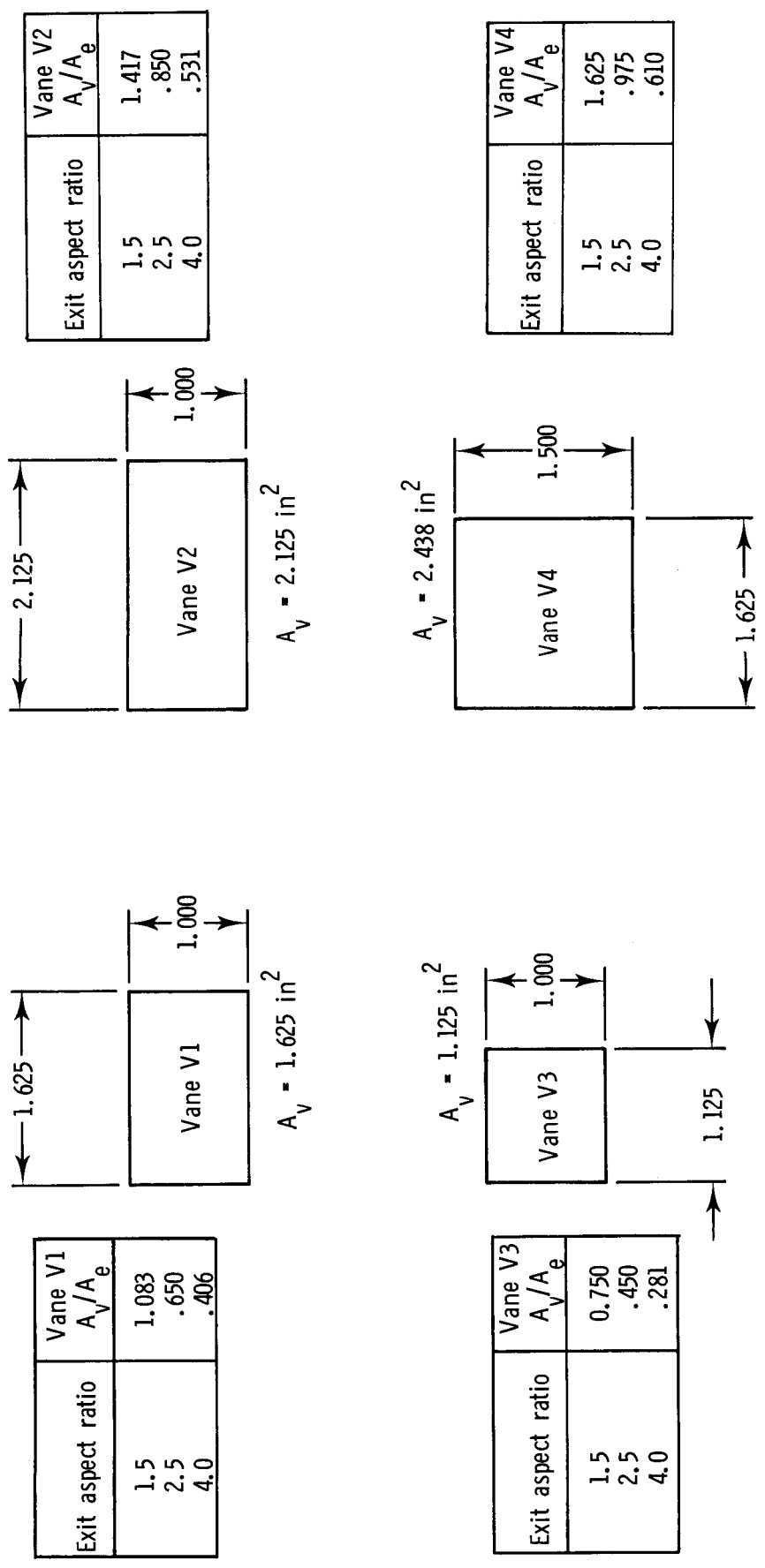
Pitch-vector nonaxisymmetric convergent-divergent nozzle



Exit aspect ratio	$\delta_{v,p}$, deg	A_t , in ²	A_e/A_t	$(NPR)_d$
1.5	-11.7	1.353	1.08	2.89
2.5	↓	2.234	1.08	2.89
4.0	↓	3.552	1.09	2.97

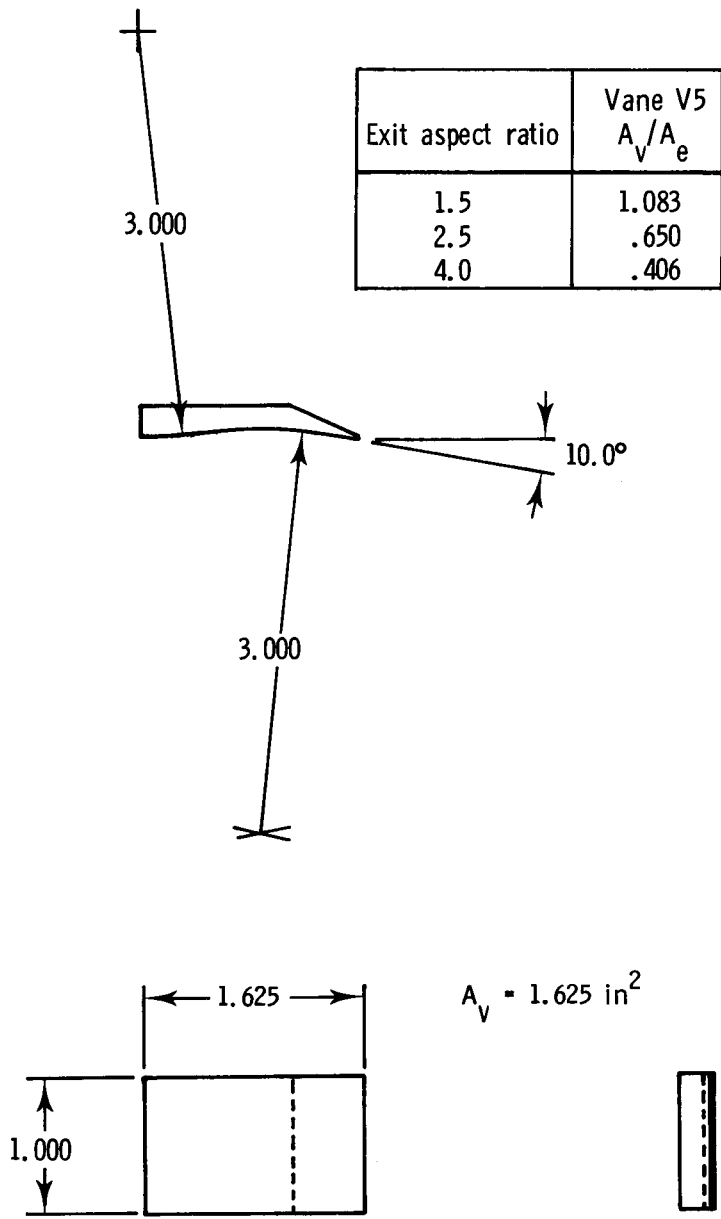
(b) Nozzle side views.

Figure 2. Concluded.



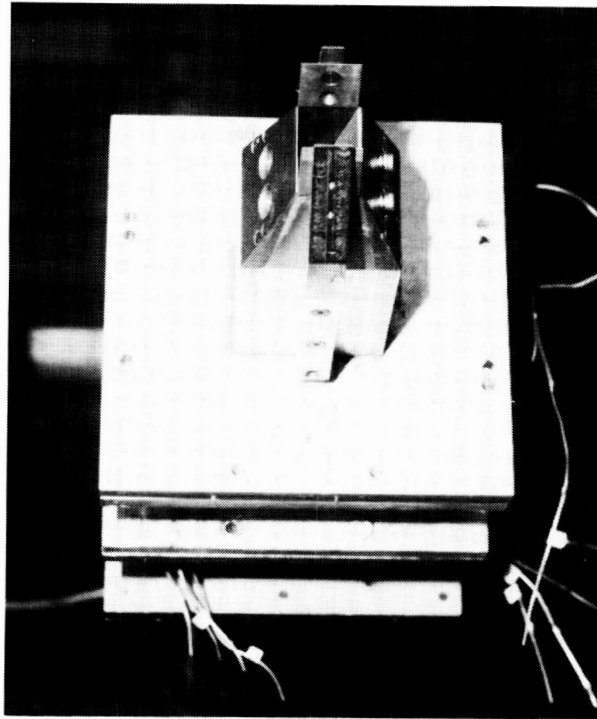
(a) Flat vanes.

Figure 3. Sketches showing geometry of yaw vector vanes. Linear dimensions are in inches.



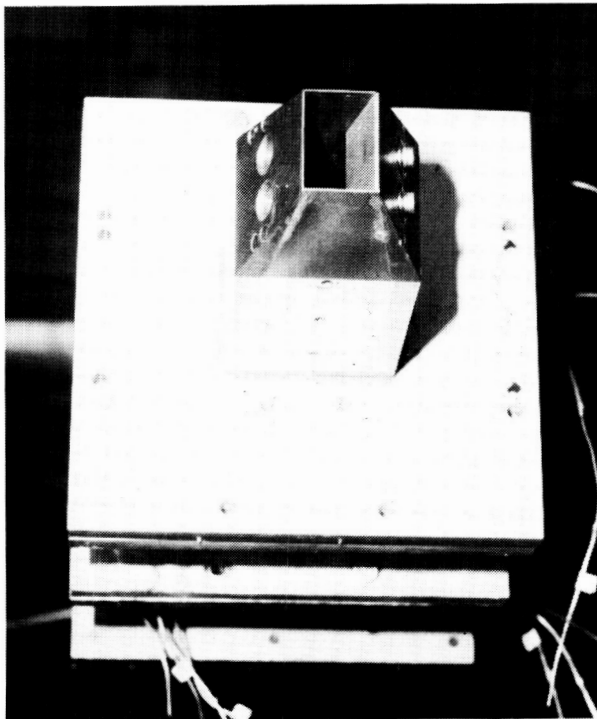
(b) Curved vane V5.

Figure 3. Concluded.



L-85-3433

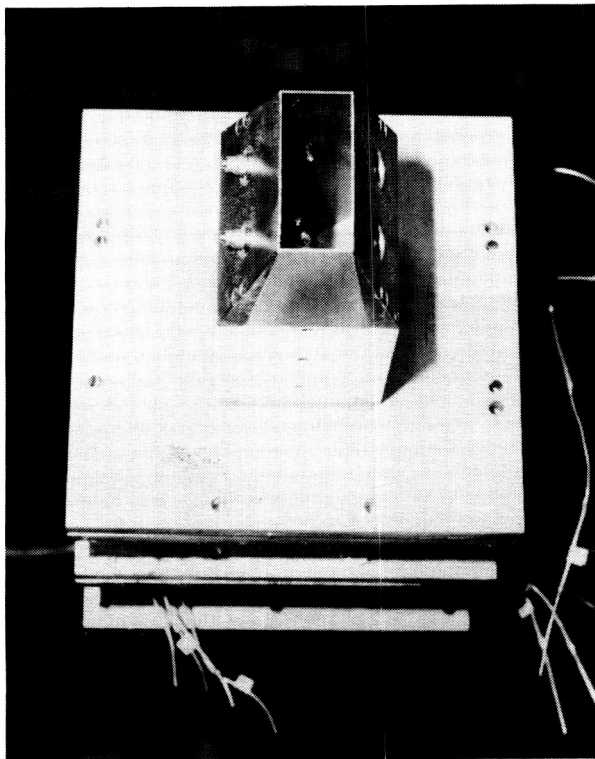
2-D C-D nozzle; $\delta_{v,p} = 0^\circ$; $\delta_{v,y} = -30^\circ$;
vane V3



L-85-3432

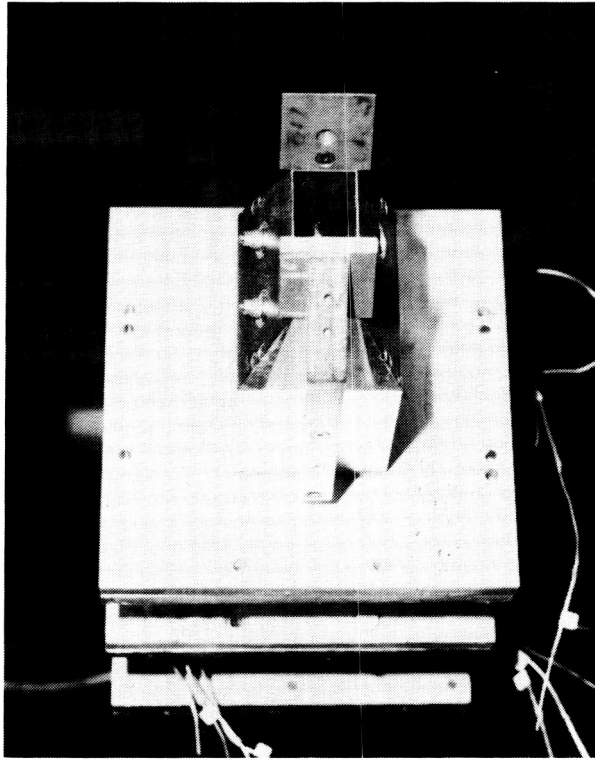
2-D C-D nozzle; $\delta_{v,p} = -11.70^\circ$; $\delta_{v,y} = 0^\circ$;
no yaw vanes

Figure 4. Two-dimensional nozzle configurations with aspect ratio of 1.5.



L-85-3429

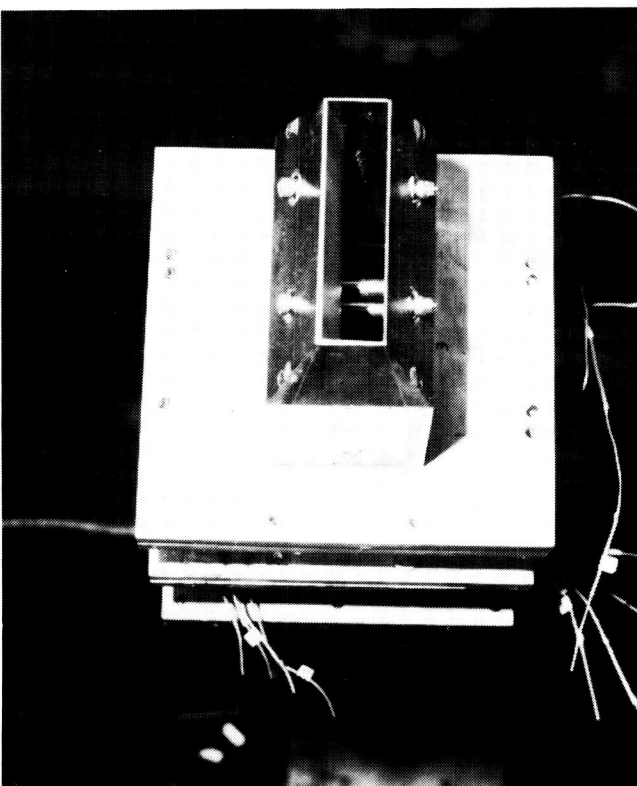
2-D C-D nozzle; $\delta_{v,p} = 0^\circ$; $\delta_{v,y} = 0^\circ$;
no yaw vanes



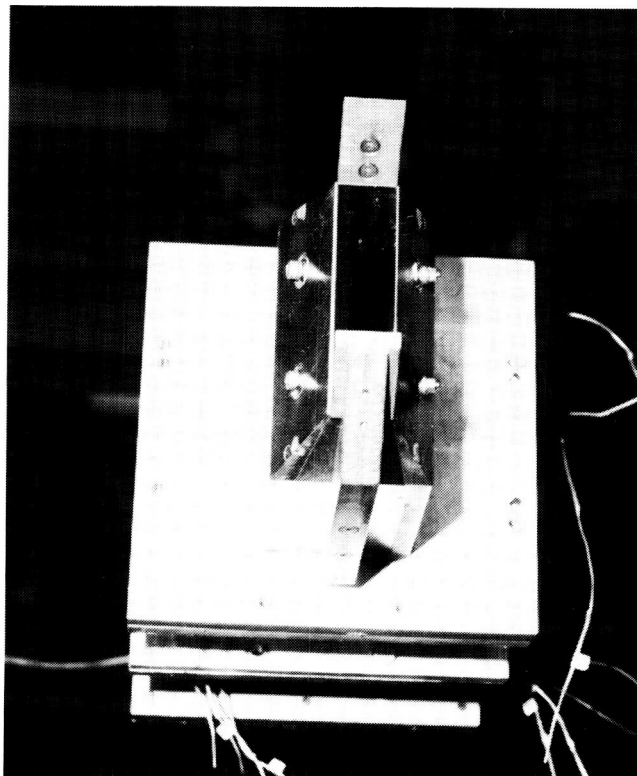
L-85-3434

2-D C-D nozzle; $\delta_{v,p} = 0^\circ$; $\delta_{v,y} = -30^\circ$;
vane V4

Figure 5. Two-dimensional nozzle configurations with aspect ratio of 2.5.



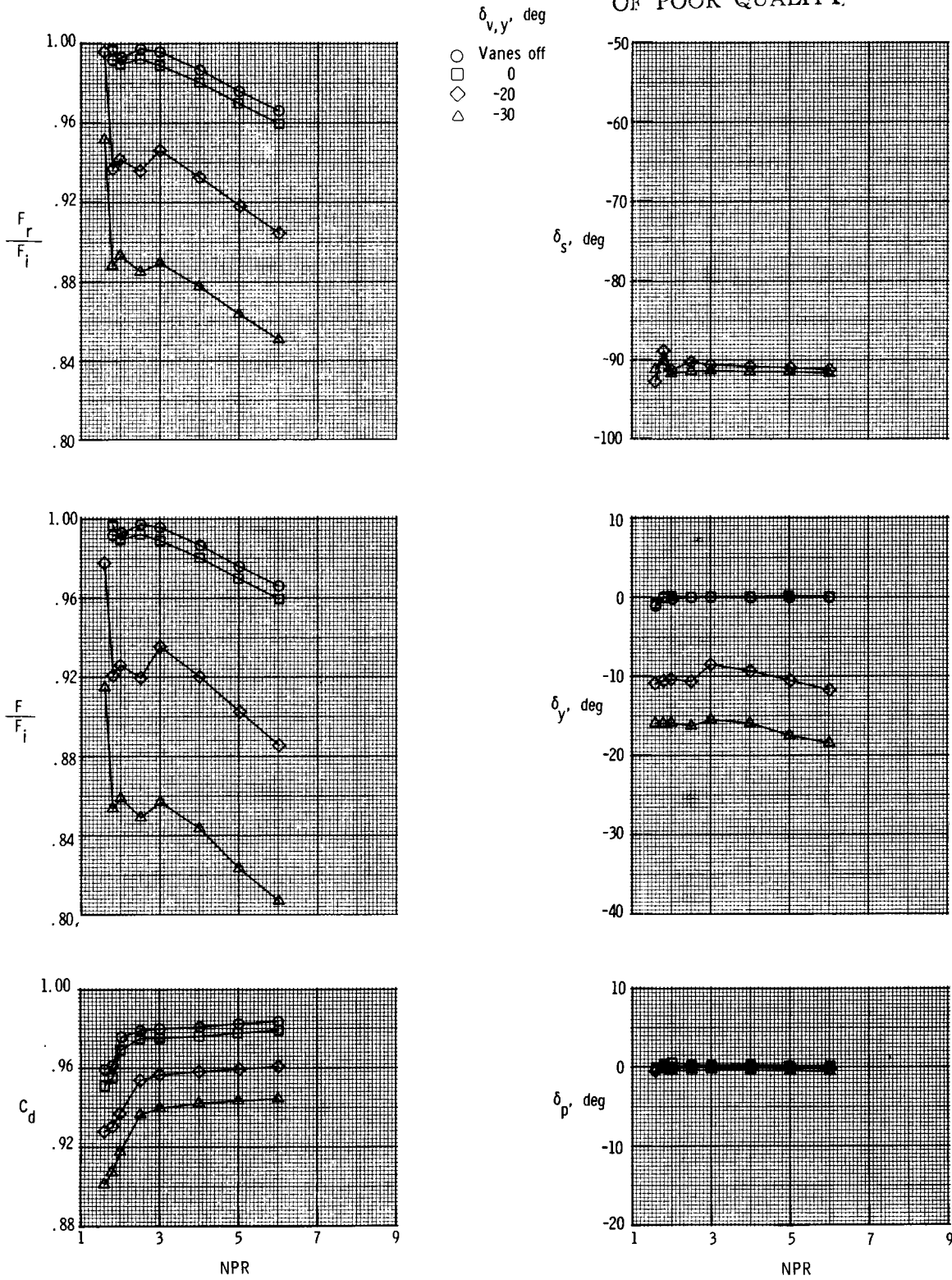
L-85-3427
2-D C-D nozzle; $\delta_{v,p} = 0^\circ$; $\delta_{v,y} = 0^\circ$;
no yaw vanes



L-85-3428
2-D C-D nozzle; $\delta_{v,p} = 0^\circ$; $\delta_{v,y} = -30^\circ$;
vane VI

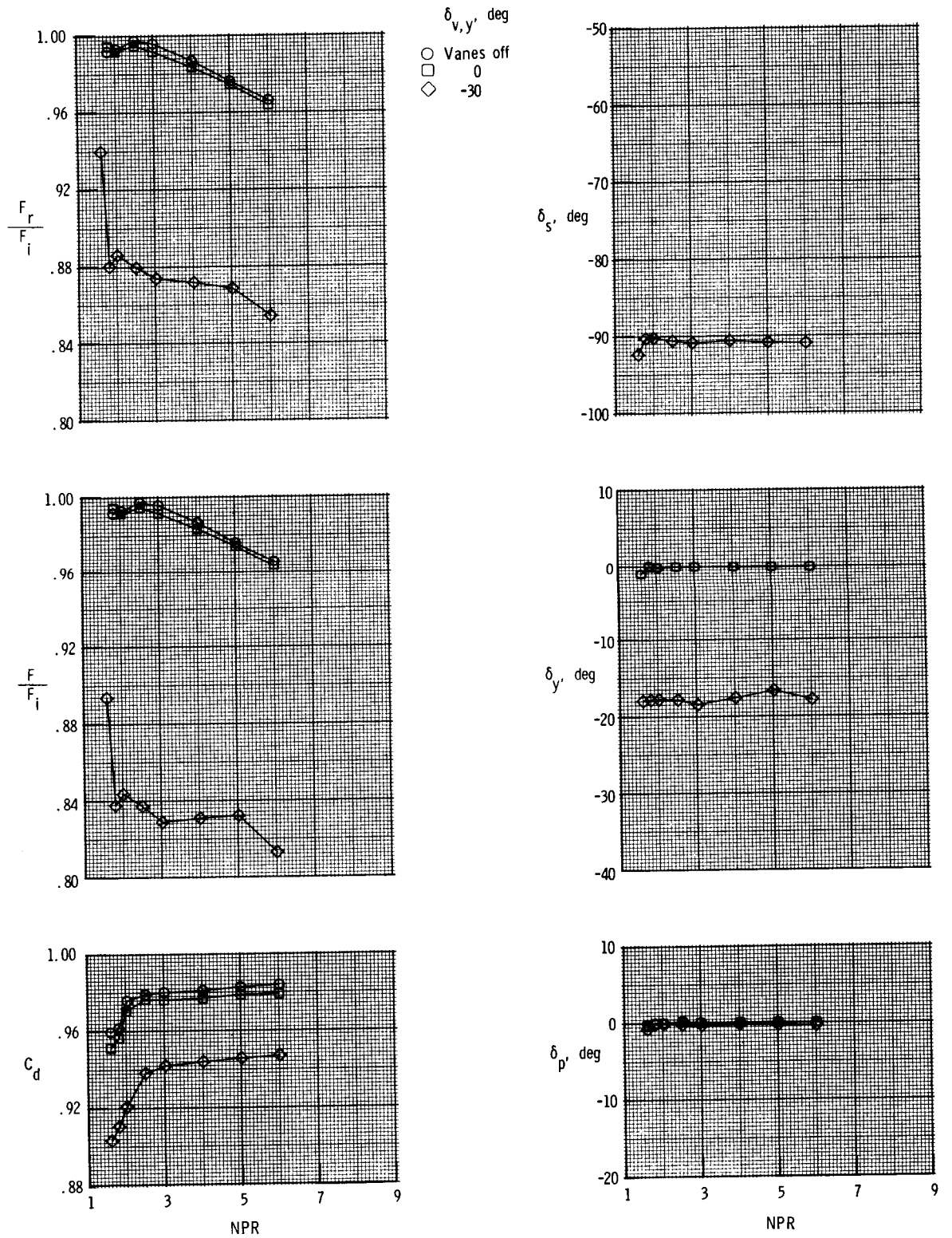
Figure 6. Two-dimensional nozzle configurations with aspect ratio of 4.0.

ORIGINAL PAGE IS
OF POOR QUALITY.



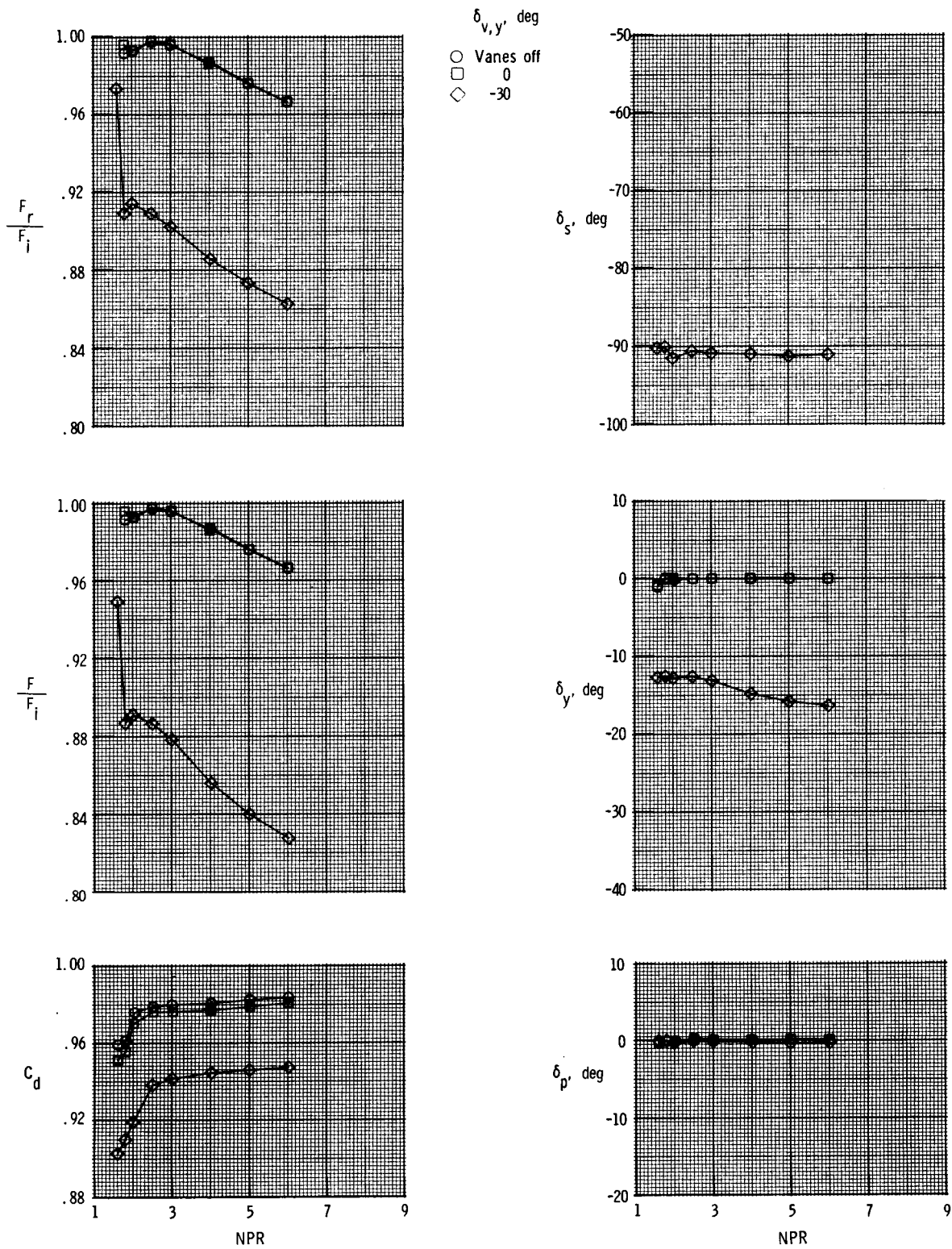
(a) Vane V1.

Figure 7. Effect of vane deflection on nozzle performance for 2-D convergent nozzle with AR = 1.5 and $\delta_{v,p} = 0^\circ$.



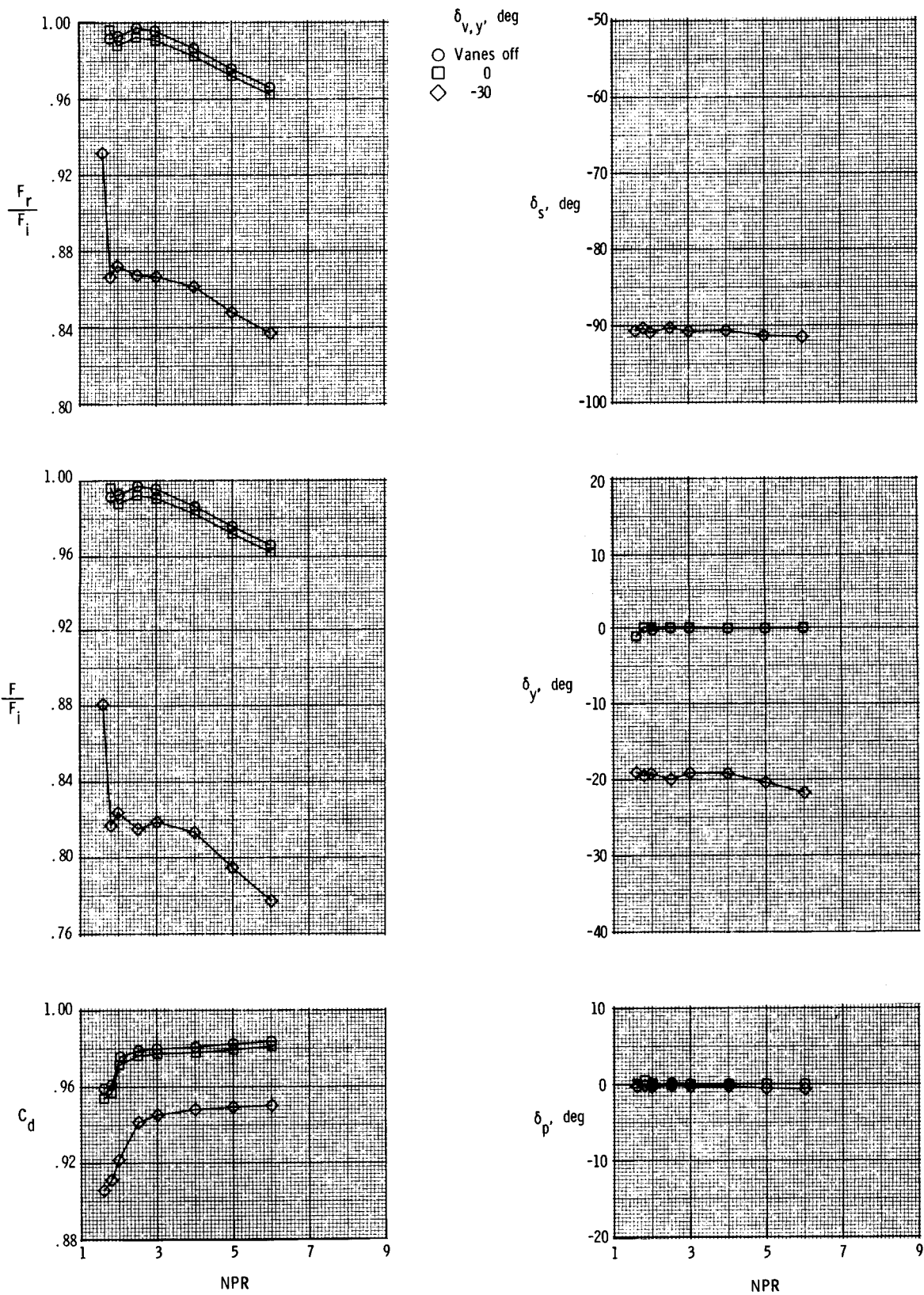
(b) Vane V2.

Figure 7. Continued.



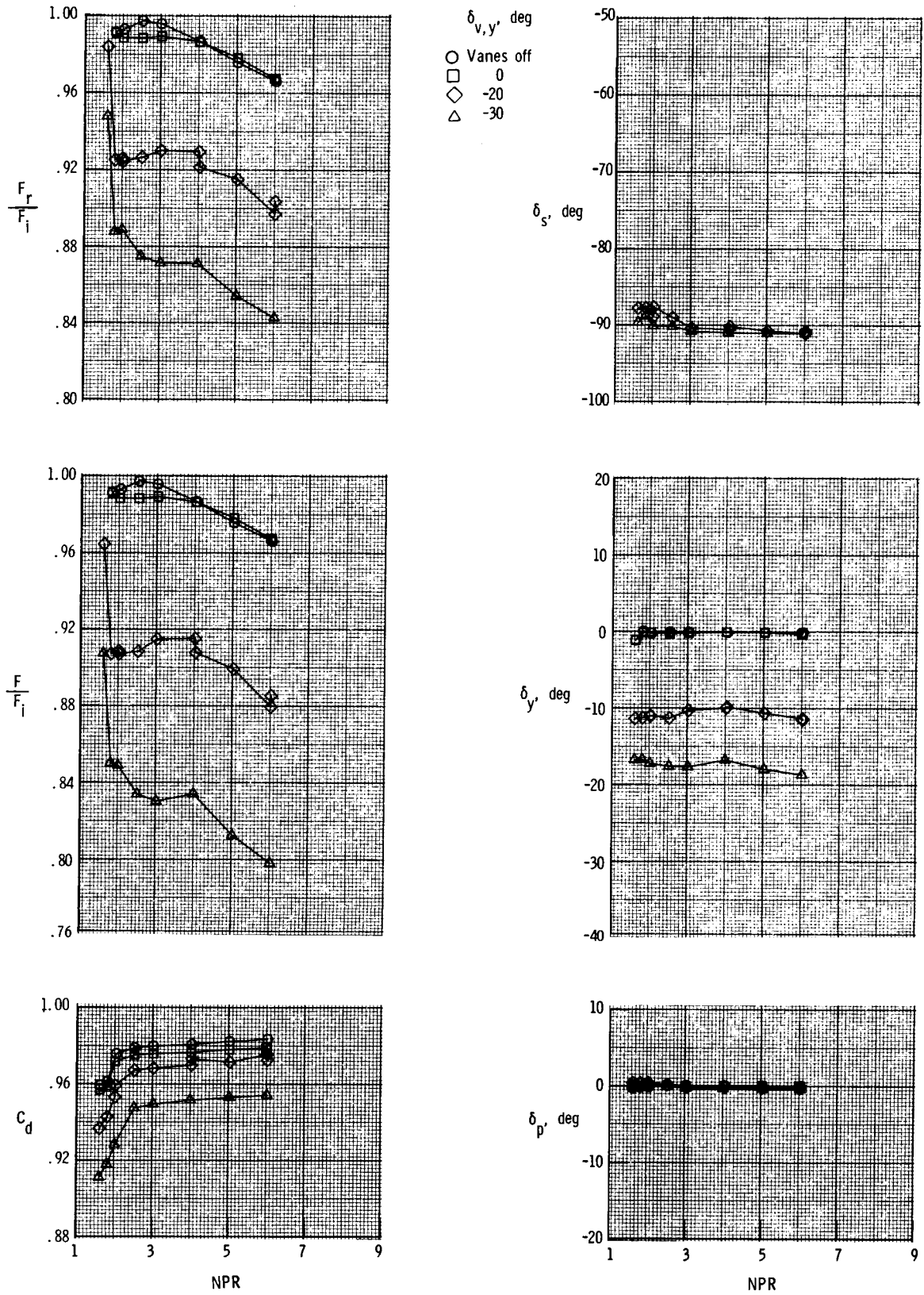
(c) Vane V3.

Figure 7. Continued.



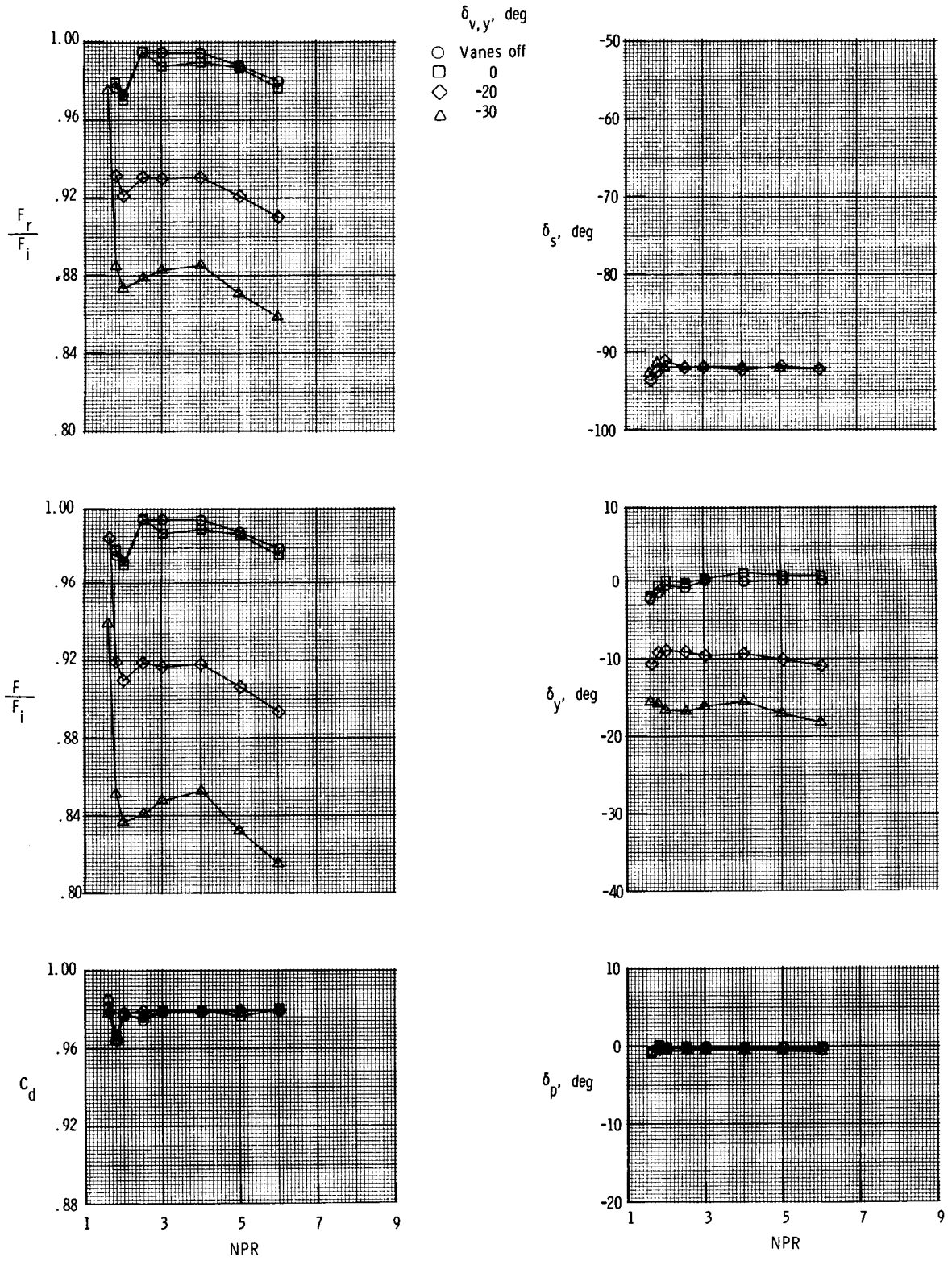
(d) Vane V4.

Figure 7. Continued.



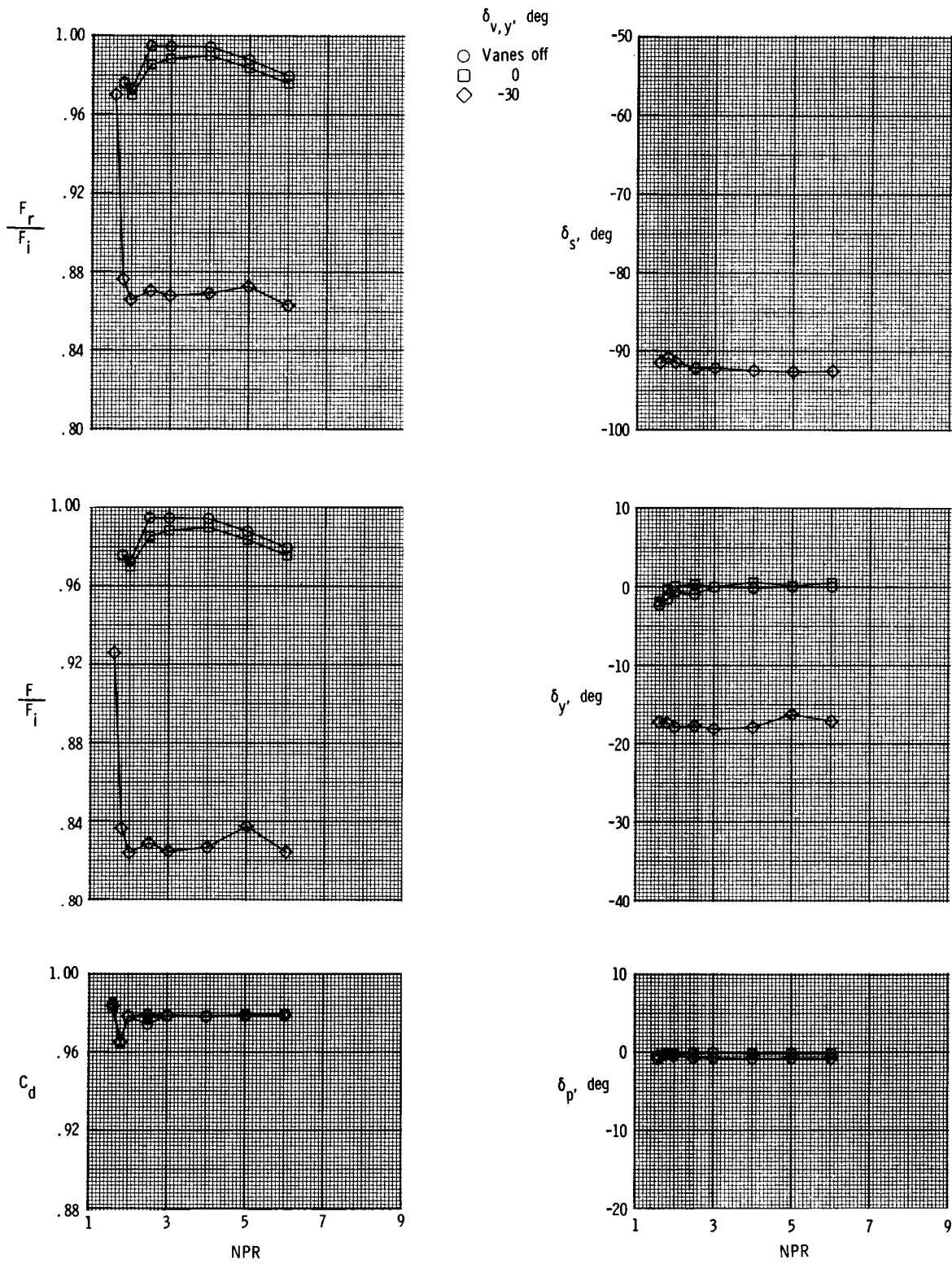
(e) Vane V5.

Figure 7. Concluded.



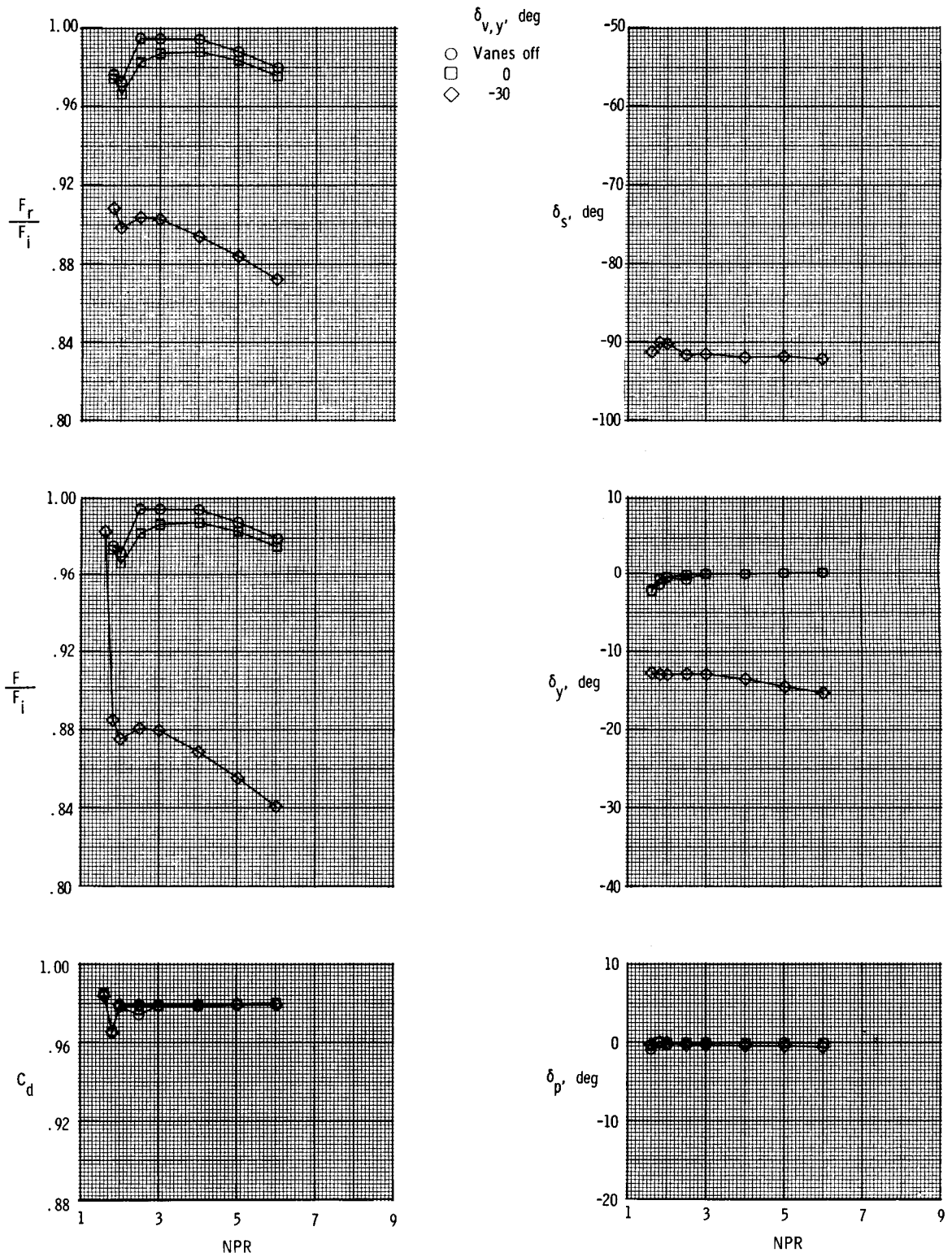
(a) Vane V1.

Figure 8. Effect of vane deflection on nozzle performance for 2-D C-D nozzle with $AR = 1.5$ and $\delta_{v,p} = 0^\circ$



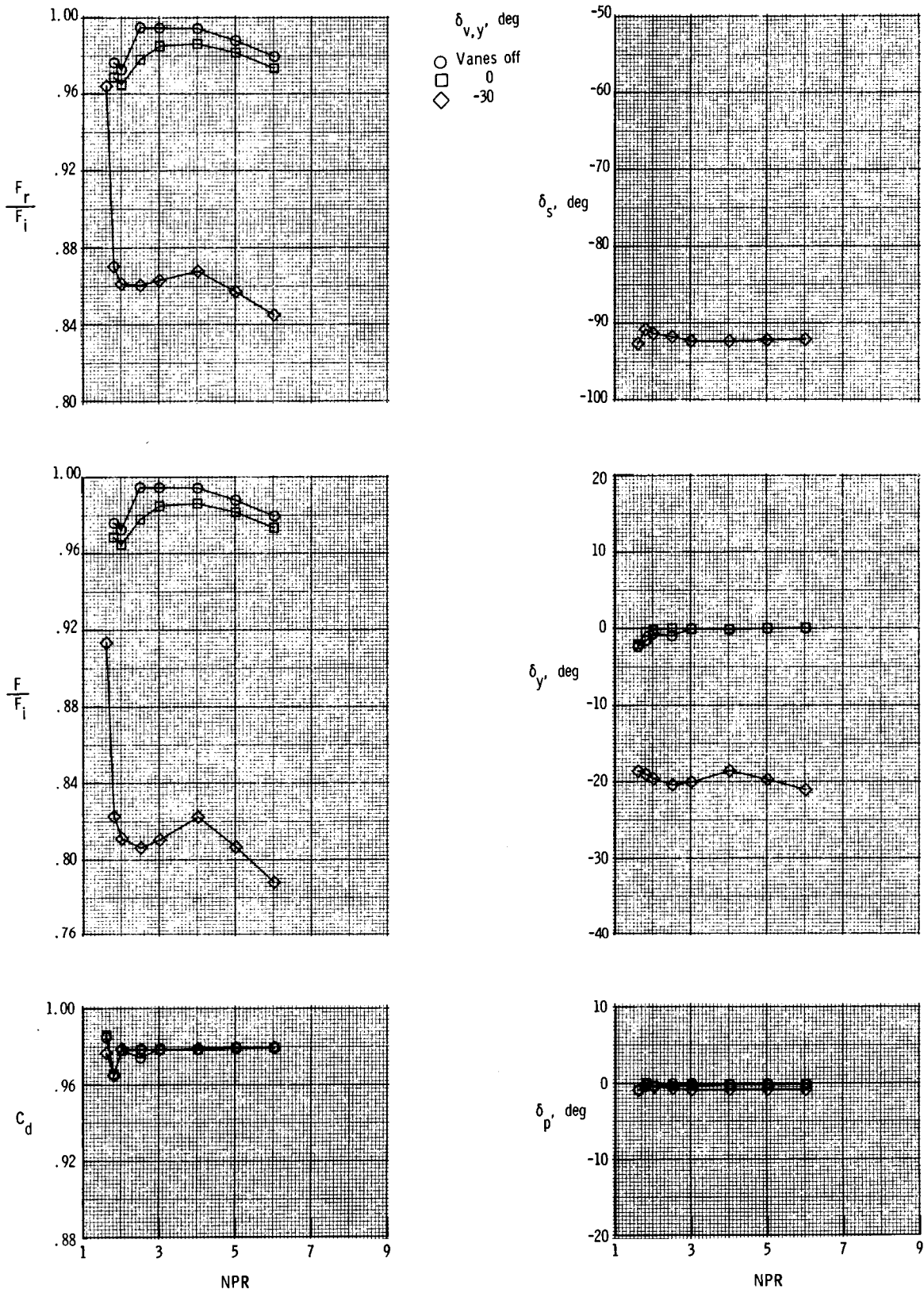
(b) Vane V2.

Figure 8. Continued.



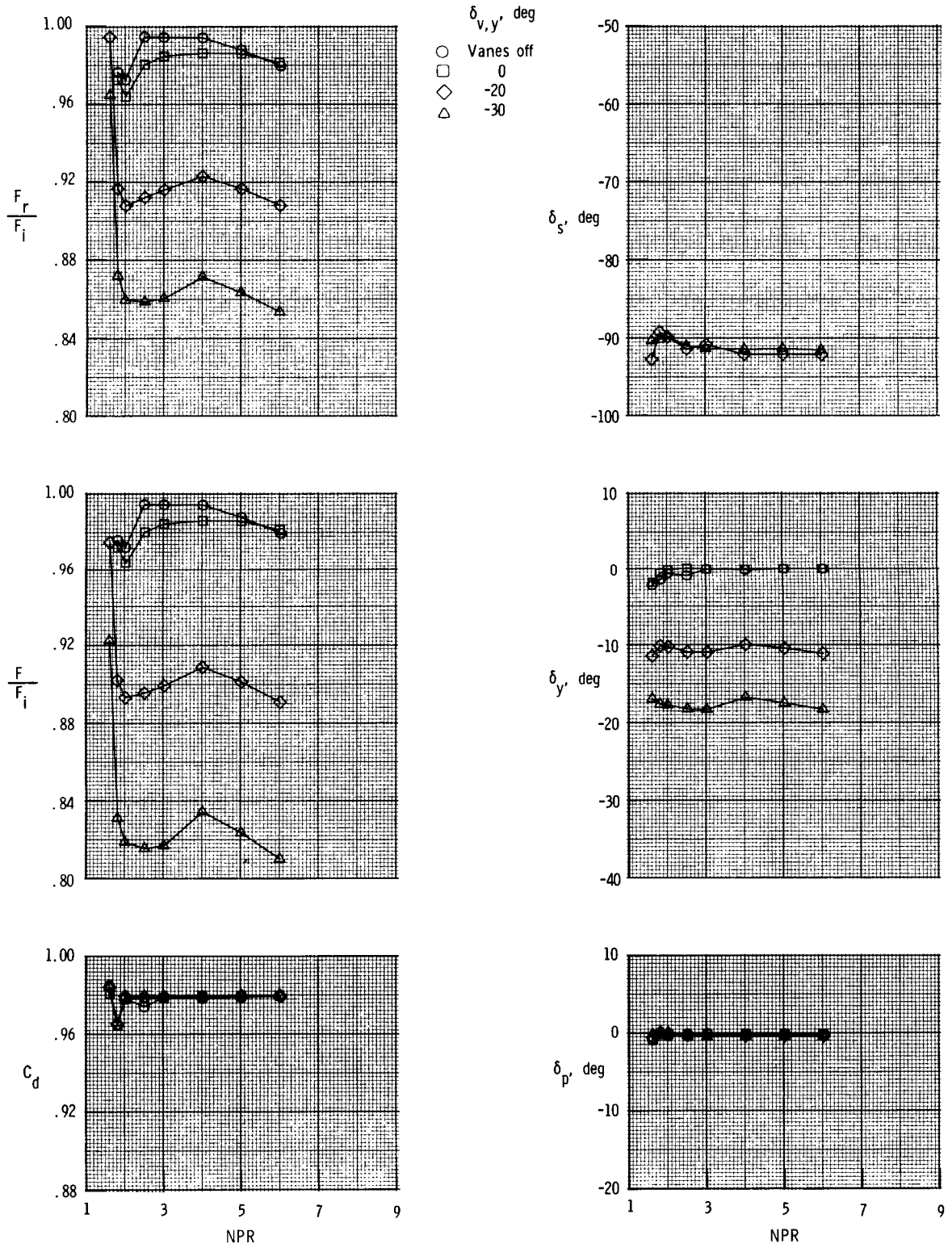
(c) Vane V3.

Figure 8. Continued.



(d) Vane V4.

Figure 8. Continued.



(e) Vane V5.

Figure 8. Concluded.

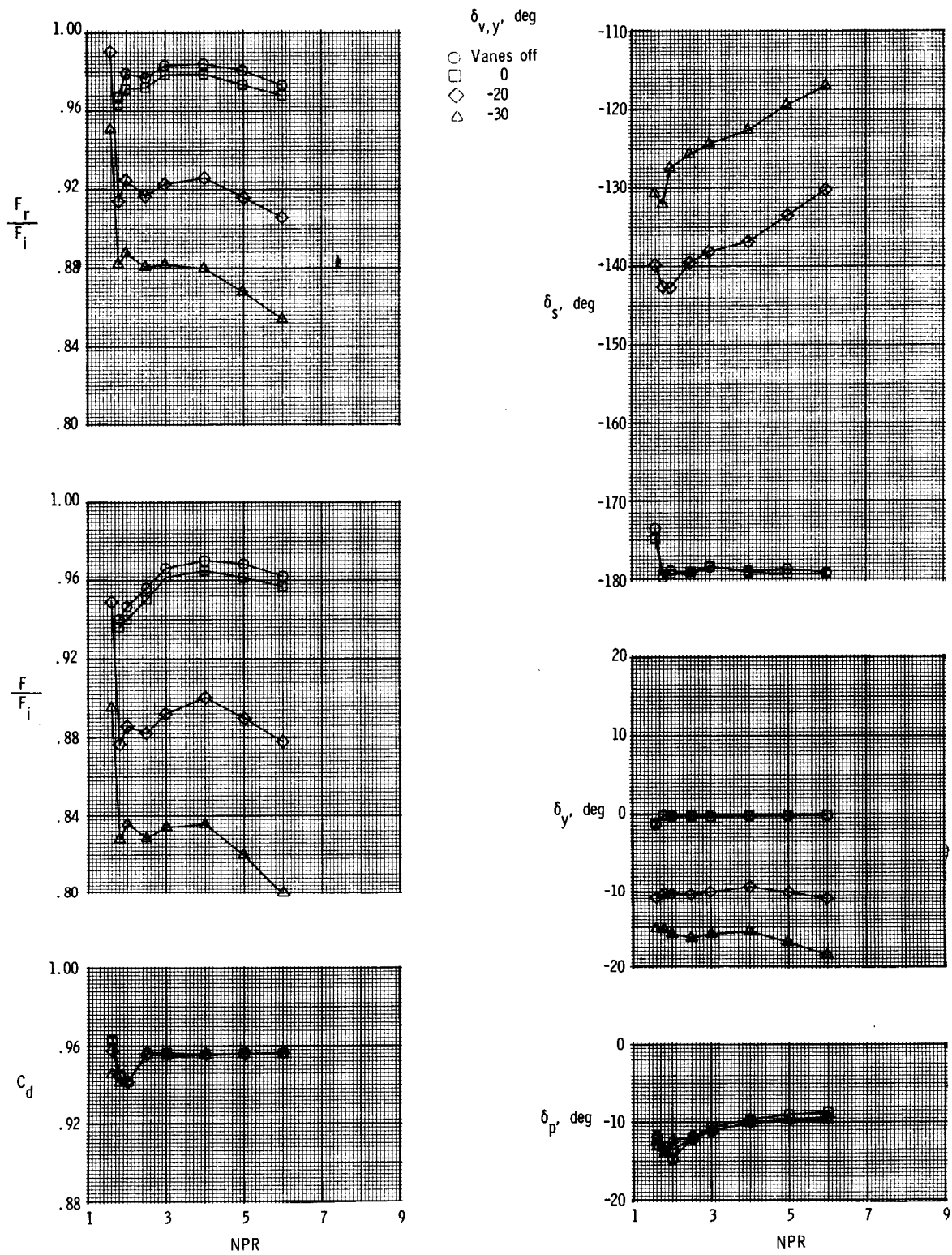
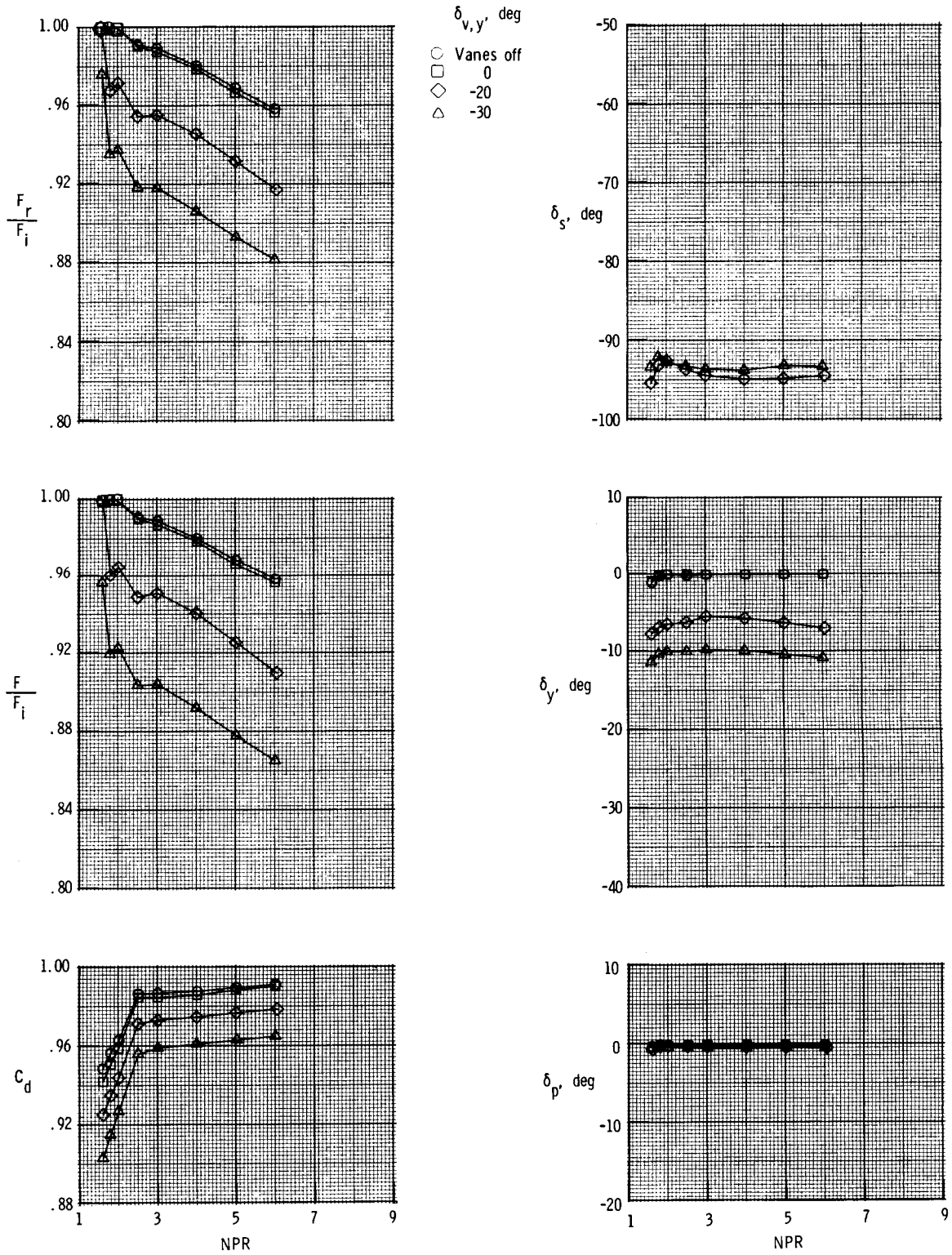
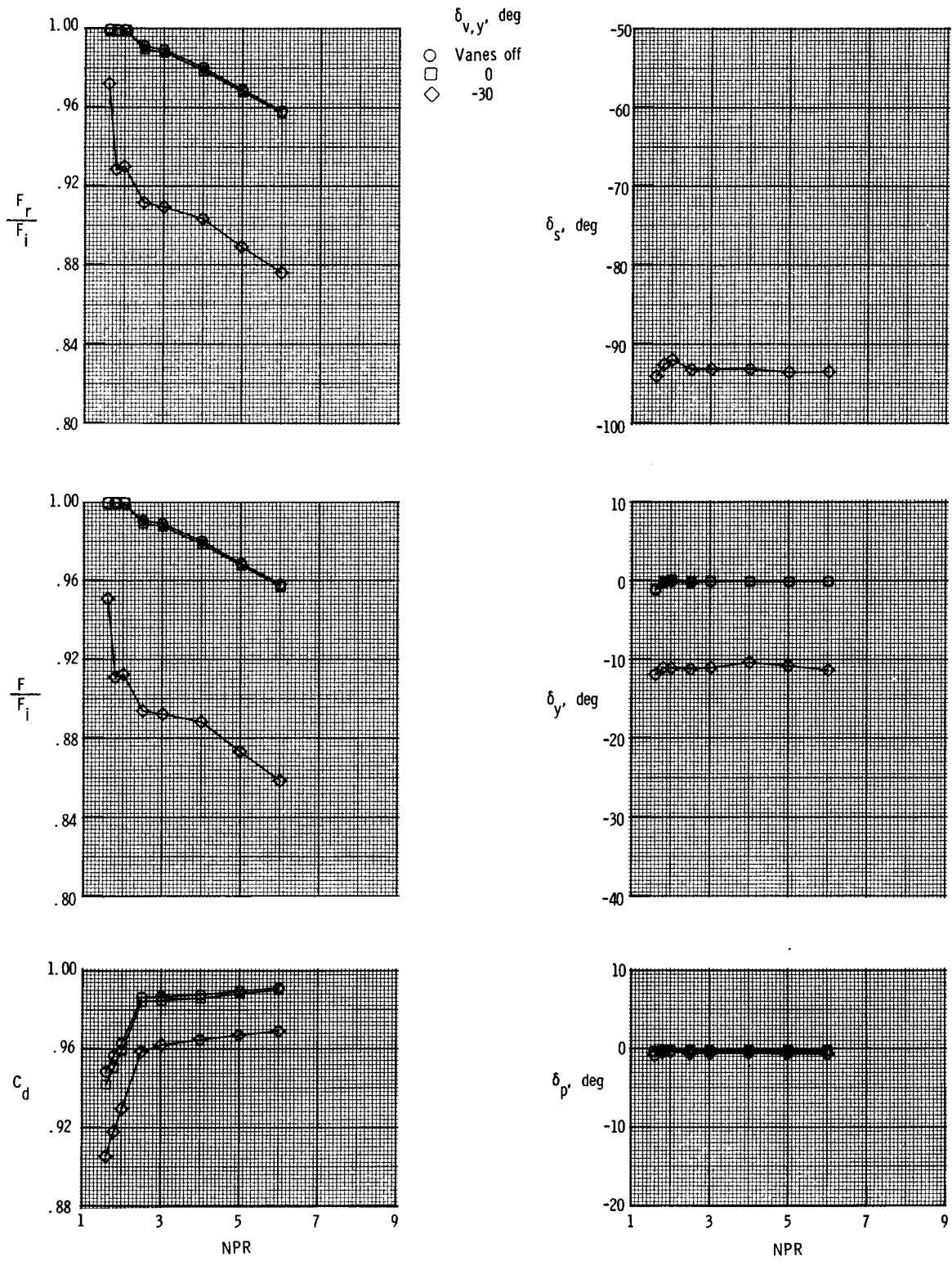


Figure 9. Effect of vane deflection on nozzle performance for 2-D C-D nozzle with AR = 1.5 and $\delta_{v,p} = -11.7^\circ$. Vane V1.



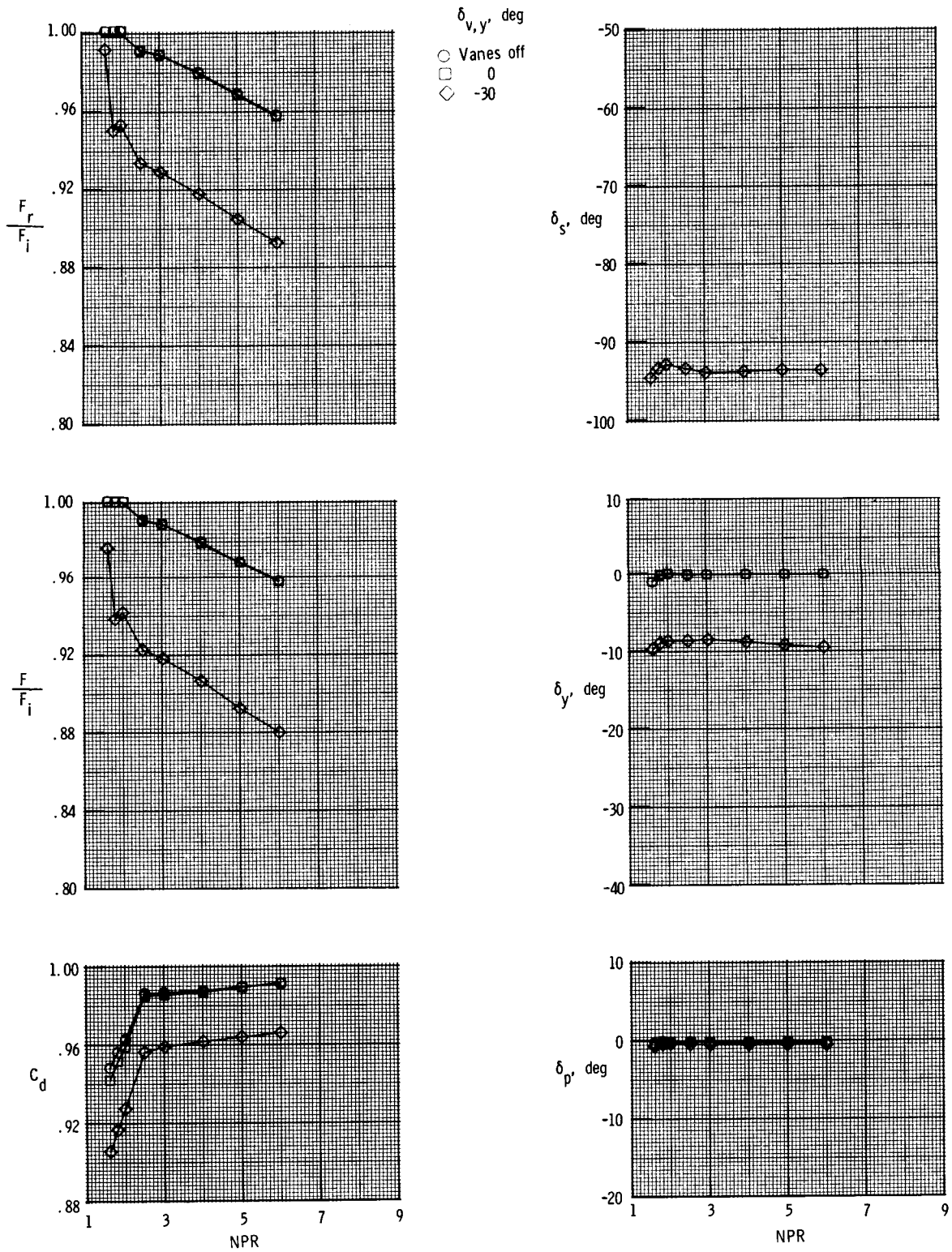
(a) Vane V1.

Figure 10. Effect of vane deflection on nozzle performance for 2-D convergent nozzle with AR = 2.5 and $\delta_{v,p} = 0^\circ$.



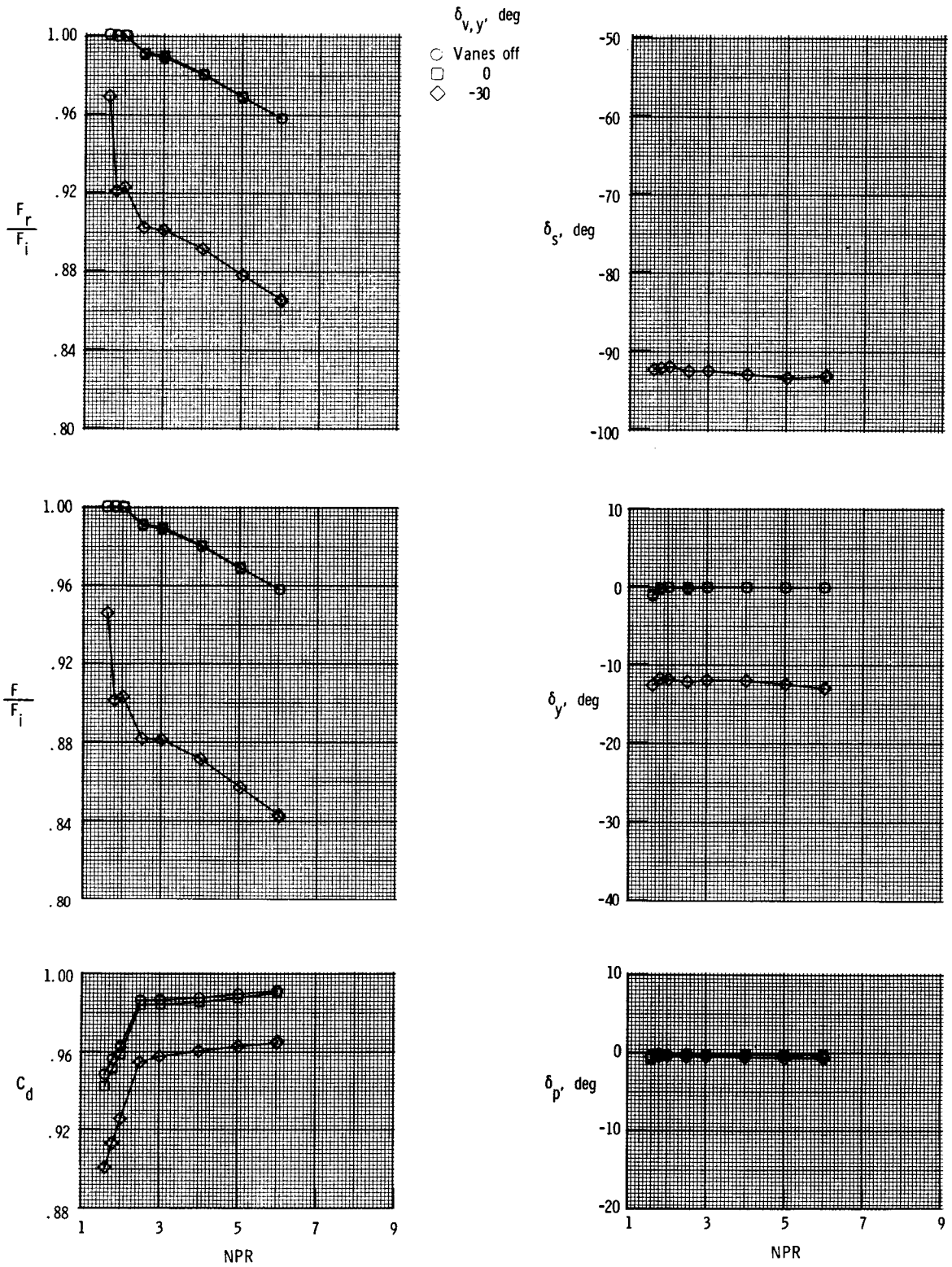
(b) Vane V2.

Figure 10. Continued.



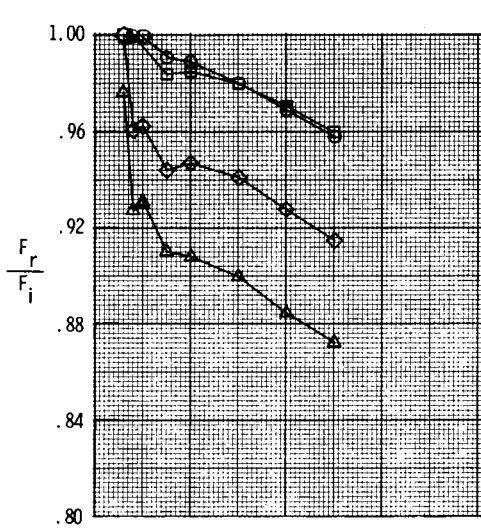
(c) Vane V3.

Figure 10. Continued.

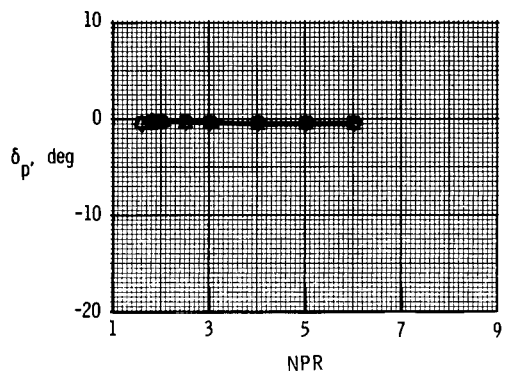
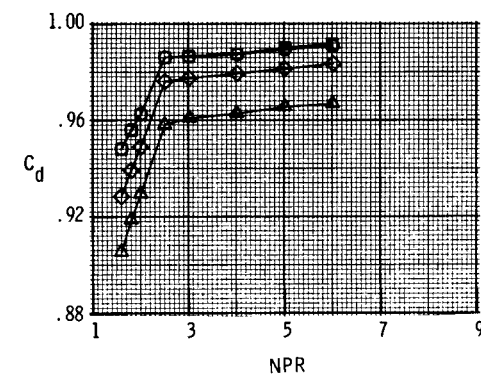
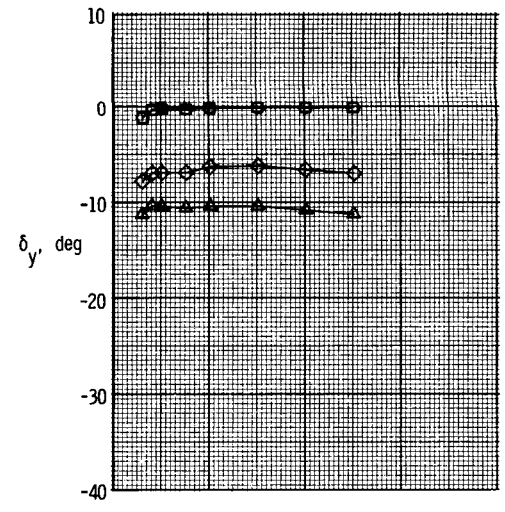
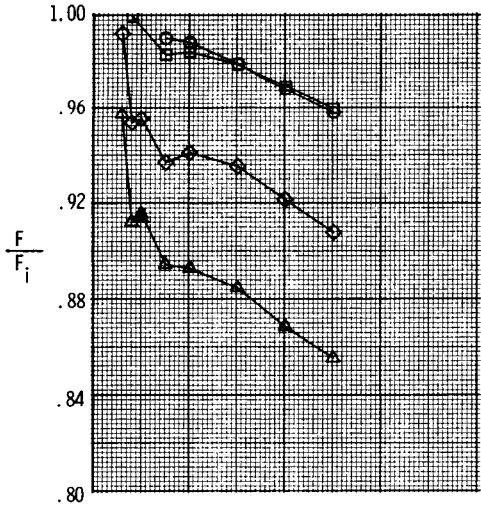
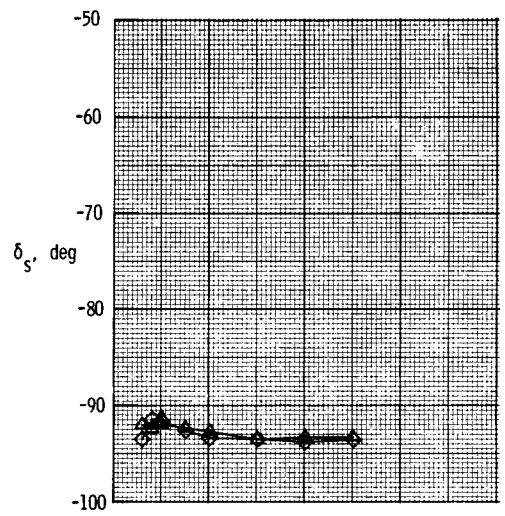


(d) Vane V4.

Figure 10. Continued.

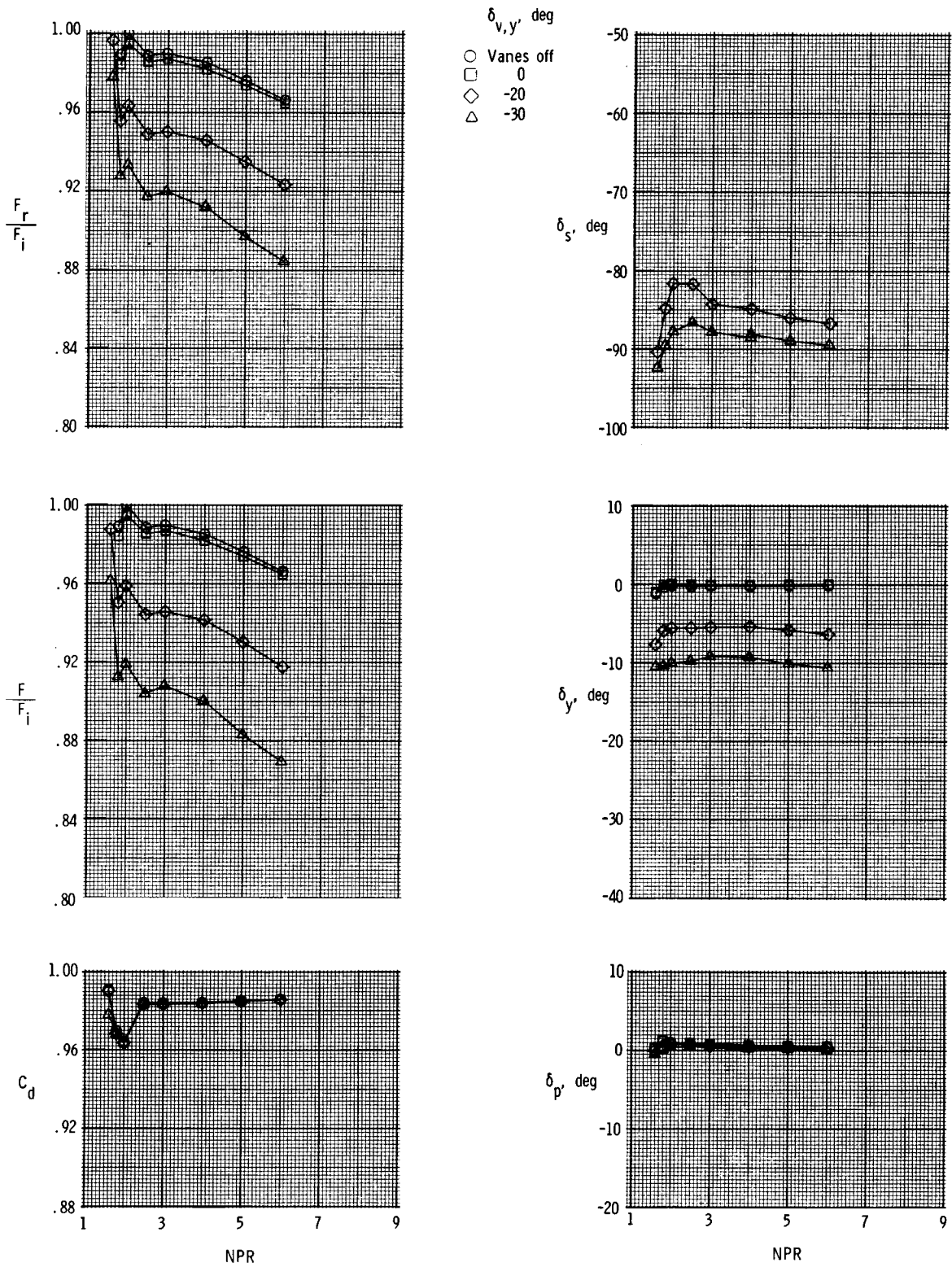


$\delta_{v,y'}$, deg
 ○ Vanes off
 □ 0
 ◇ -20
 △ -30



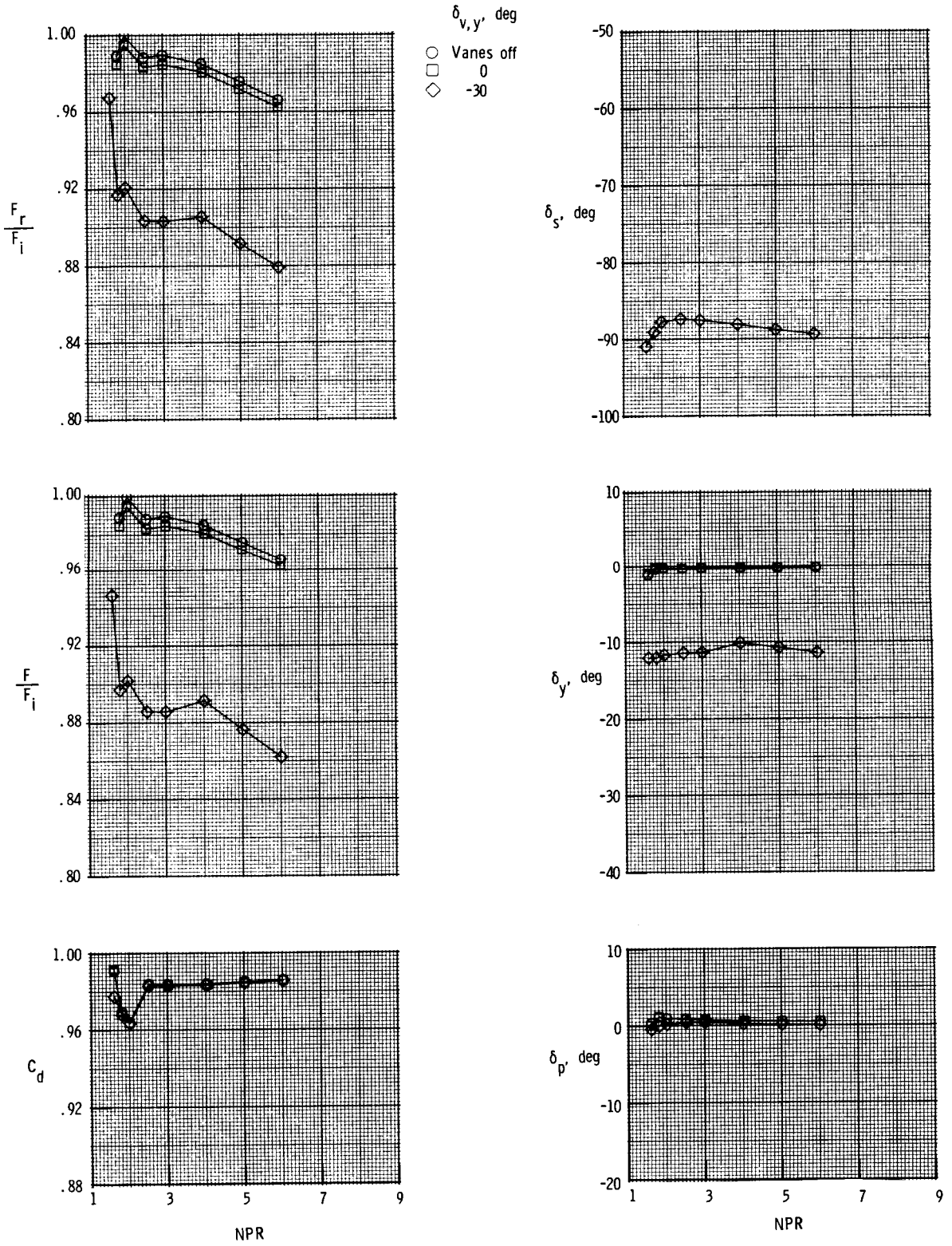
(e) Vane V5.

Figure 10. Concluded.



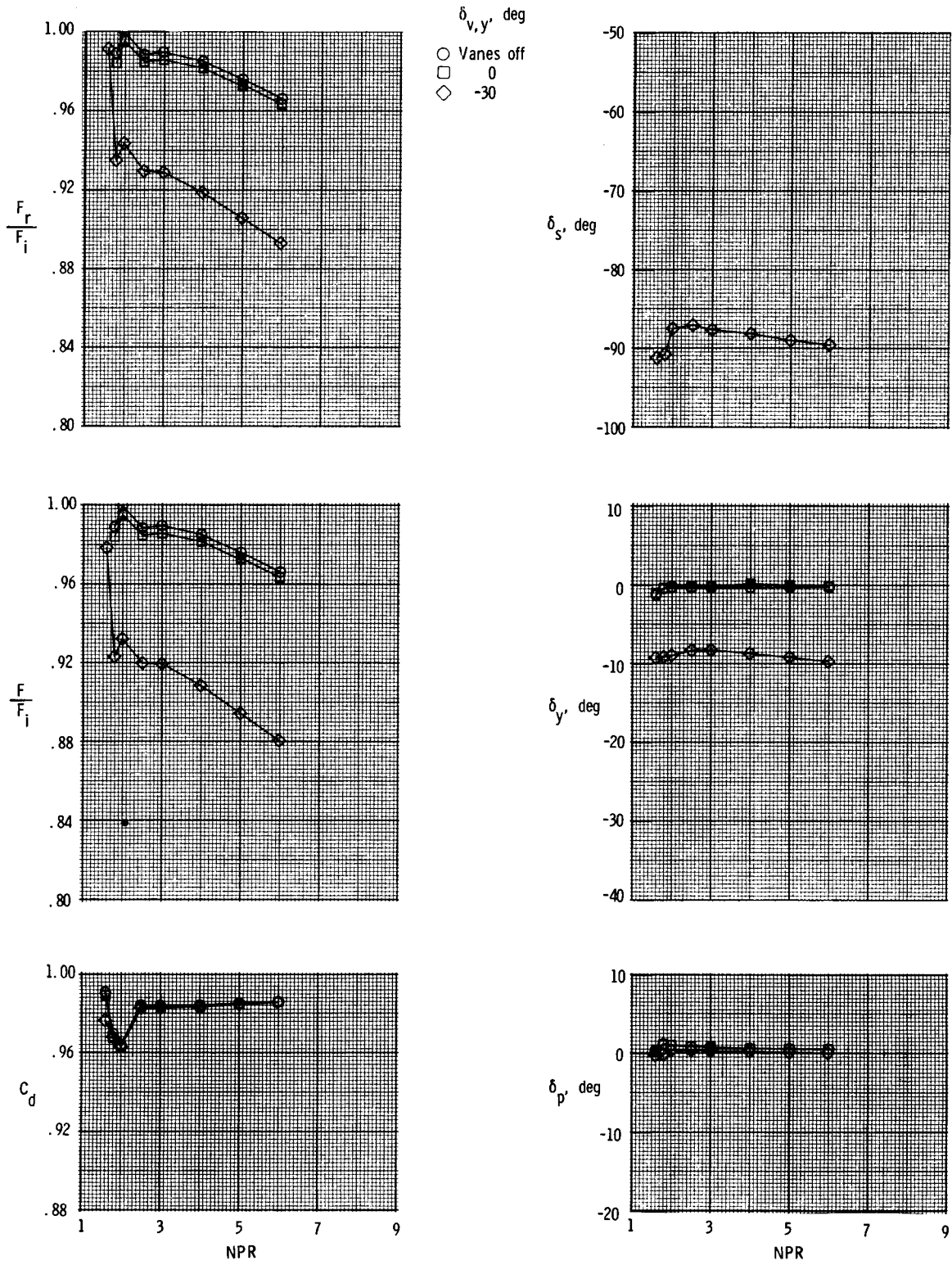
(a) Vane V1.

Figure 11. Effect of vane deflection on nozzle performance for 2-D C-D nozzle with AR = 2.5 and $\delta_{v,p} = 0^\circ$.



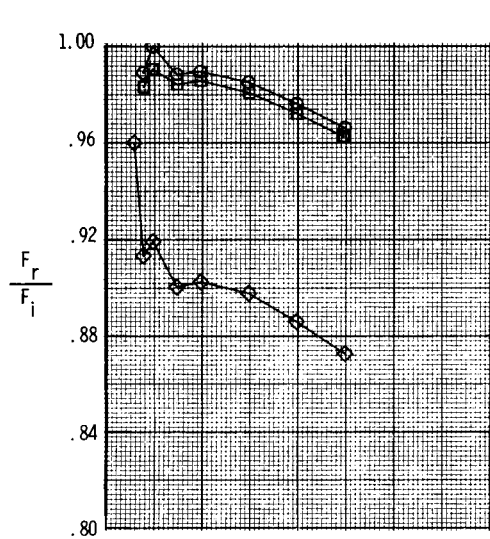
(b) Vane V2.

Figure 11. Continued.

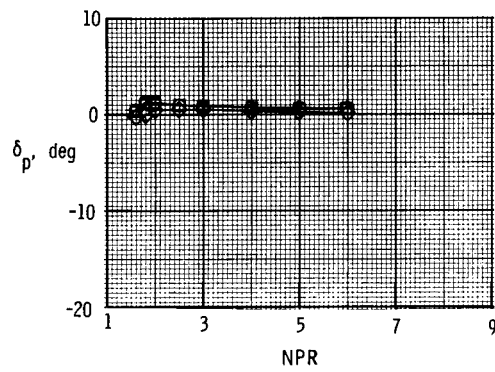
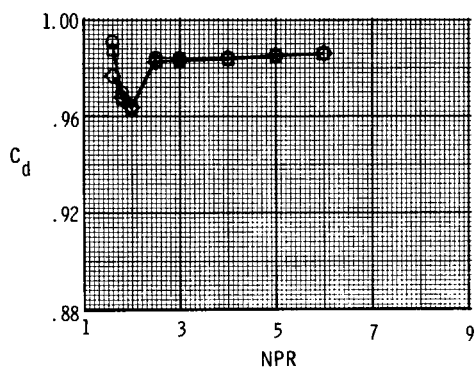
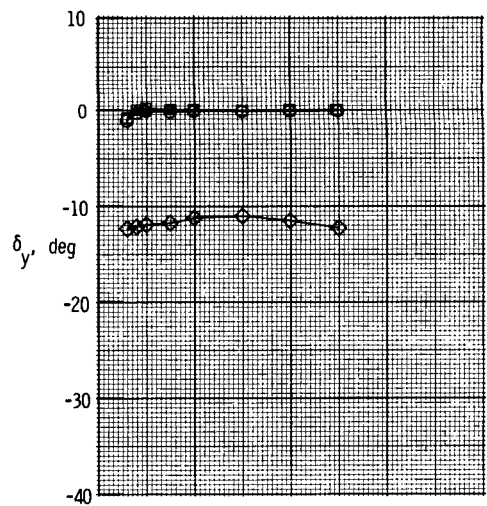
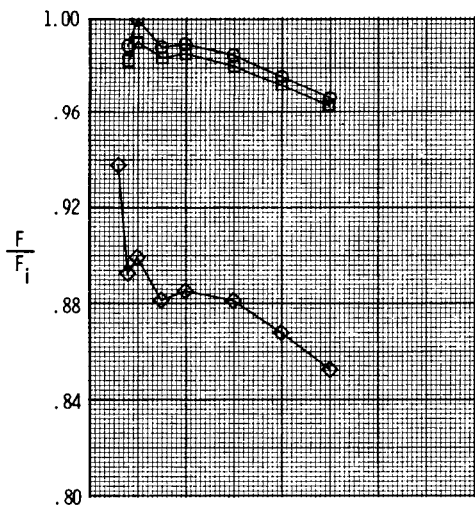
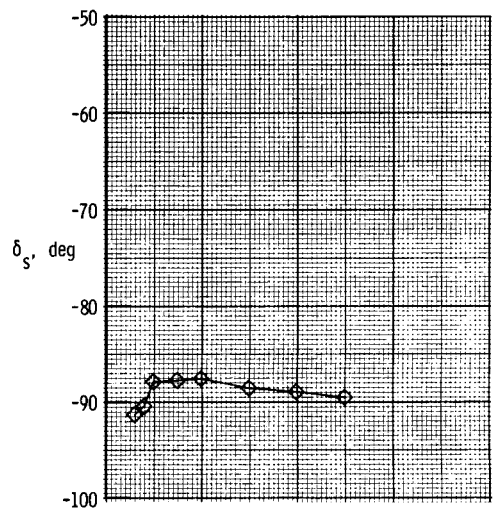


(c) Vane V3.

Figure 11. Continued.

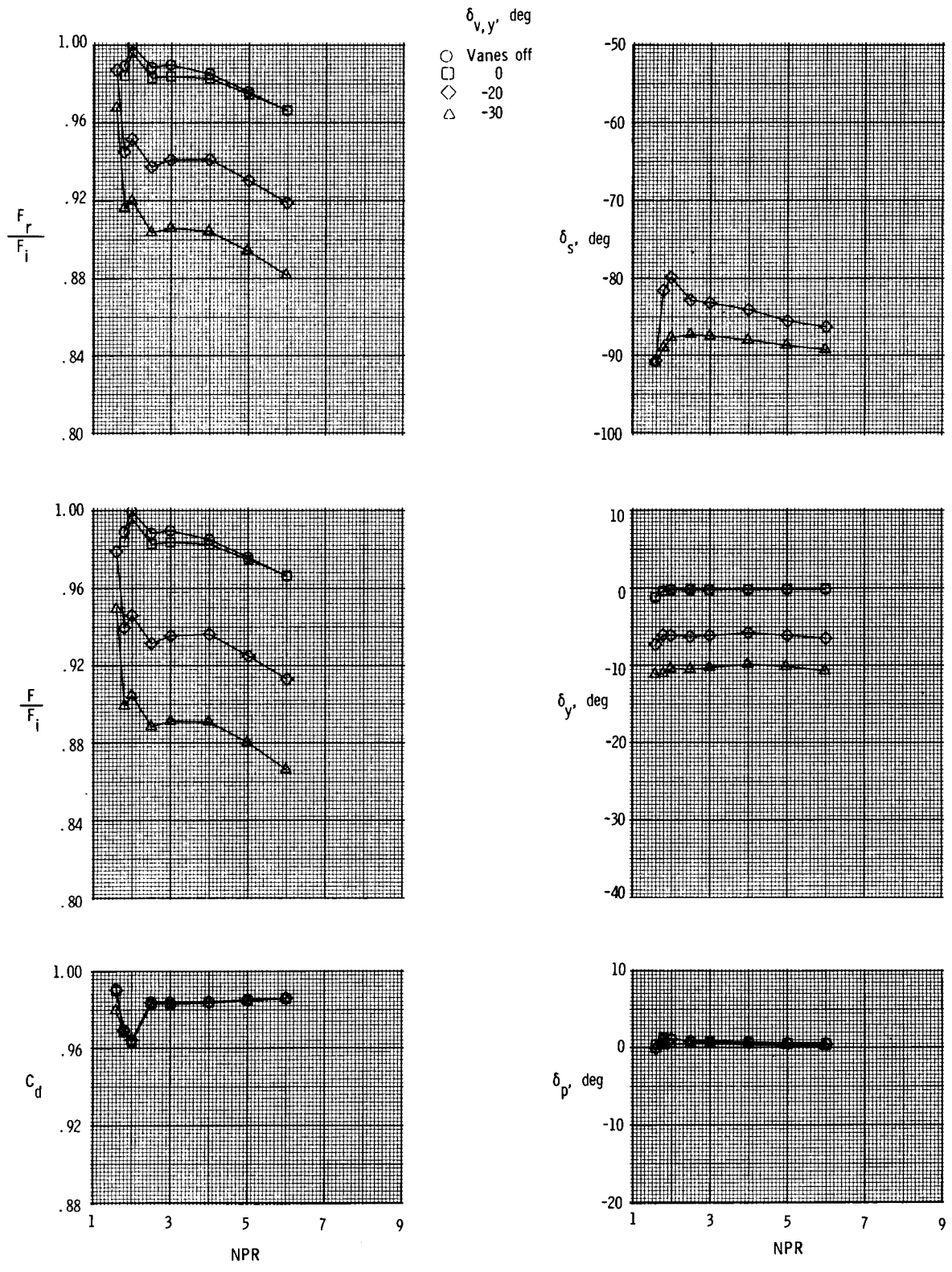


$\delta_{v,y}$, deg
 ○ Vanes off
 □ 0
 ◇ -30



(d) Vane V4.

Figure 11. Continued.



(e) Vane V5.

Figure 11. Concluded.

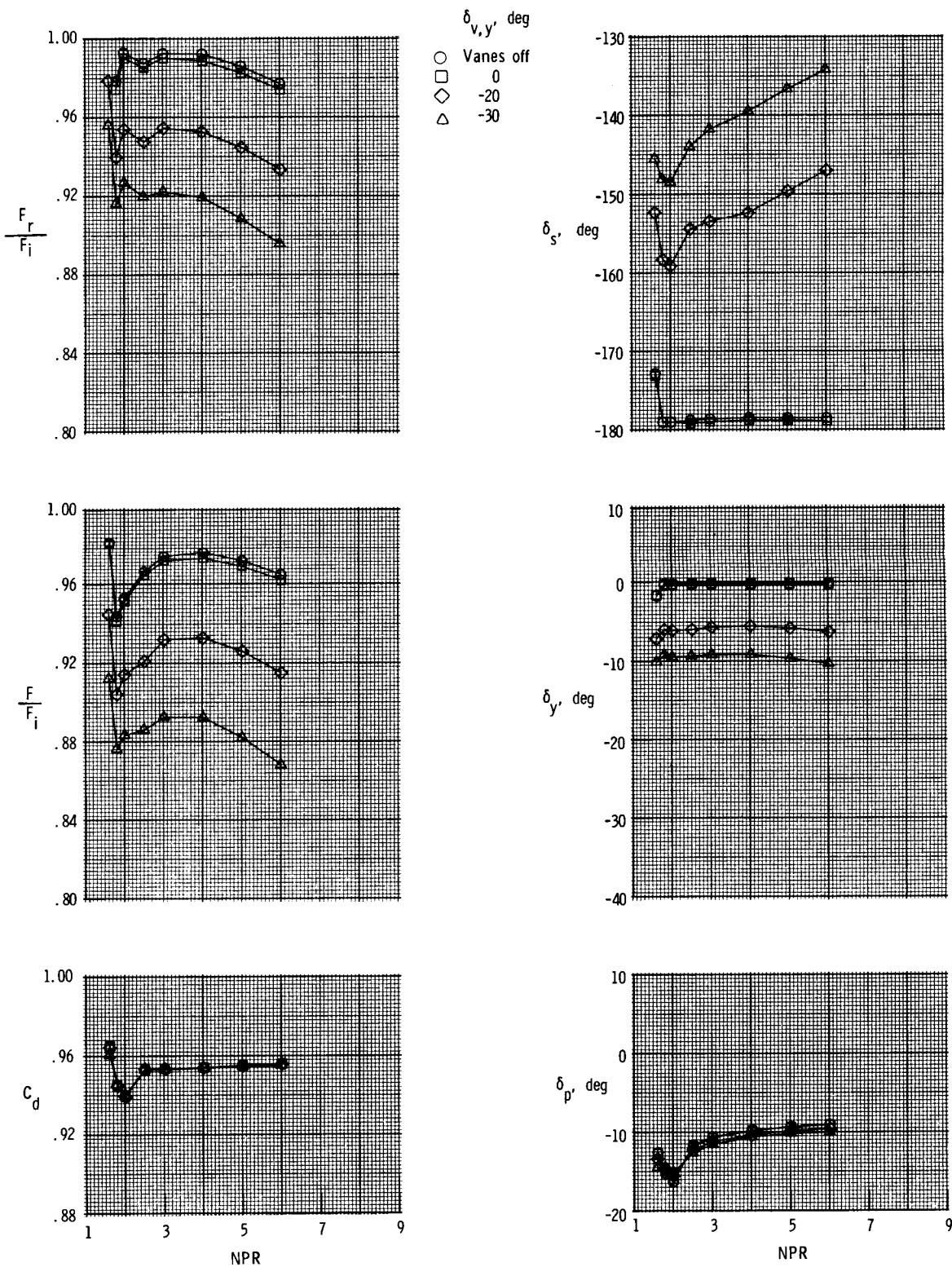
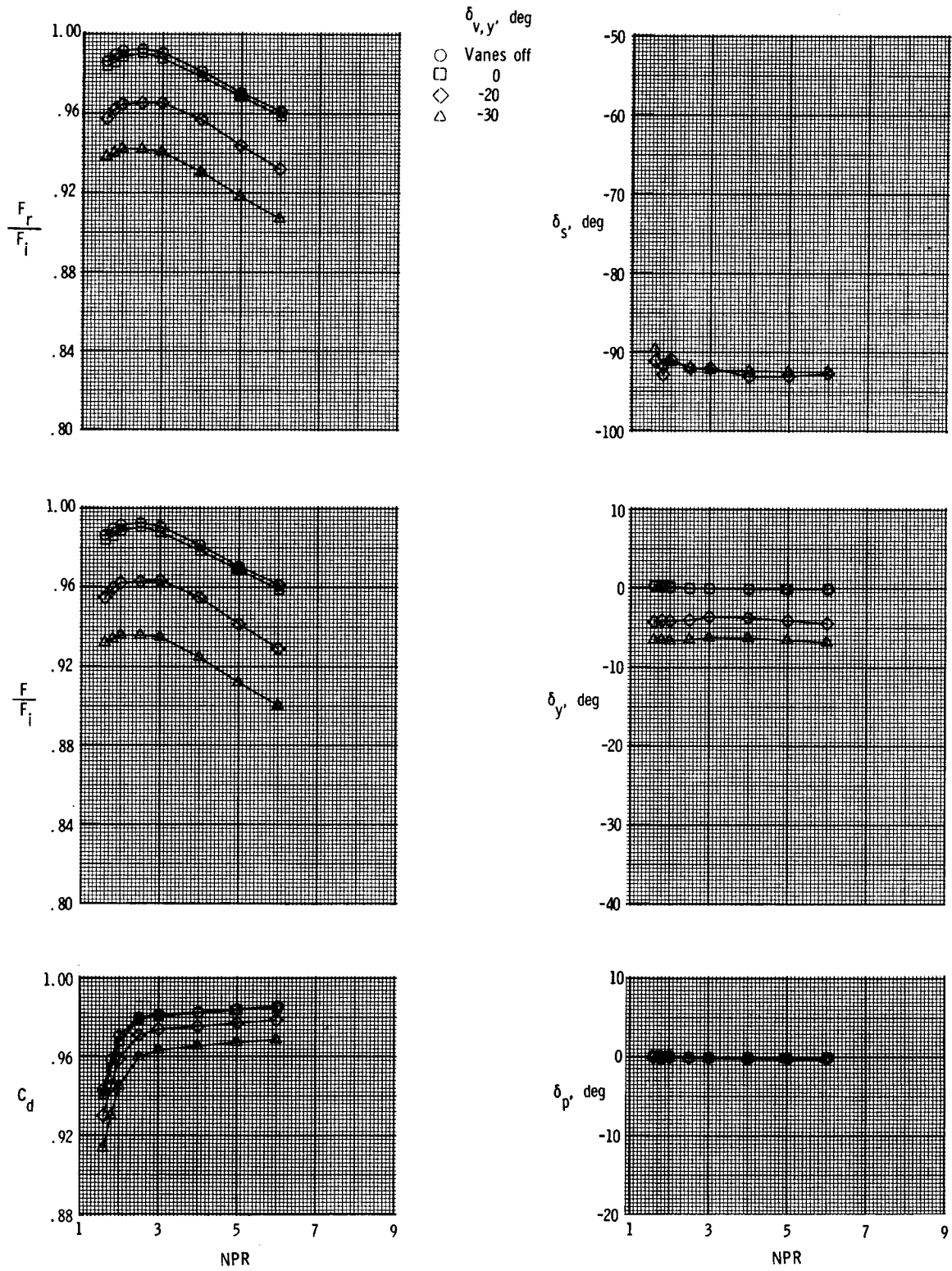
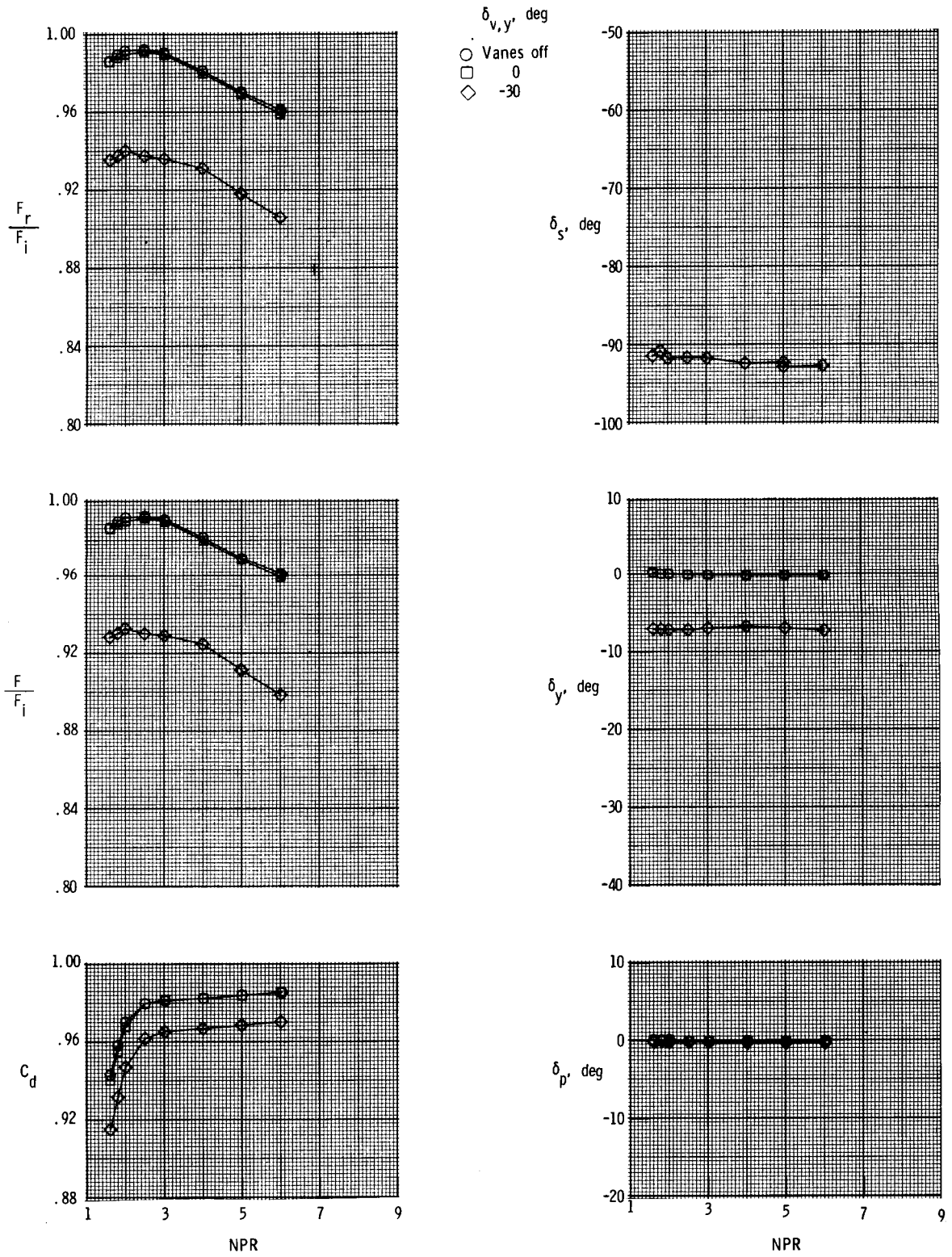


Figure 12. Effect of vane deflection on nozzle performance for pitch-vectored 2-D C-D nozzle with AR = 2.5 and $\delta_{v,p} = -11.7^\circ$. Vane V1.



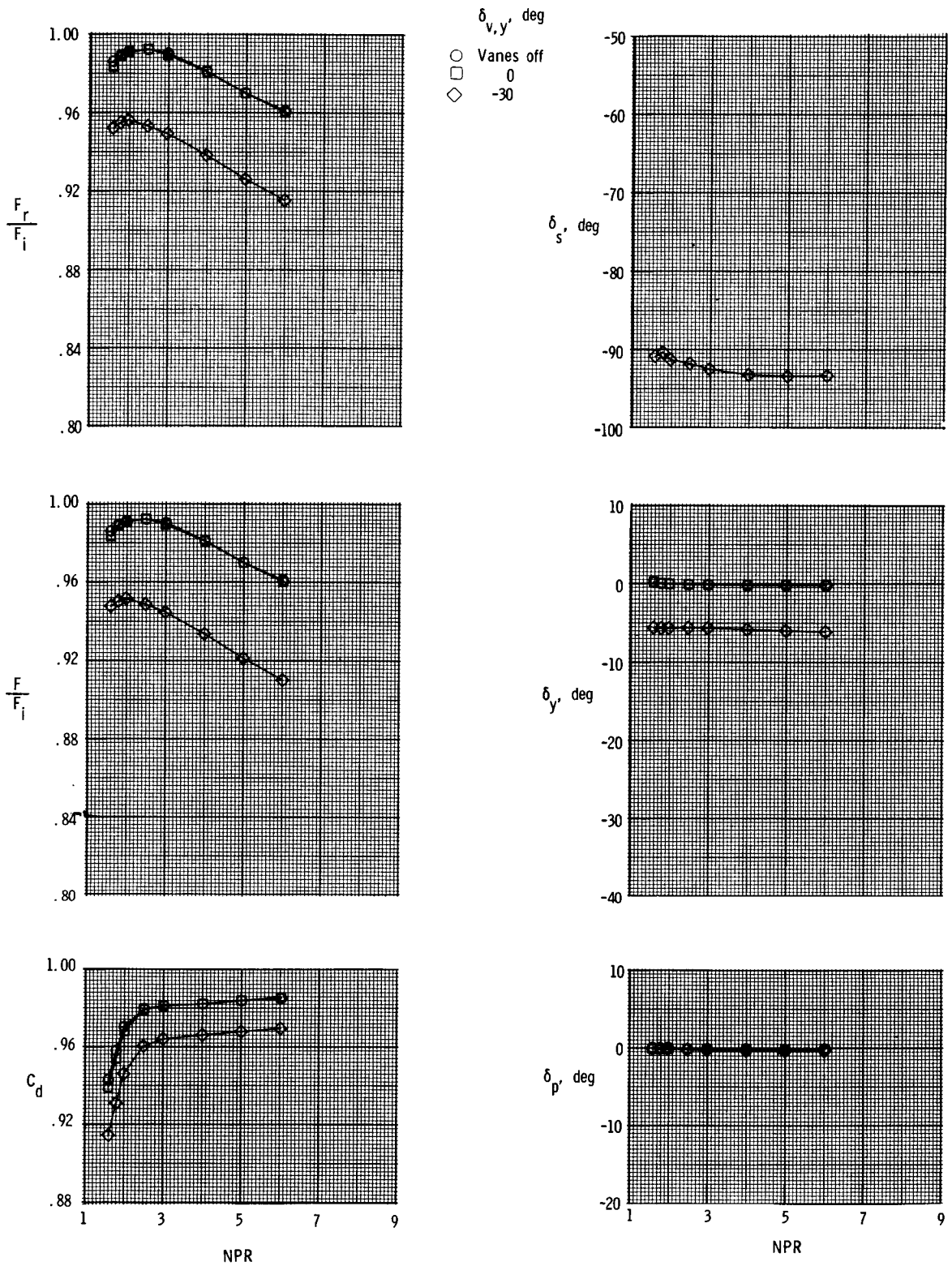
(a) Vane V1.

Figure 13. Effect of vane deflection on nozzle performance for 2-D convergent nozzle with $AR = 4.0$ and $\delta_{v,p} = 0^\circ$.



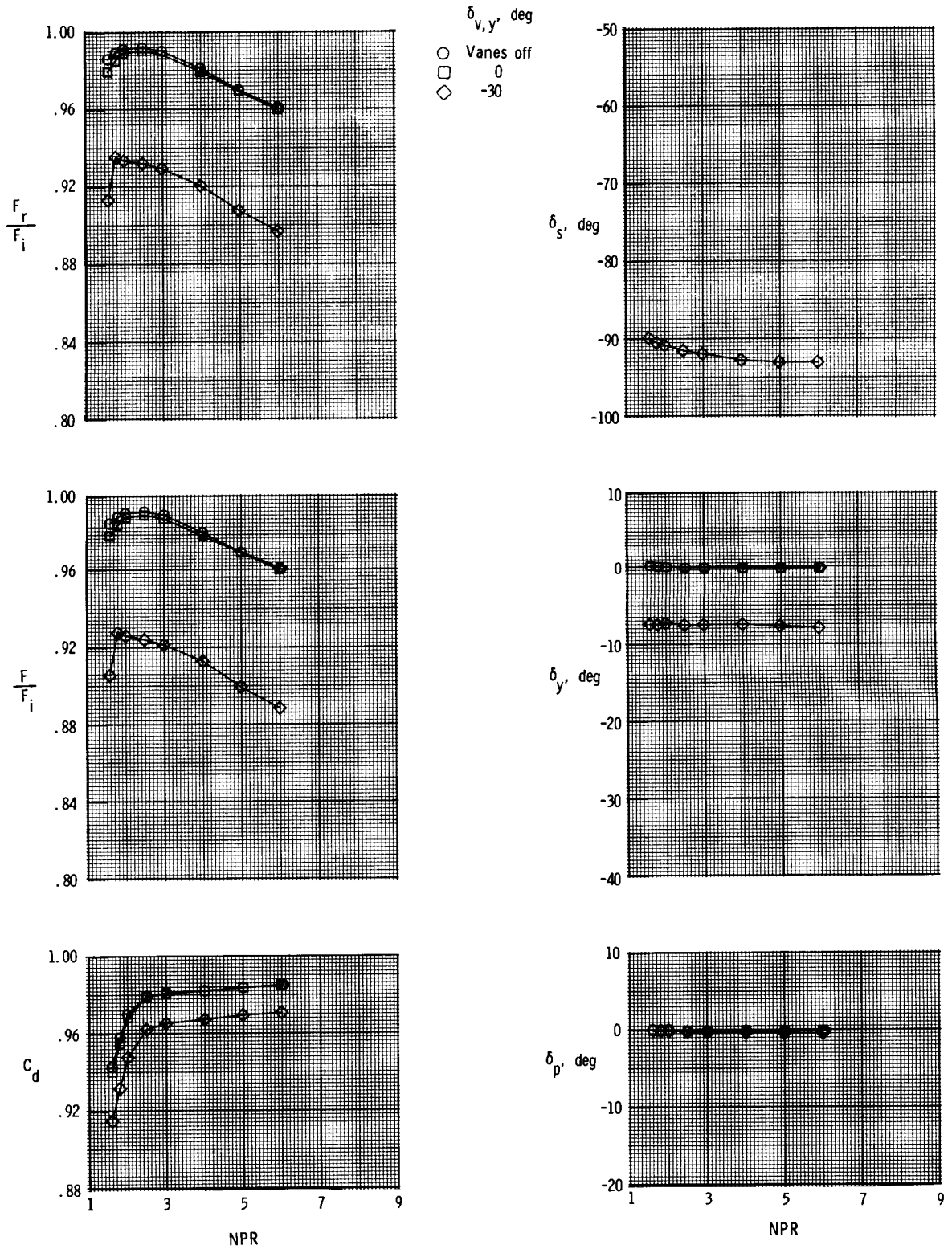
(b) Vane V2.

Figure 13. Continued.



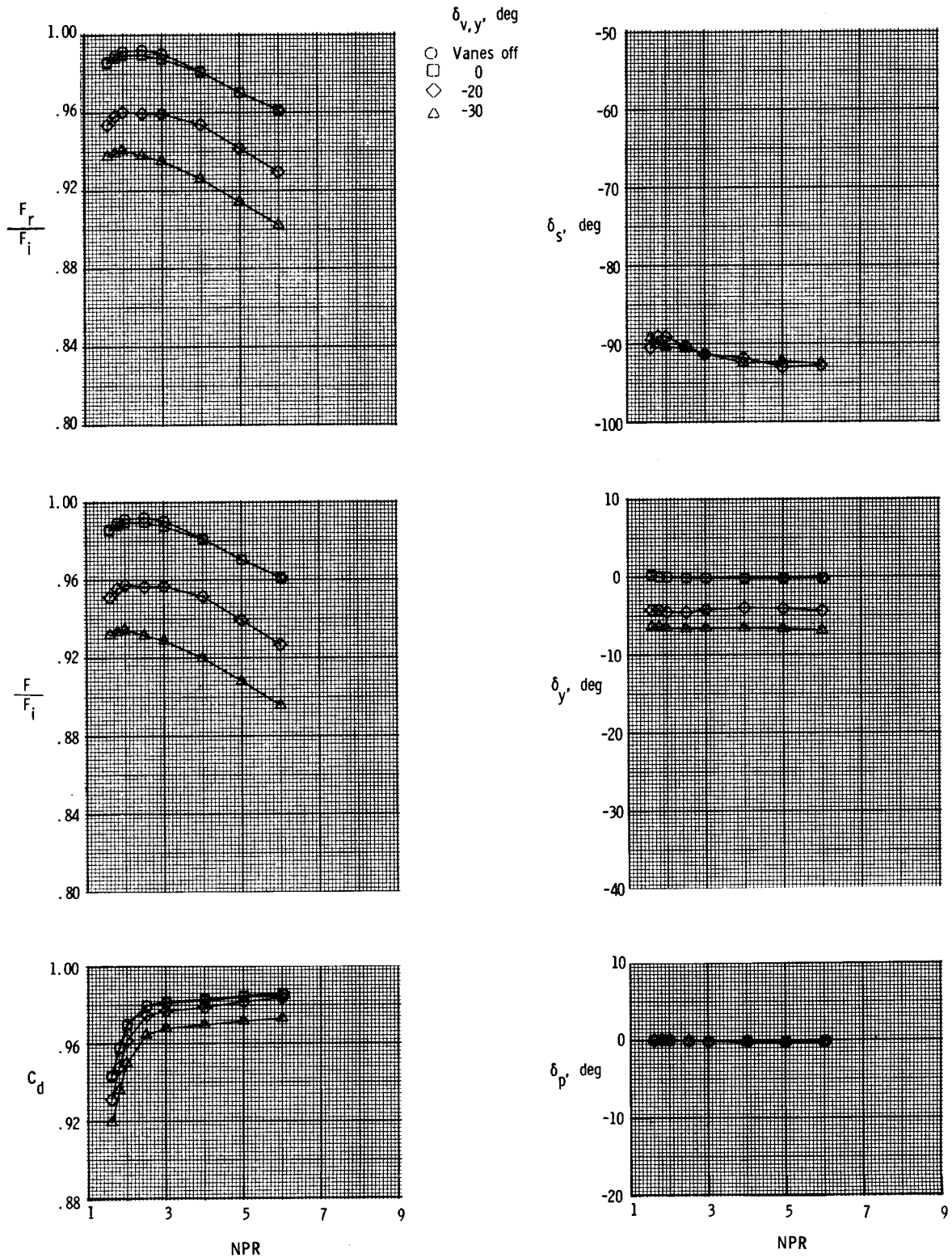
(c) Vane V3.

Figure 13. Continued.



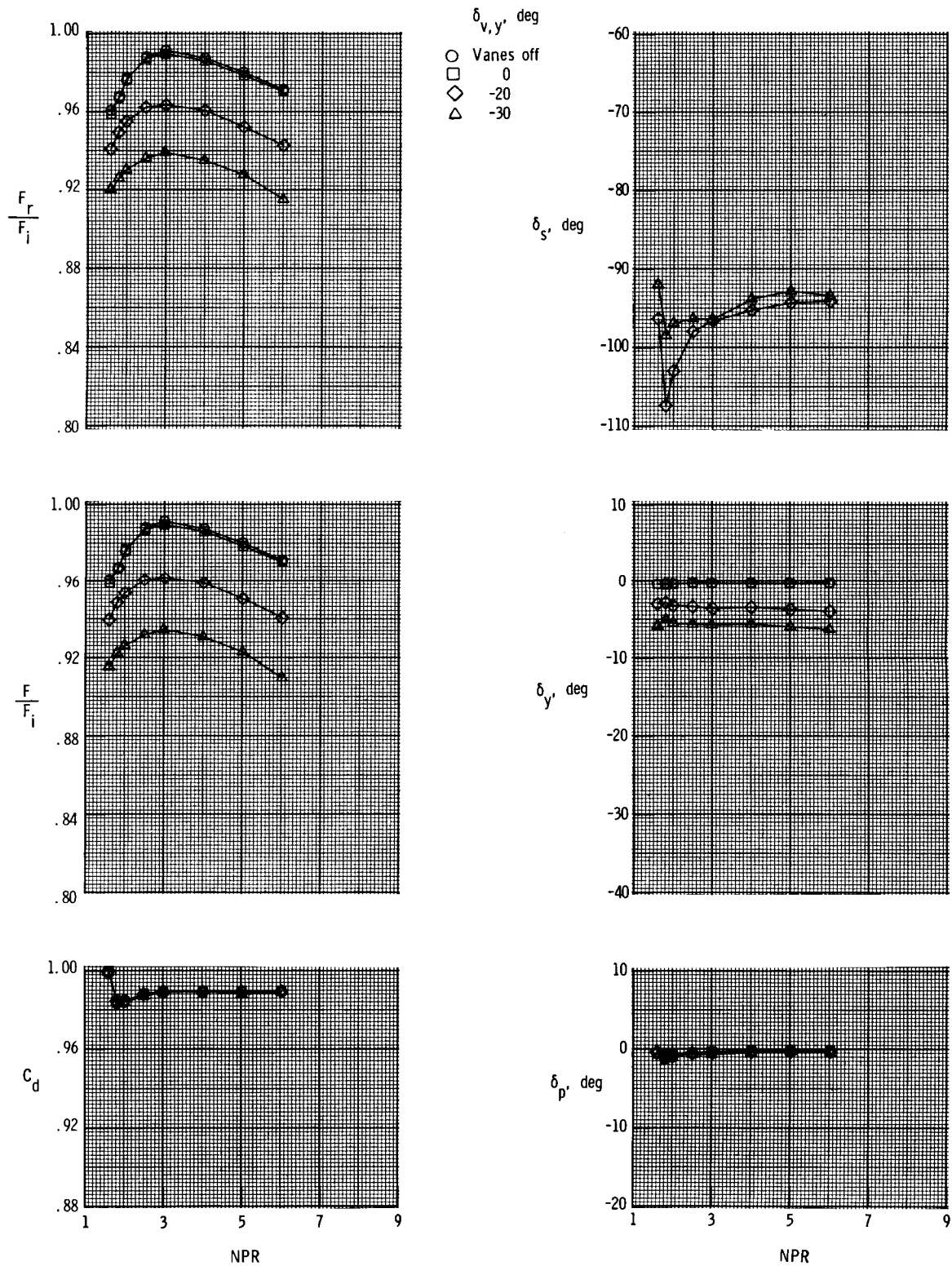
(d) Vane V4.

Figure 13. Continued.



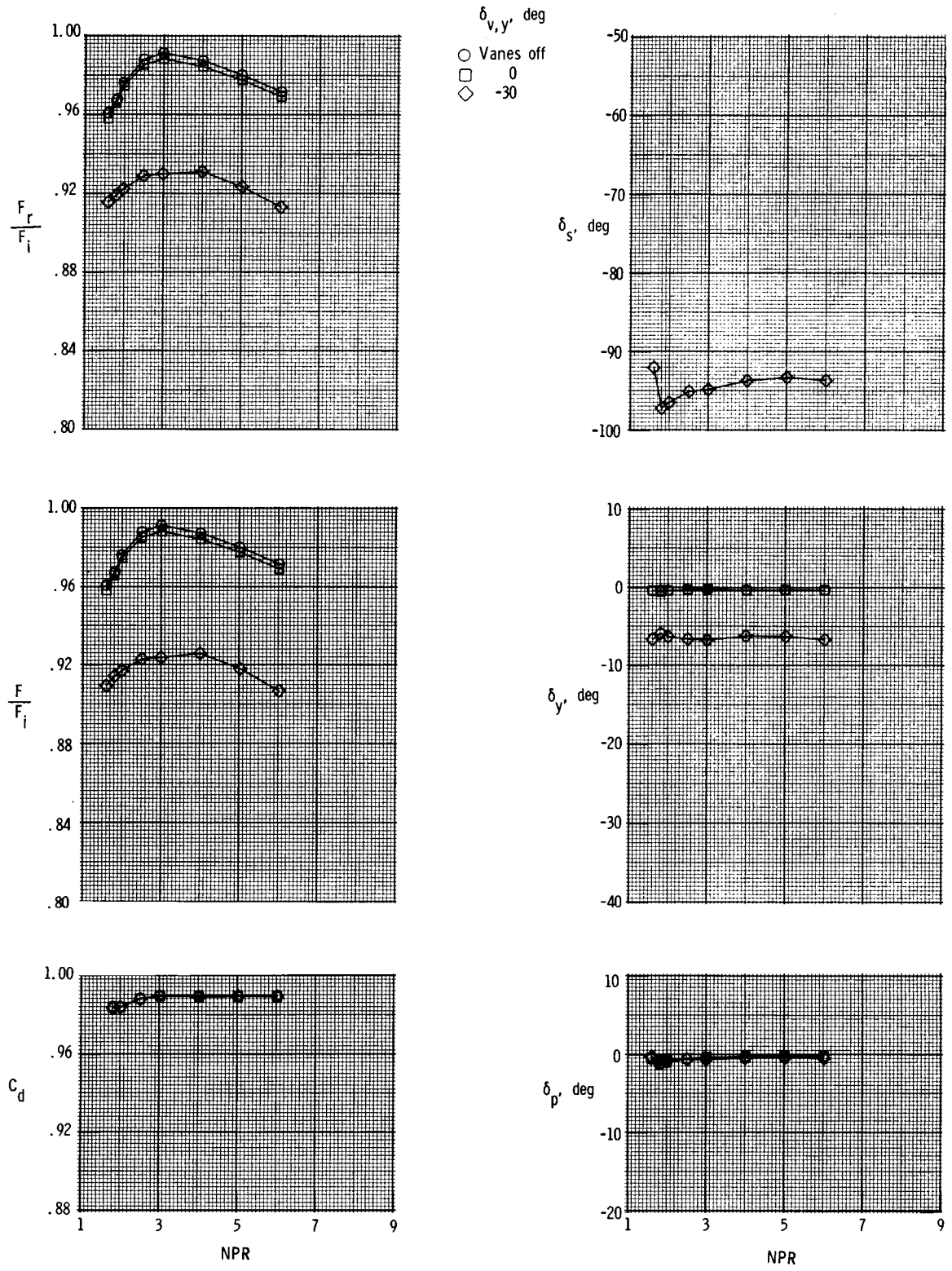
(e) Vane V5.

Figure 13. Concluded.



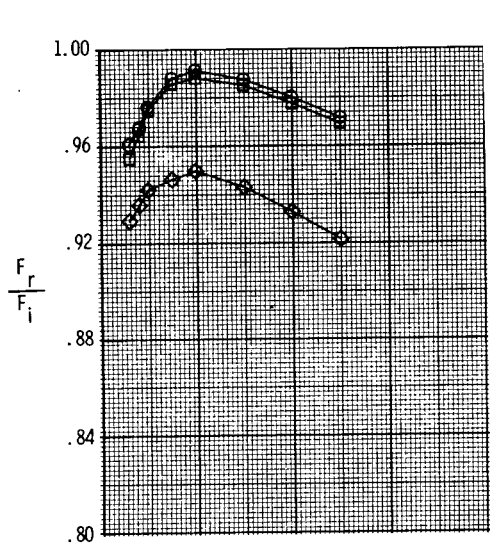
(a) Vane V1.

Figure 14. Effect of vane deflection on nozzle performance for 2-D C-D nozzle with $AR = 4.0$ and $\delta_{v,p} = 0^\circ$.

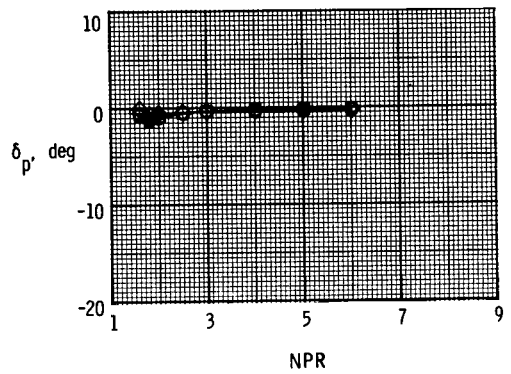
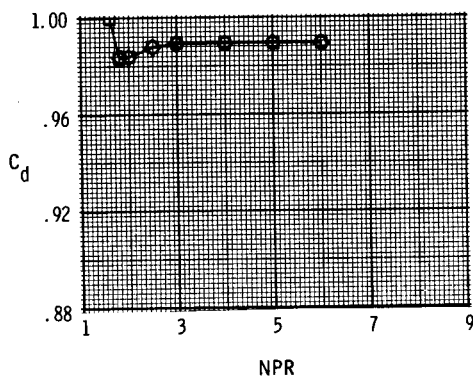
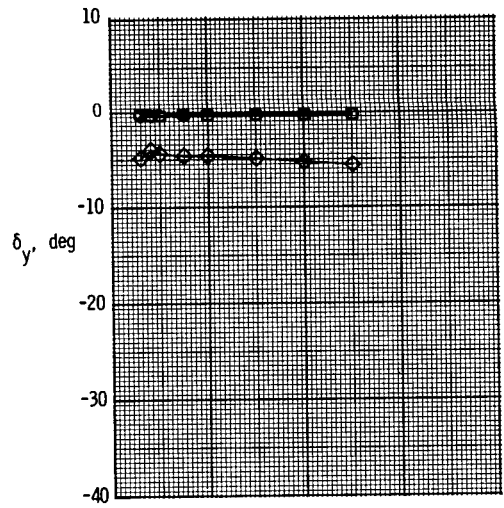
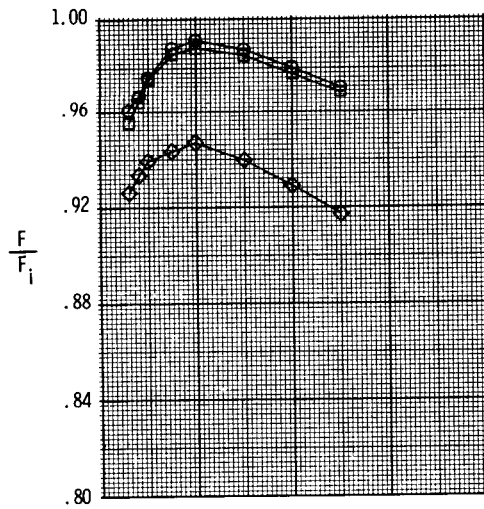
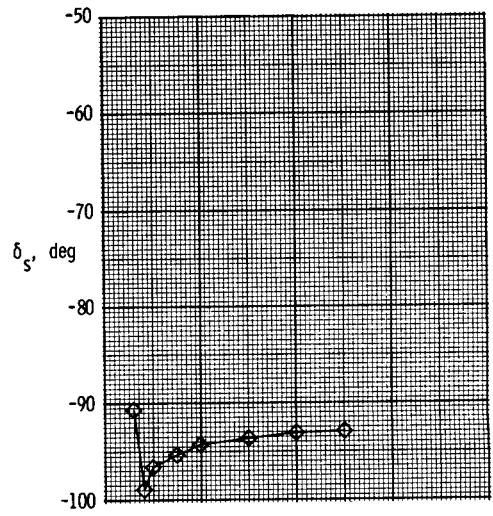


(b) Vane V2.

Figure 14. Continued.

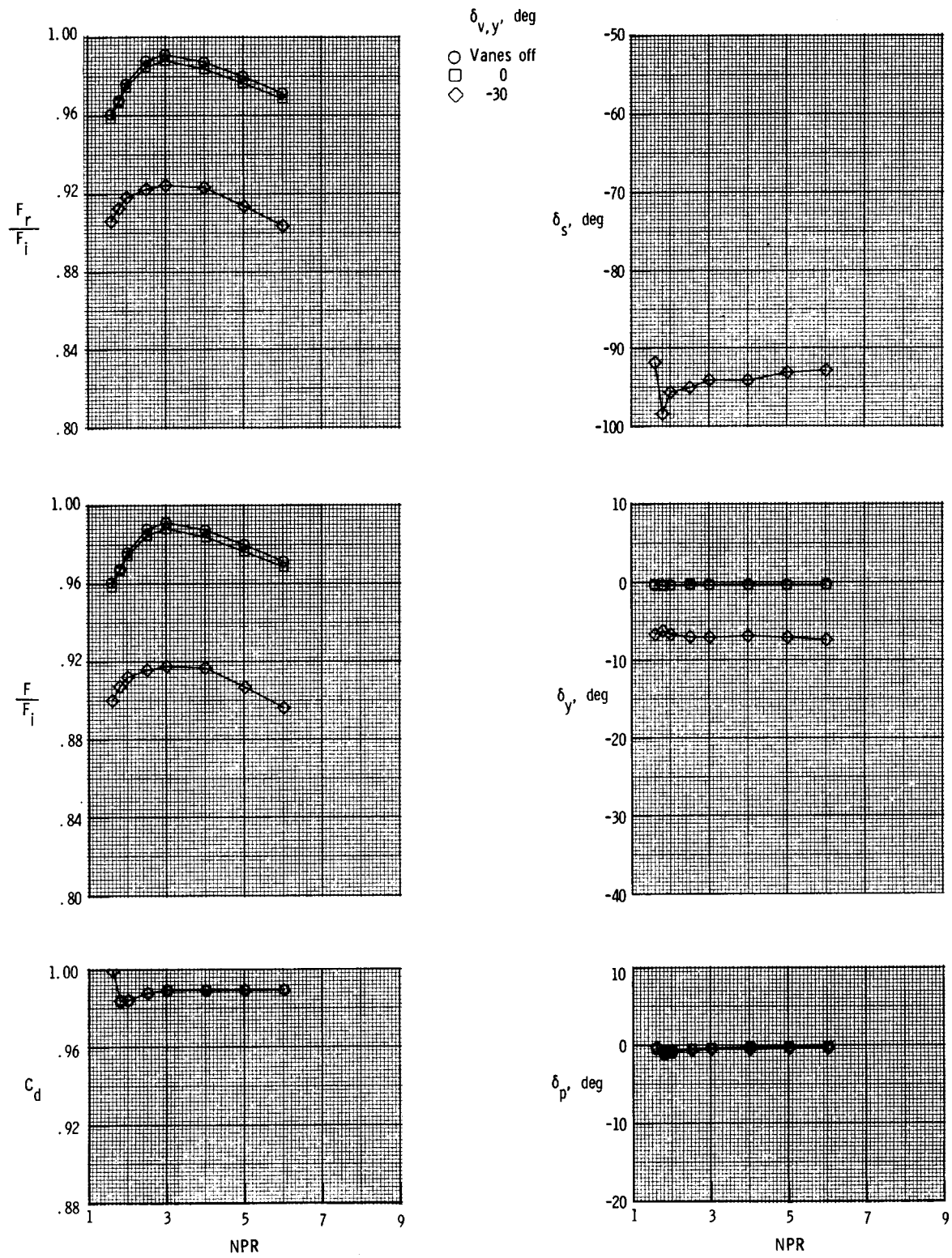


$\delta_{v,y}$, deg
 ○ Vanes off
 □ 0
 ◇ -30



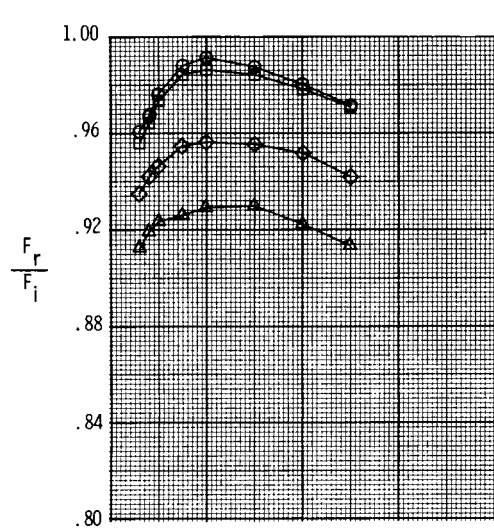
(c) Vane V3.

Figure 14. Continued.

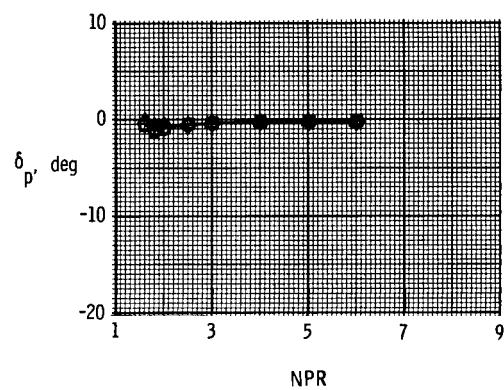
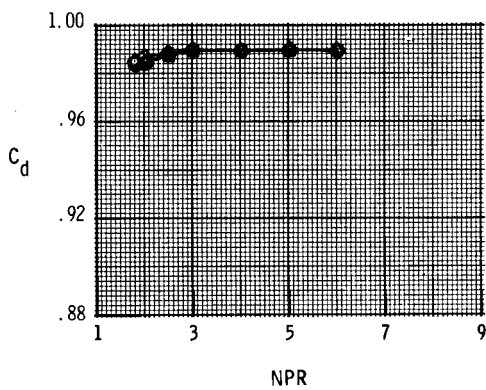
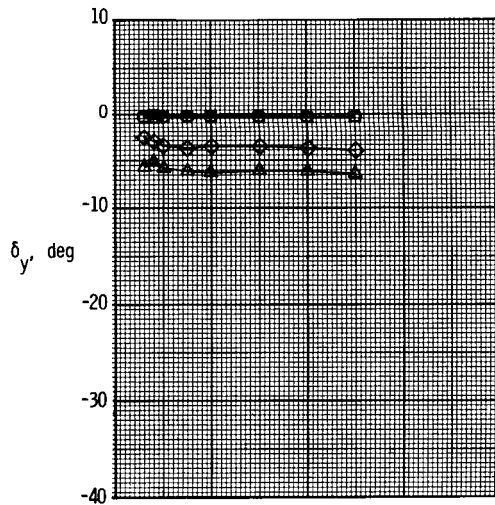
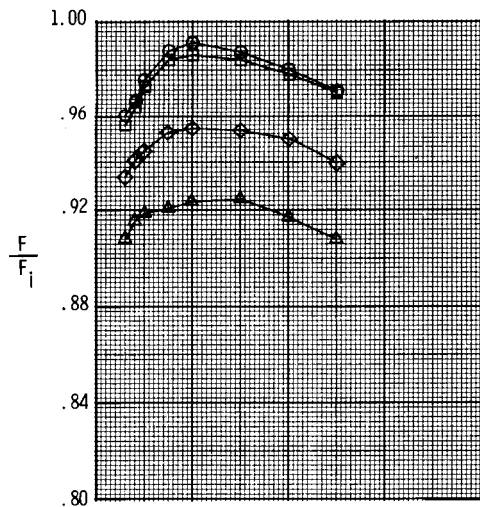
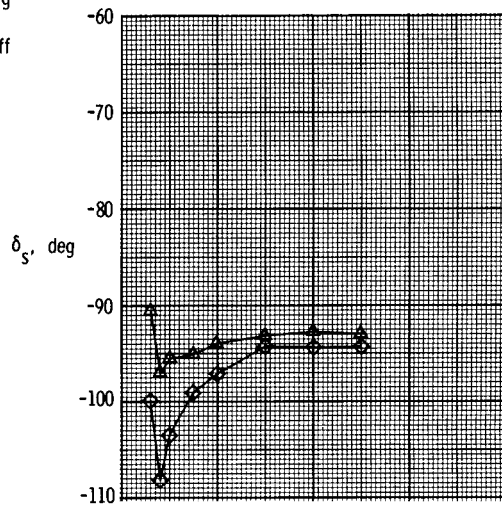


(d) Vane V4.

Figure 14. Continued.



$\delta_{v,y'}$ deg
 ○ Vanes off
 □ 0
 ◇ -20
 △ -30



(e) Vane V5.

Figure 14. Concluded.

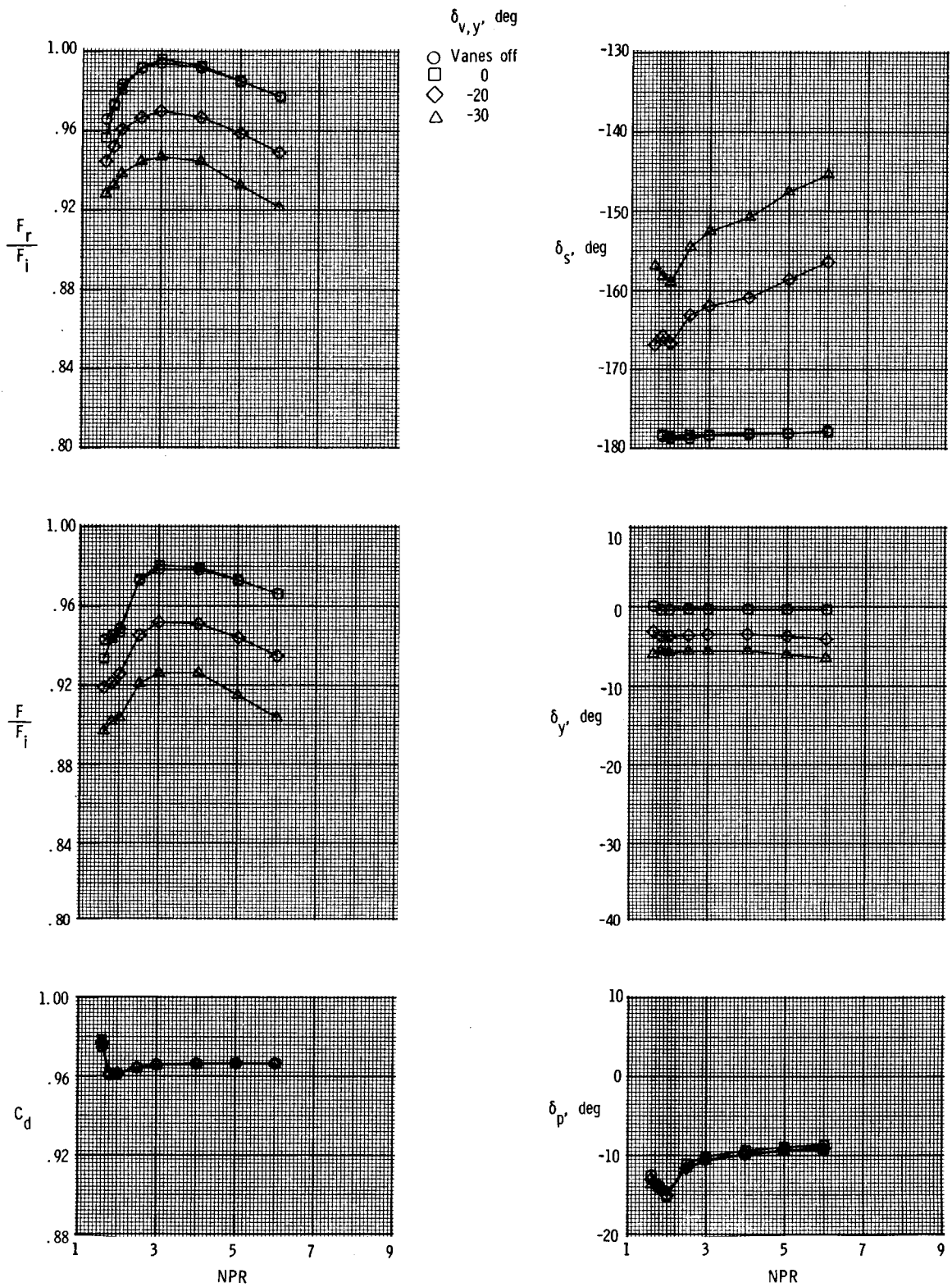
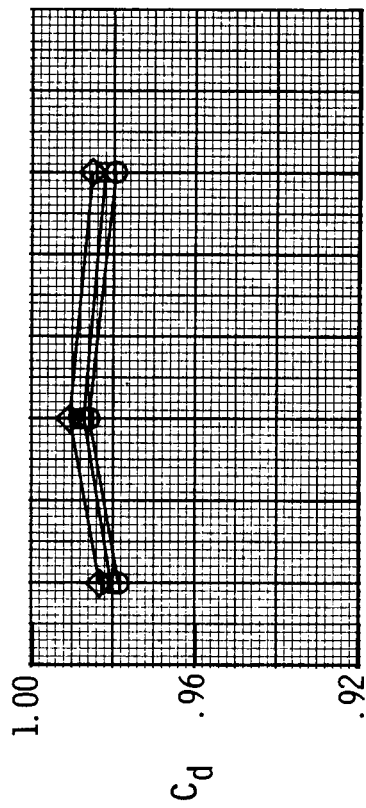
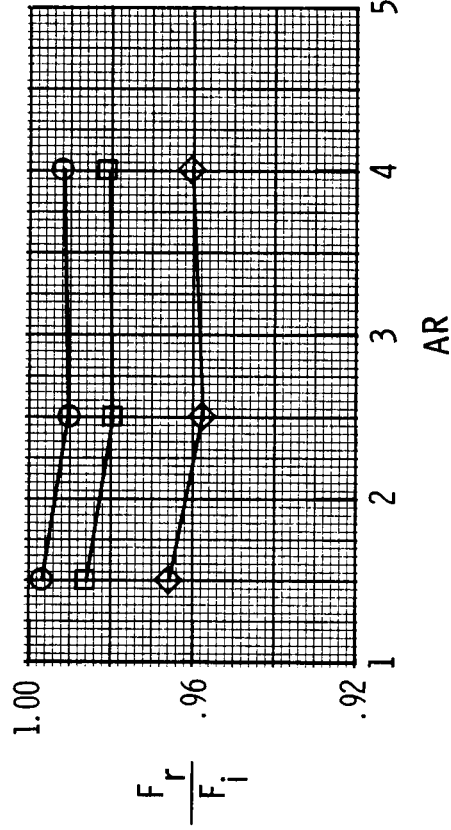
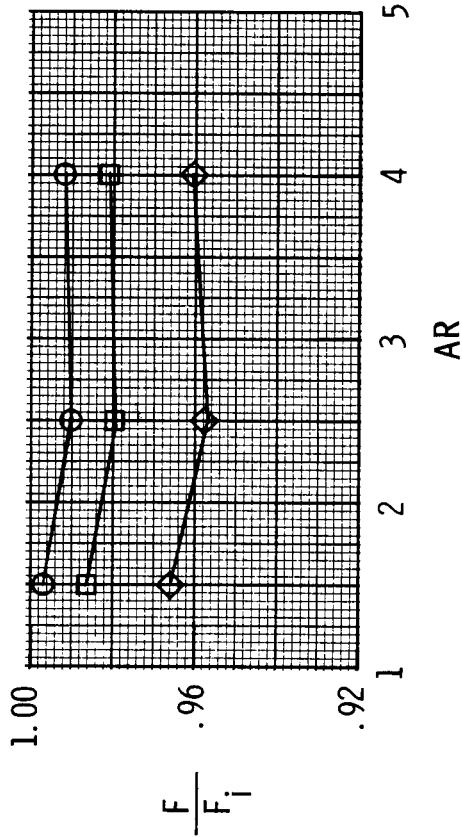


Figure 15. Effect of vane deflection on nozzle performance for pitched-vectored 2-D C-D nozzle with AR = 4.0 and $\delta_{v,p} = -11.7^\circ$. Vane V1.

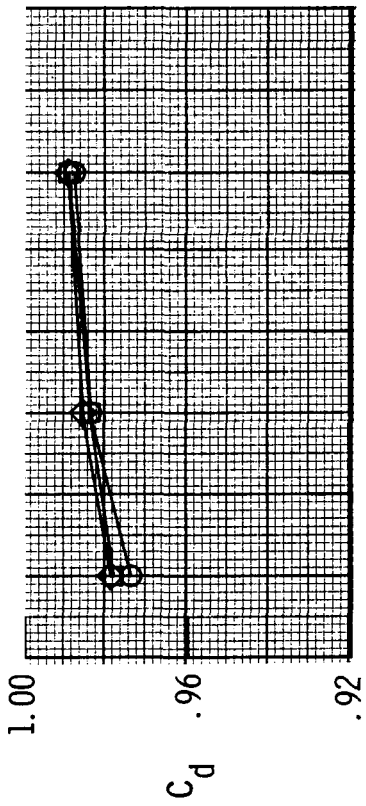


NPR
 ○ 2.5
 □ 4.0
 ◇ 6.0

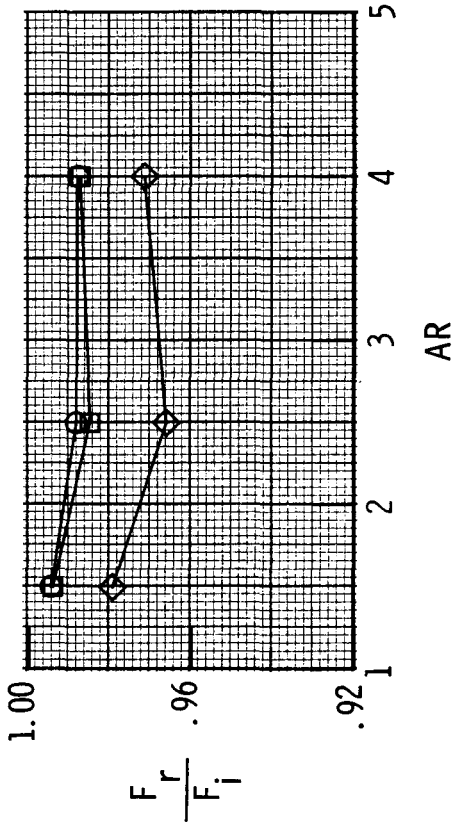
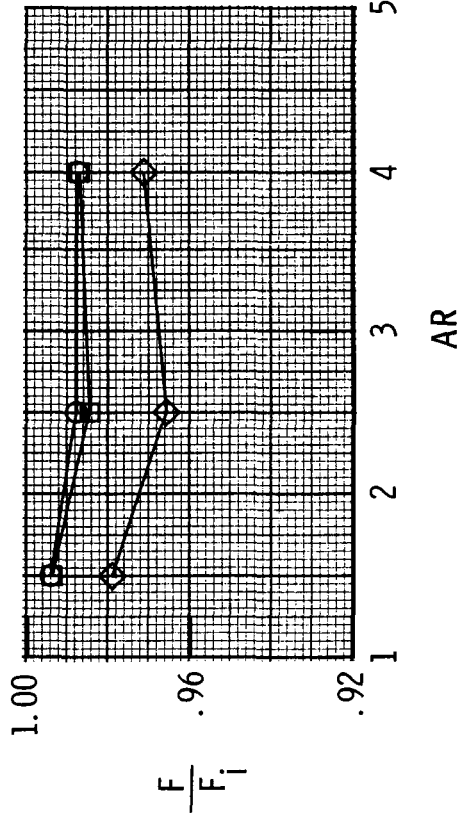


(a) 2-D convergent nozzle; $\delta_{v,p} = 0^\circ$

Figure 16. Effect of exit aspect ratio on nozzle performance for 2-D nozzles without post-exit vanes.



NPR
 ○ 2.5
 □ 4.0
 ◇ 6.0

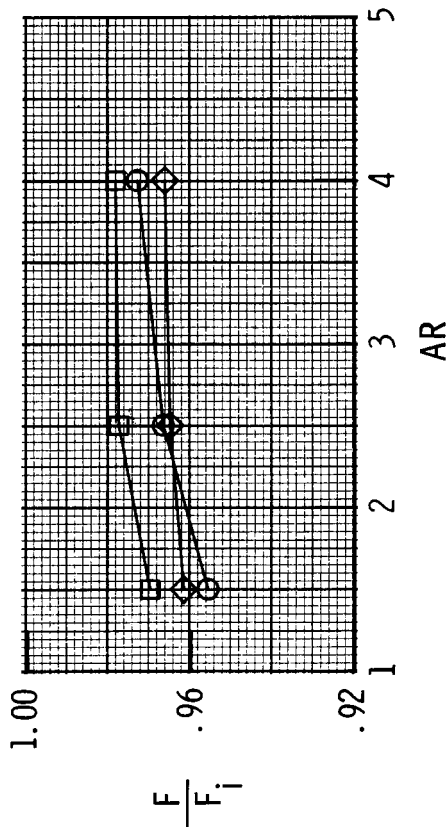
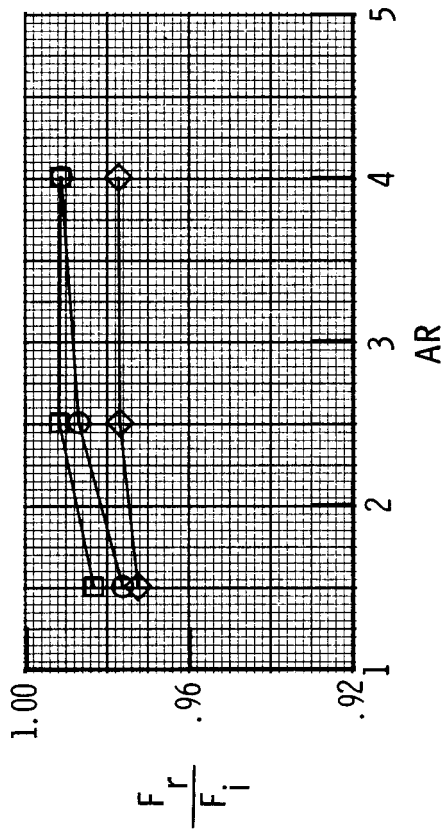
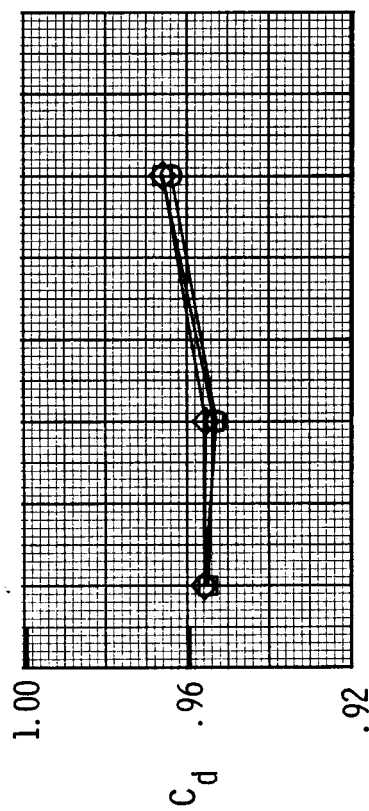
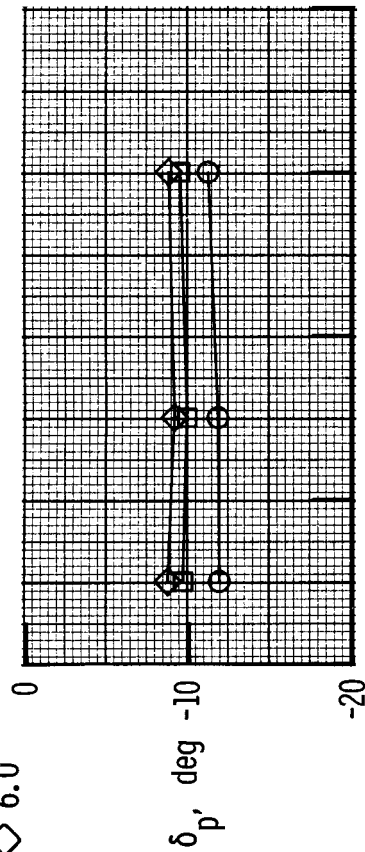


(b) 2-D C-D nozzle; $\delta_{v,p} = 0^\circ$.

Figure 16. Continued.

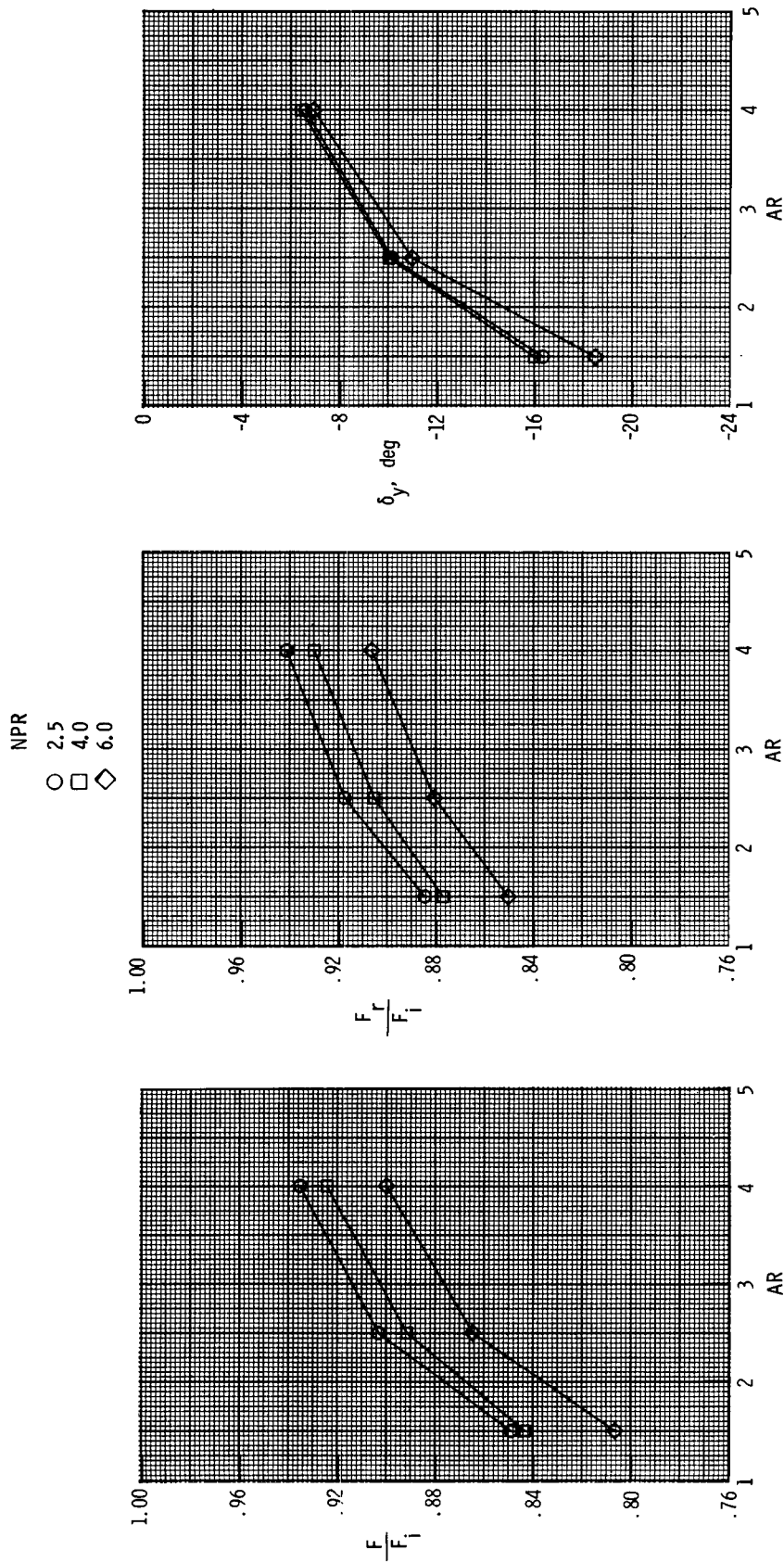
NPR

- 2.5
- 4.0
- ◇ 6.0

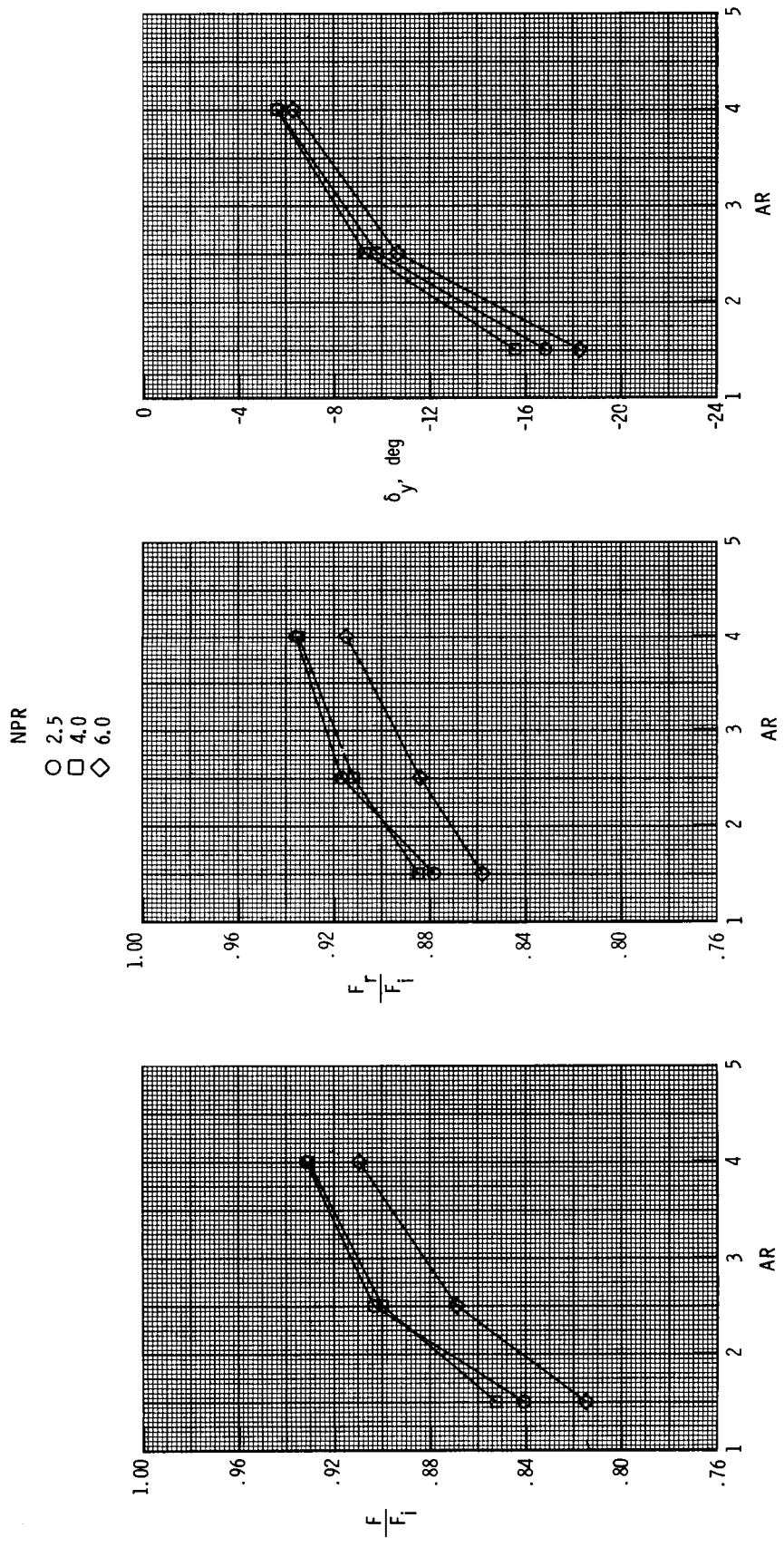


(c) 2-D C-D nozzle; $\delta_{v,p} = -11.7^\circ$.

Figure 16. Concluded.

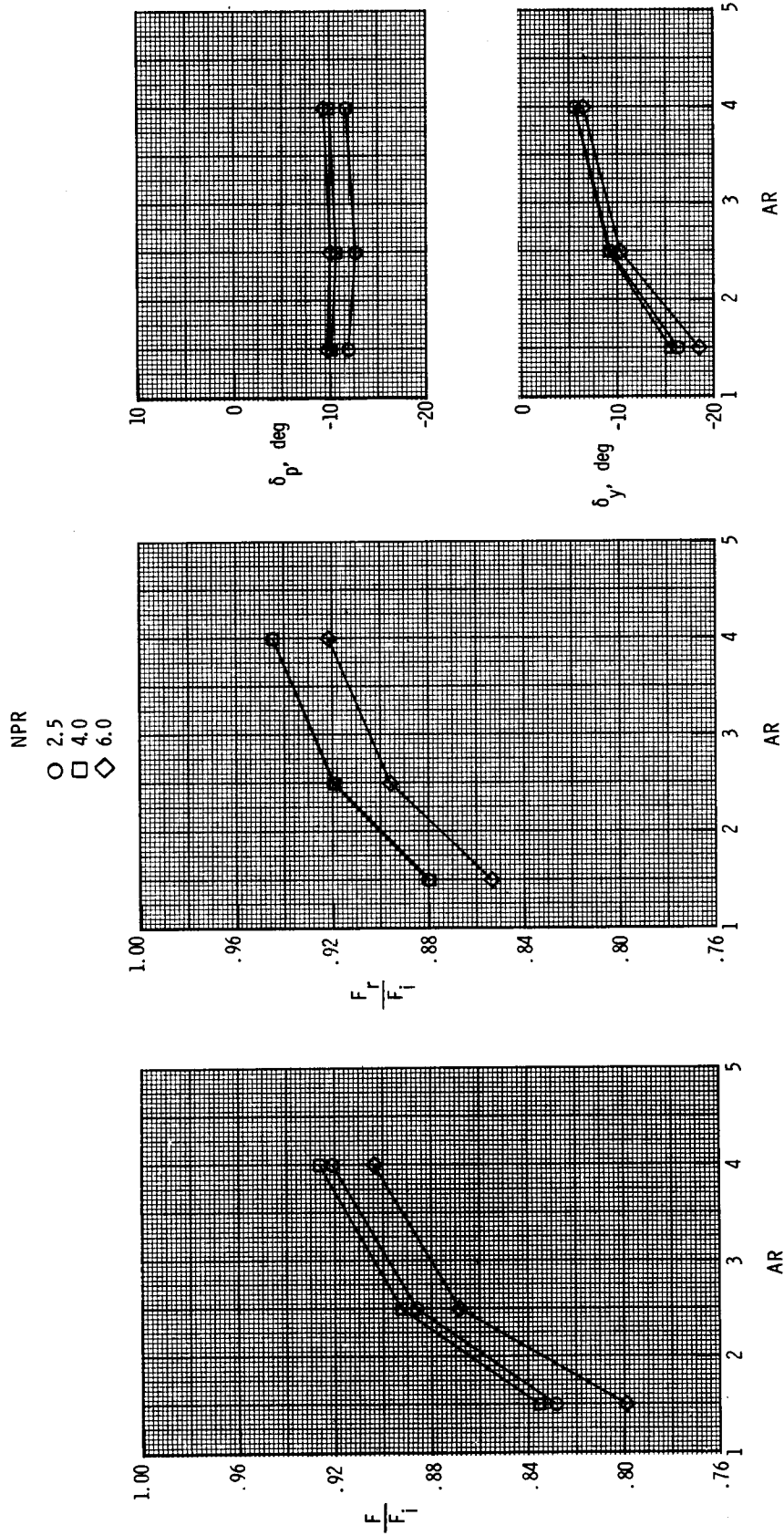


(a) 2-D convergent nozzle; $\delta_{v,p} = 0^\circ$.
 Figure 17. Effect of exit aspect ratio on nozzle performance for 2-D nozzles with vane V1 and $\delta_{v,y} = -30^\circ$.



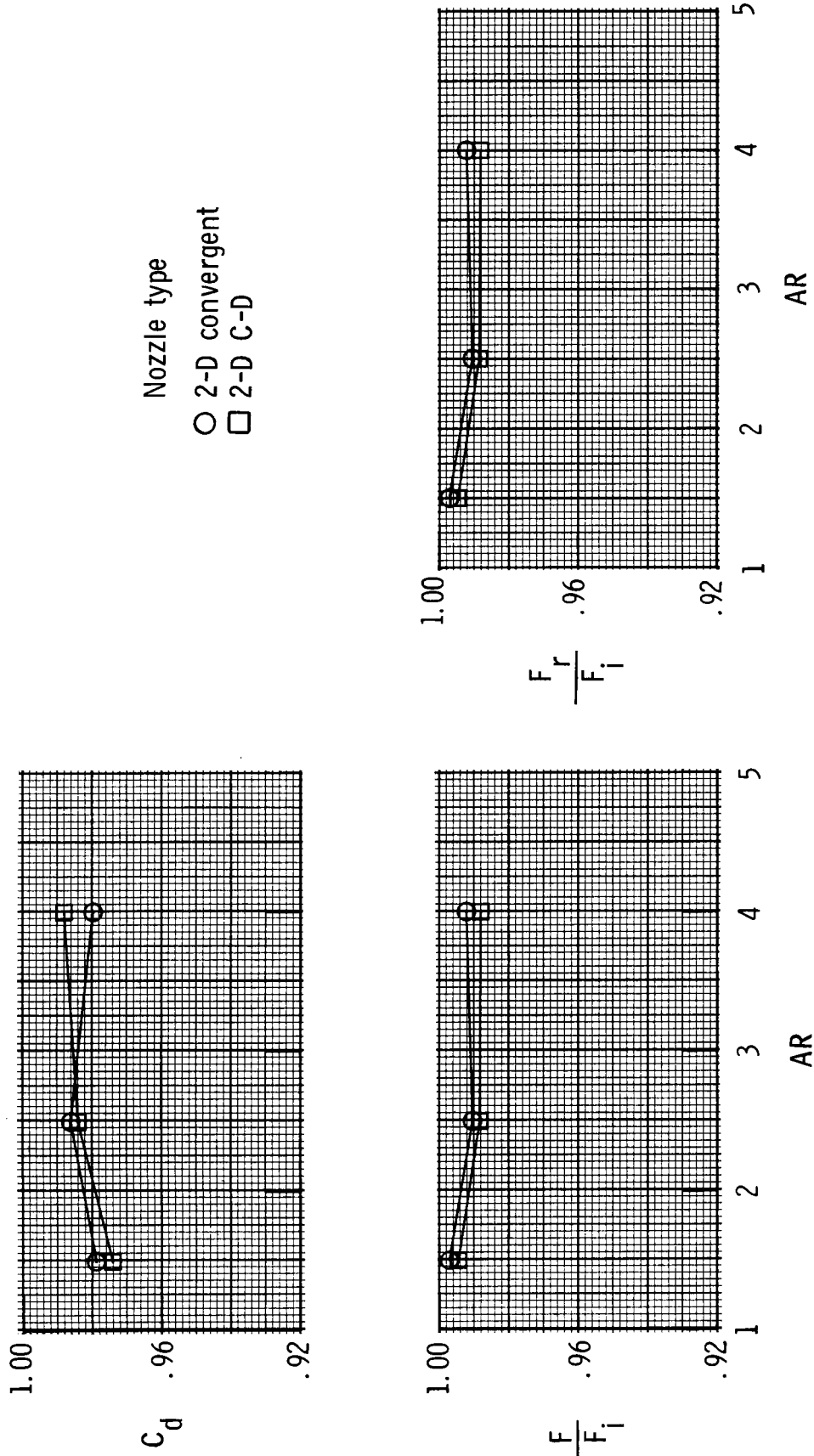
(b) 2-D C-D nozzle; $\delta_{v,p} = 0^\circ$.

Figure 17. Continued.



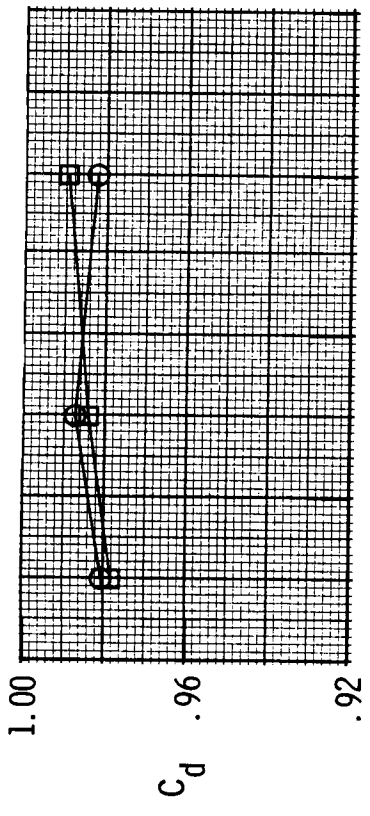
(c) 2-D C-D nozzle; $\delta_{v,p} = -11.7^\circ$.

Figure 17. Concluded.

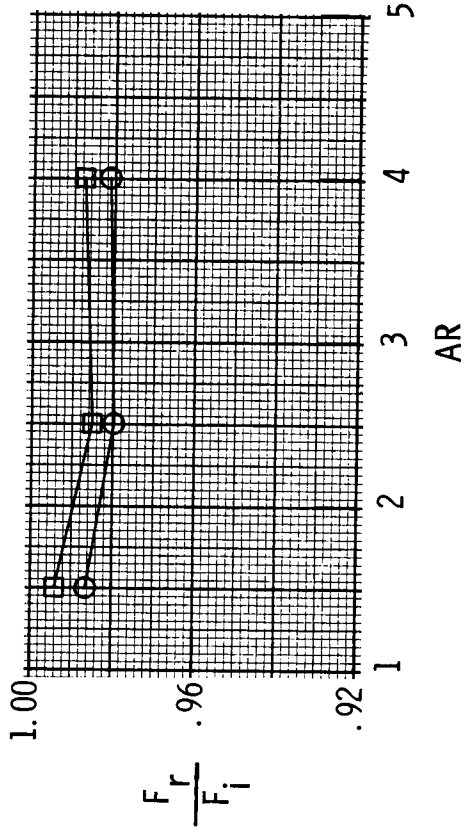
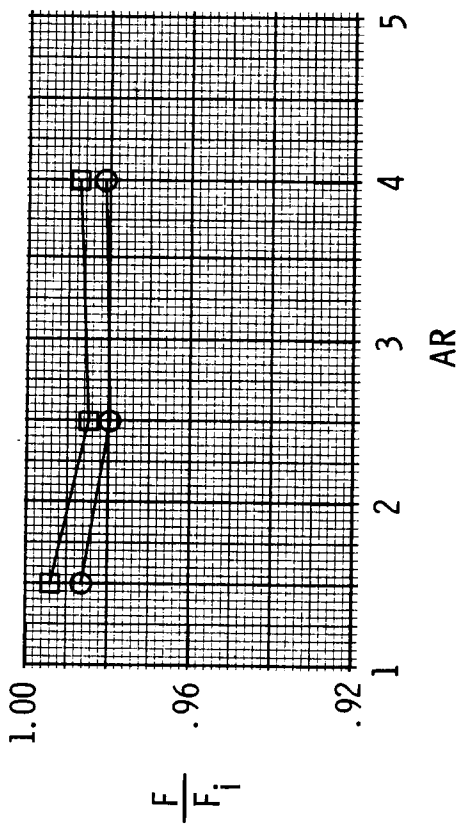


(a) NPR = 2.5.

Figure 18. Effect of nozzle type on nozzle performance for 2-D nozzles without post-exit vanes and $\delta_{v,p} = 0^\circ$, $\delta_{v,y} = 0^\circ$.

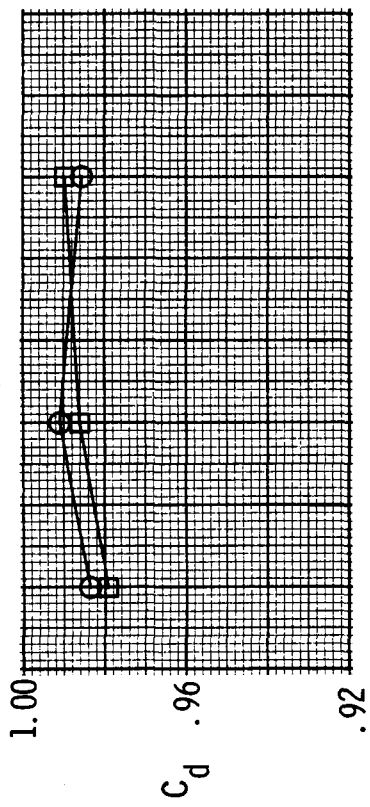


Nozzle type
 ○ 2-D convergent
 □ 2-D C-D

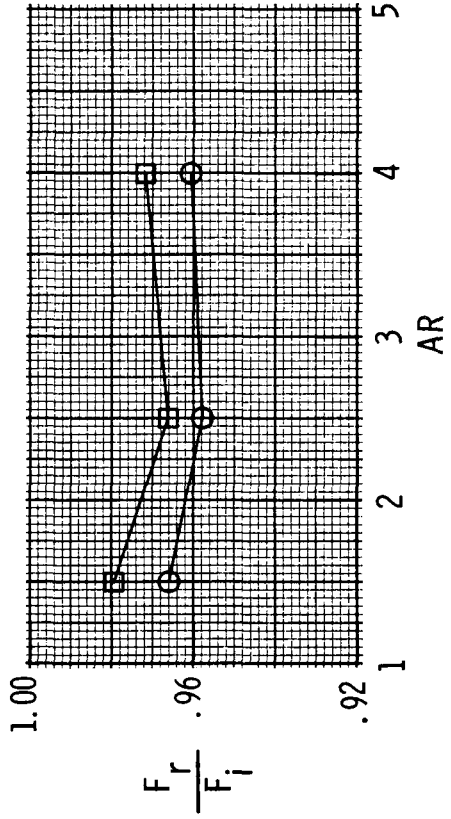
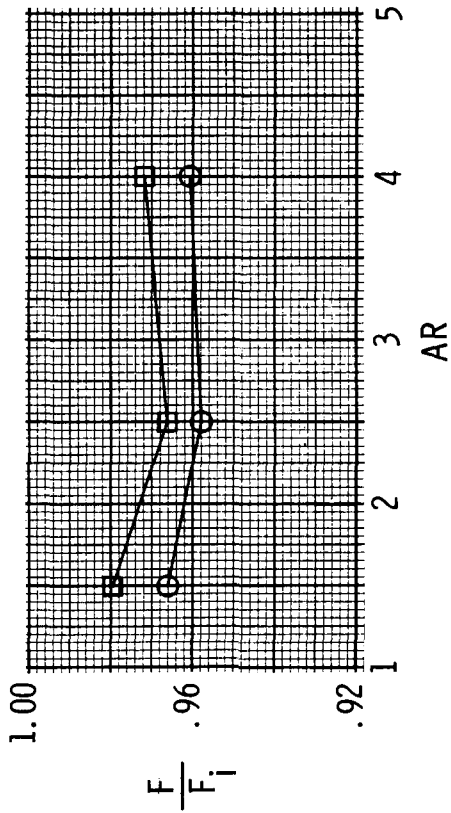


(b) $NPR = 4.0$.

Figure 18. Continued.



Nozzle type
 ○ 2-D convergent
 □ 2-D C-D

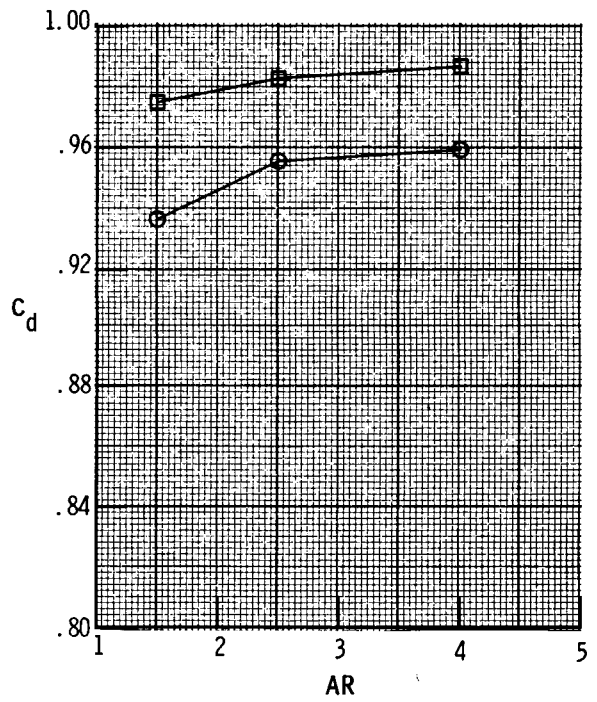
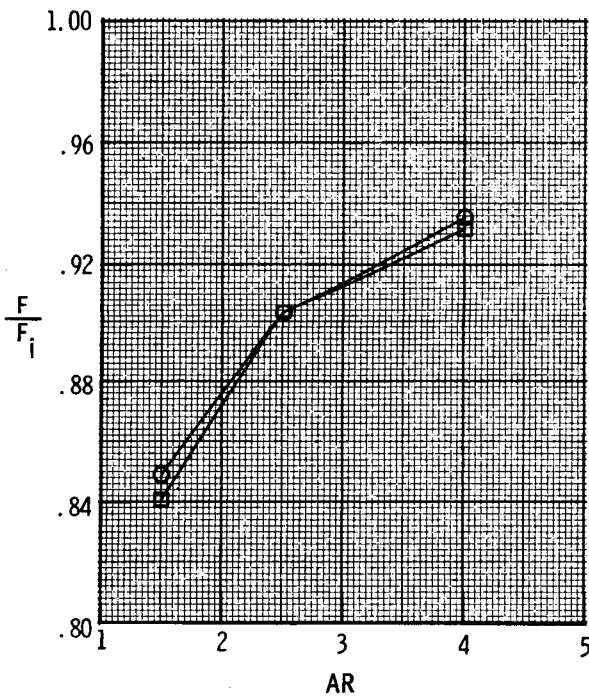
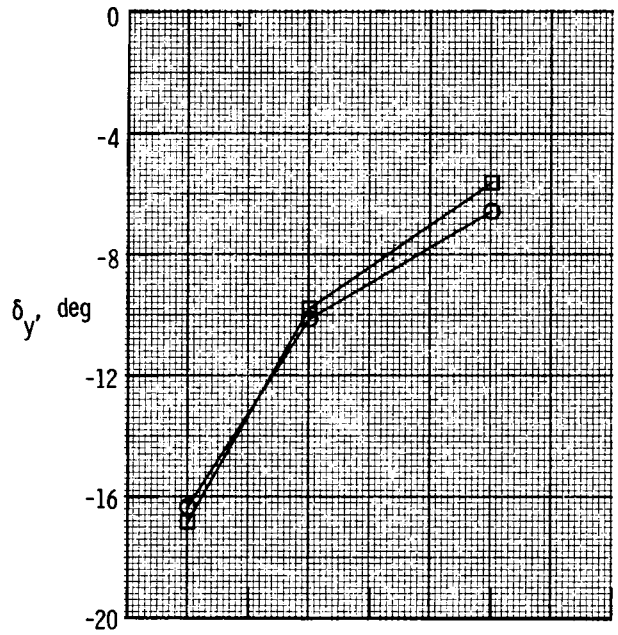
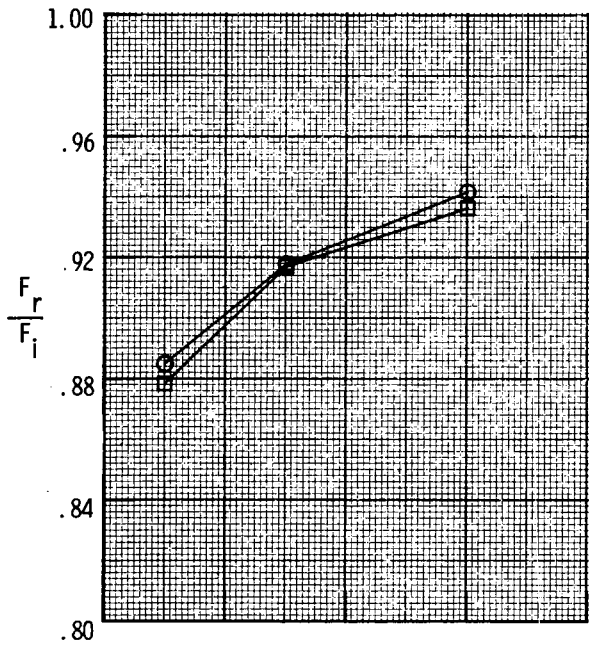


(c) NPR = 6.0.

Figure 18. Concluded.

Nozzle type

- 2-D convergent
- 2-D C-D

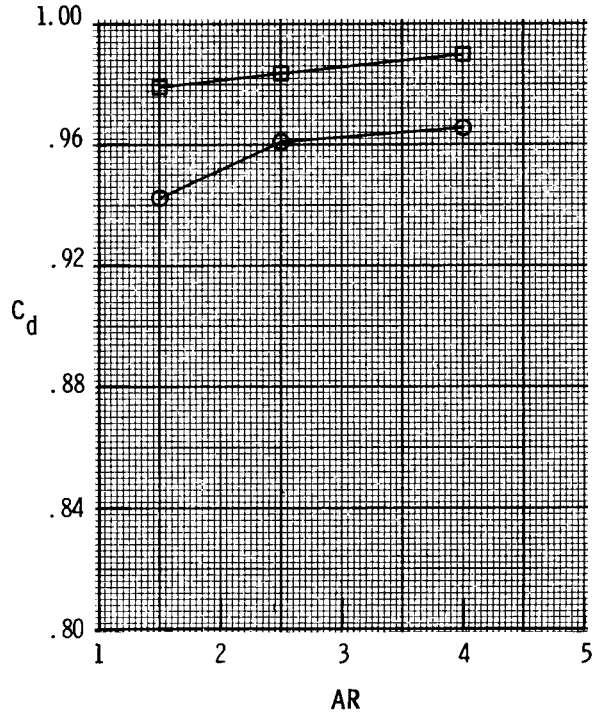
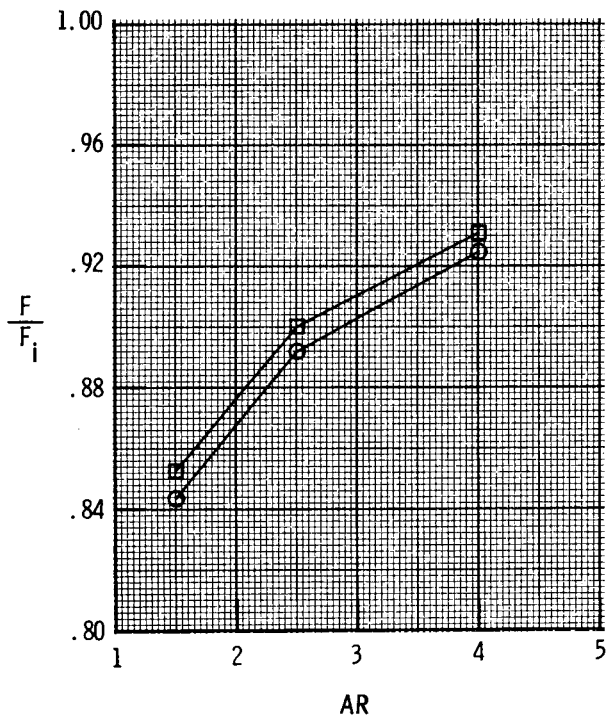
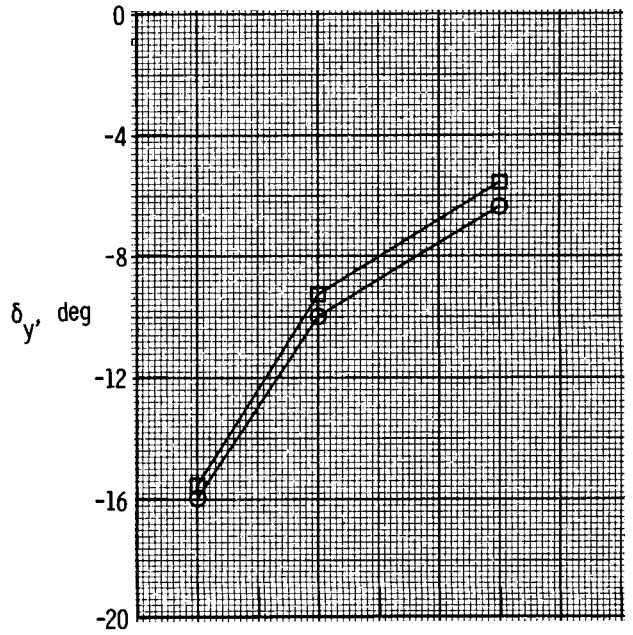
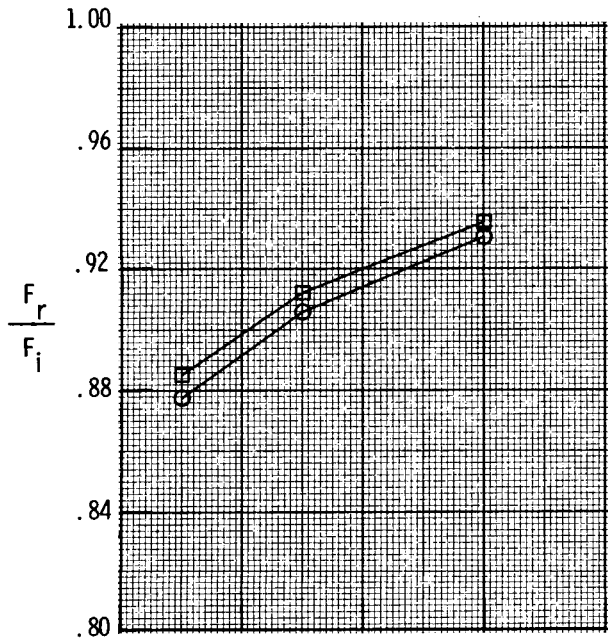


(a) NPR = 2.5.

Figure 19. Effect of nozzle type on nozzle performance for 2-D nozzles with post-exit vane V1, $\delta_{v,p} = 0^\circ$, and $\delta_{v,y} = -30^\circ$.

Nozzle type

- 2-D convergent
- 2-D C-D

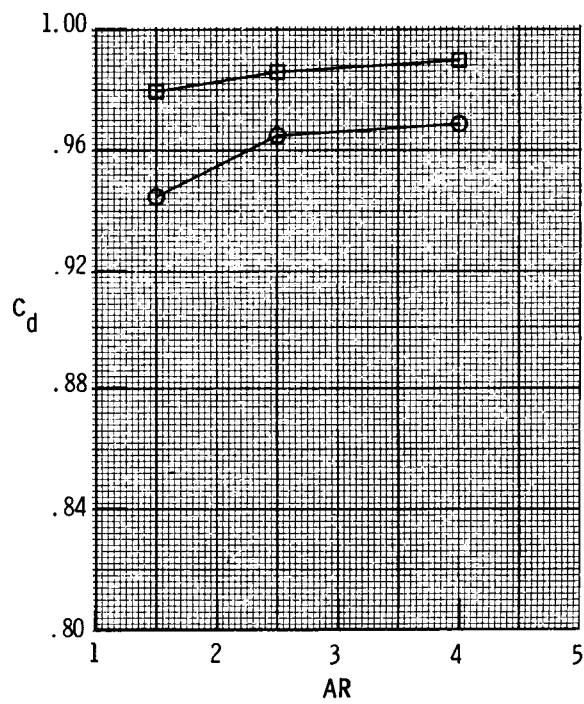
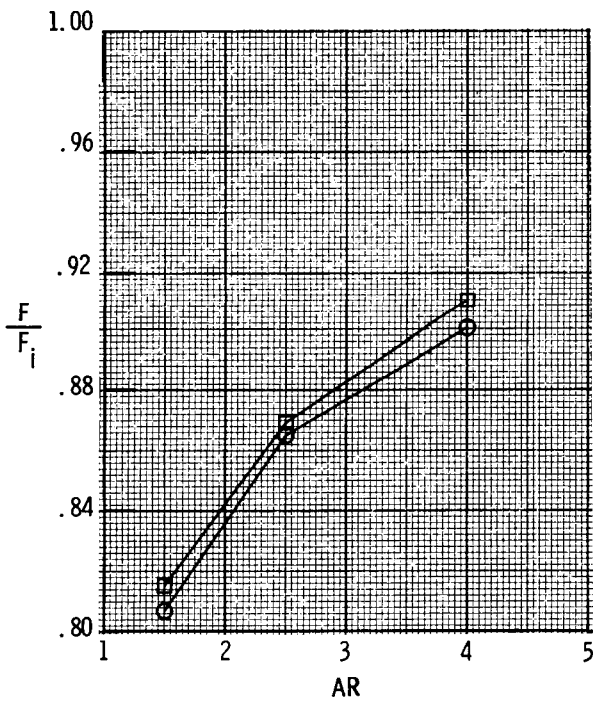
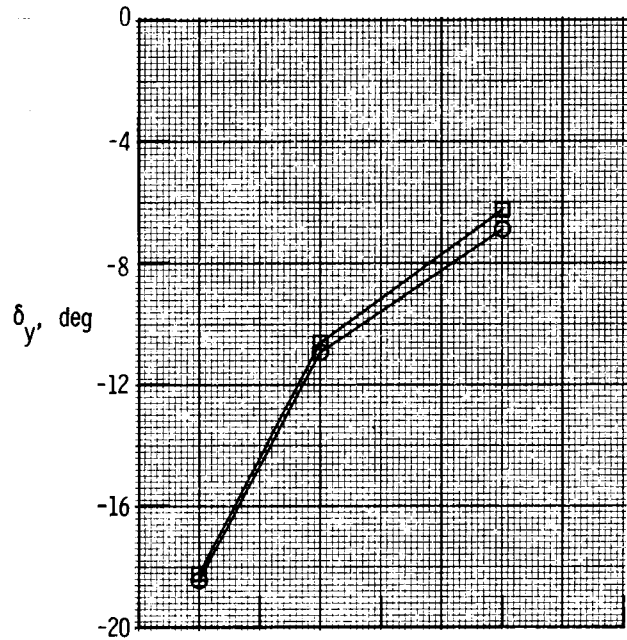
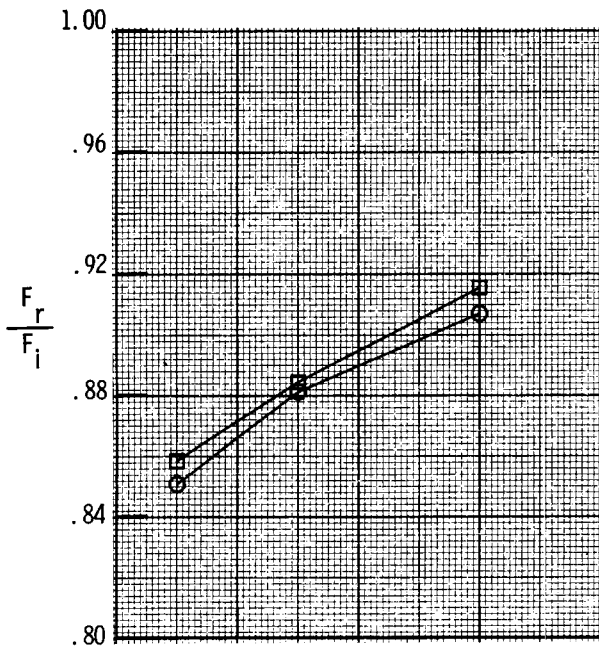


(b) NPR = 4.0.

Figure 19. Continued.

Nozzle type

- 2-D convergent
- 2-D C-D



(c) NPR = 6.0.

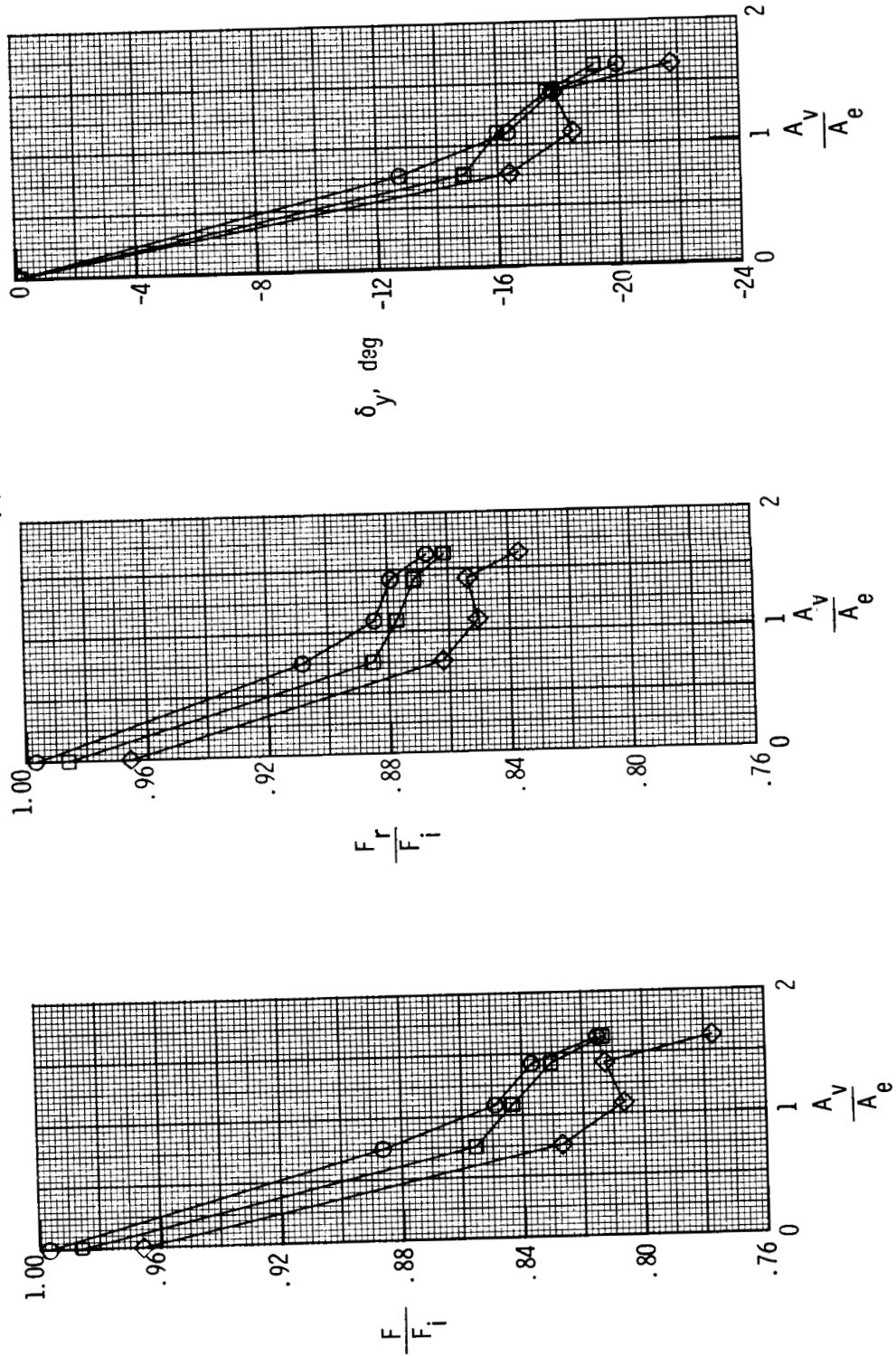
Figure 19. Concluded.

Vane A_v/A_e

Off	0.0
V3	.750
V1	1.083
V2	1.417
V4	1.625

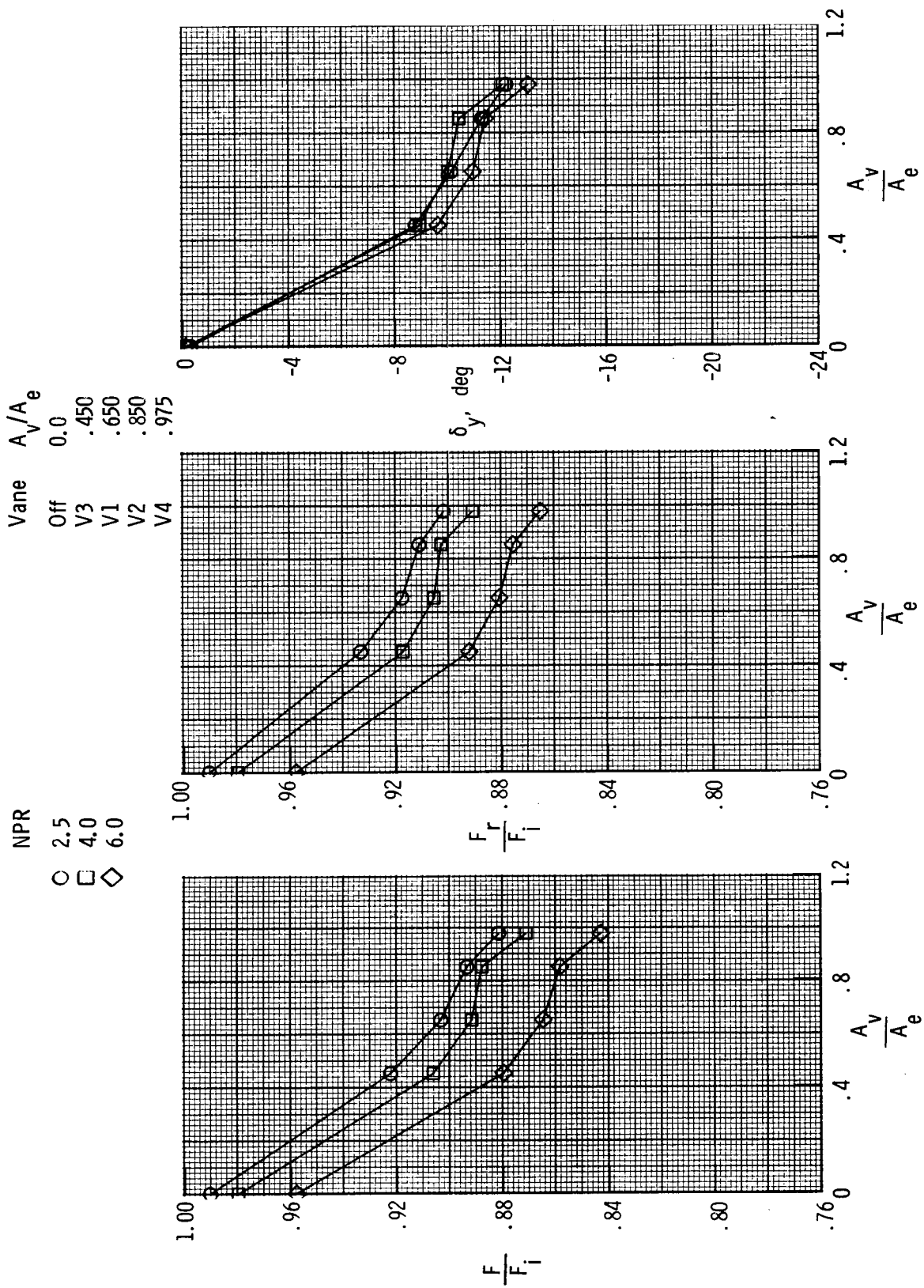
NPR

○	2.5
□	4.0
◇	6.0



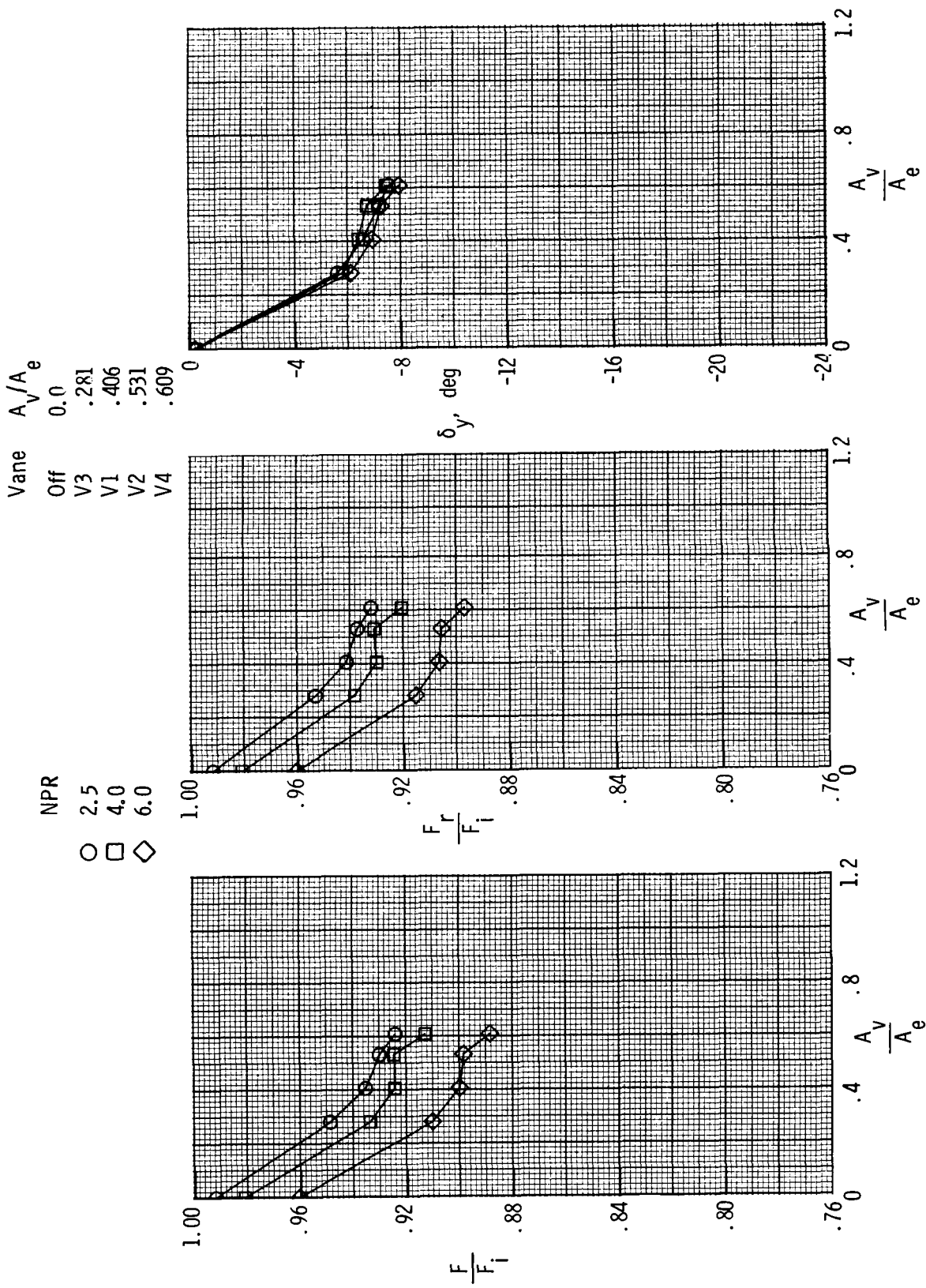
(a) AR = 1.5.

Figure 20. Effect of flat post-exit vane area on nozzle performance for 2-D convergent nozzle with $\delta_{v,p} = 0^\circ$ and $\delta_{v,y} = -30^\circ$.



(b) AR = 2.5.

Figure 20. Continued.

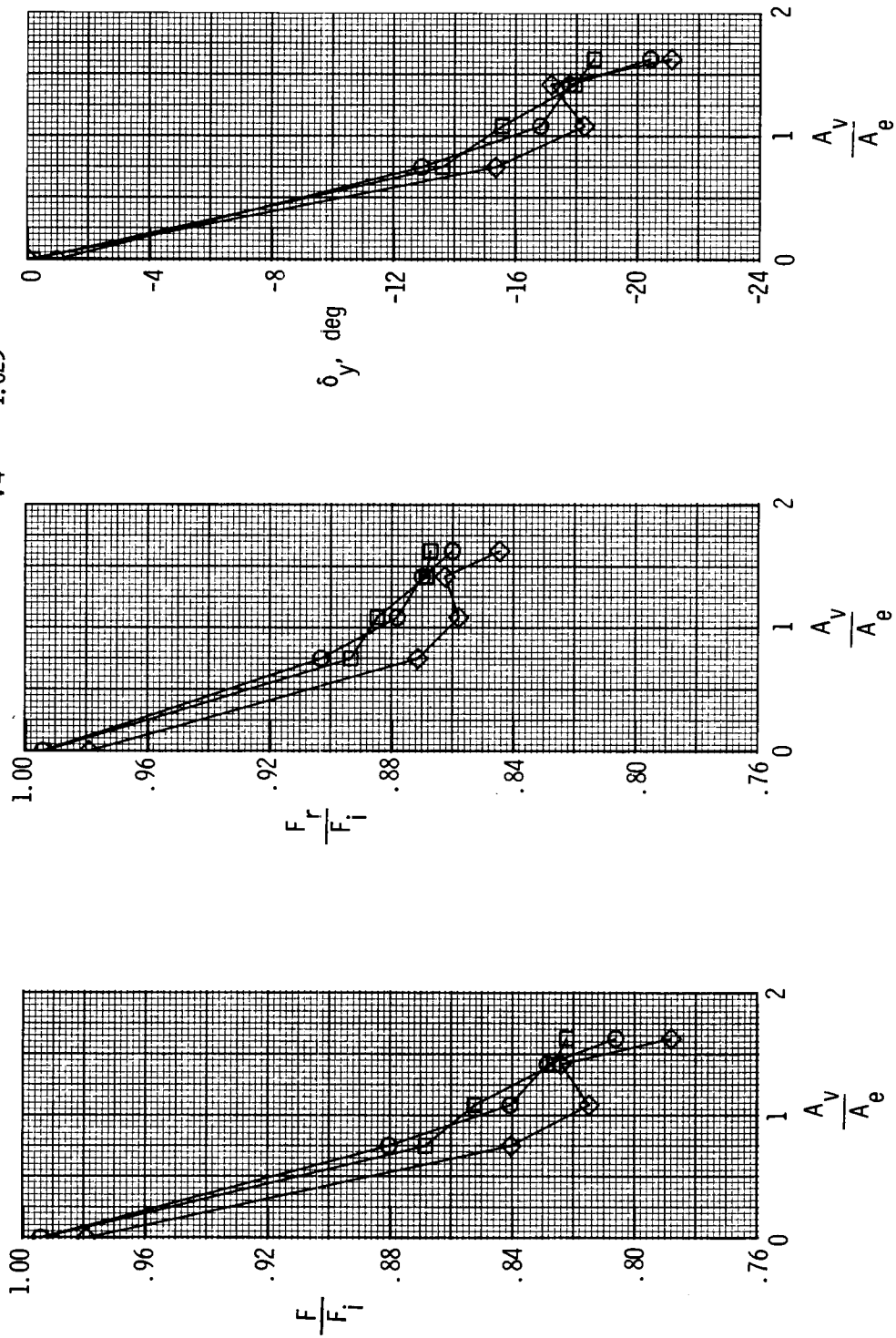


(c) AR = 4.0.

Figure 20. Concluded.

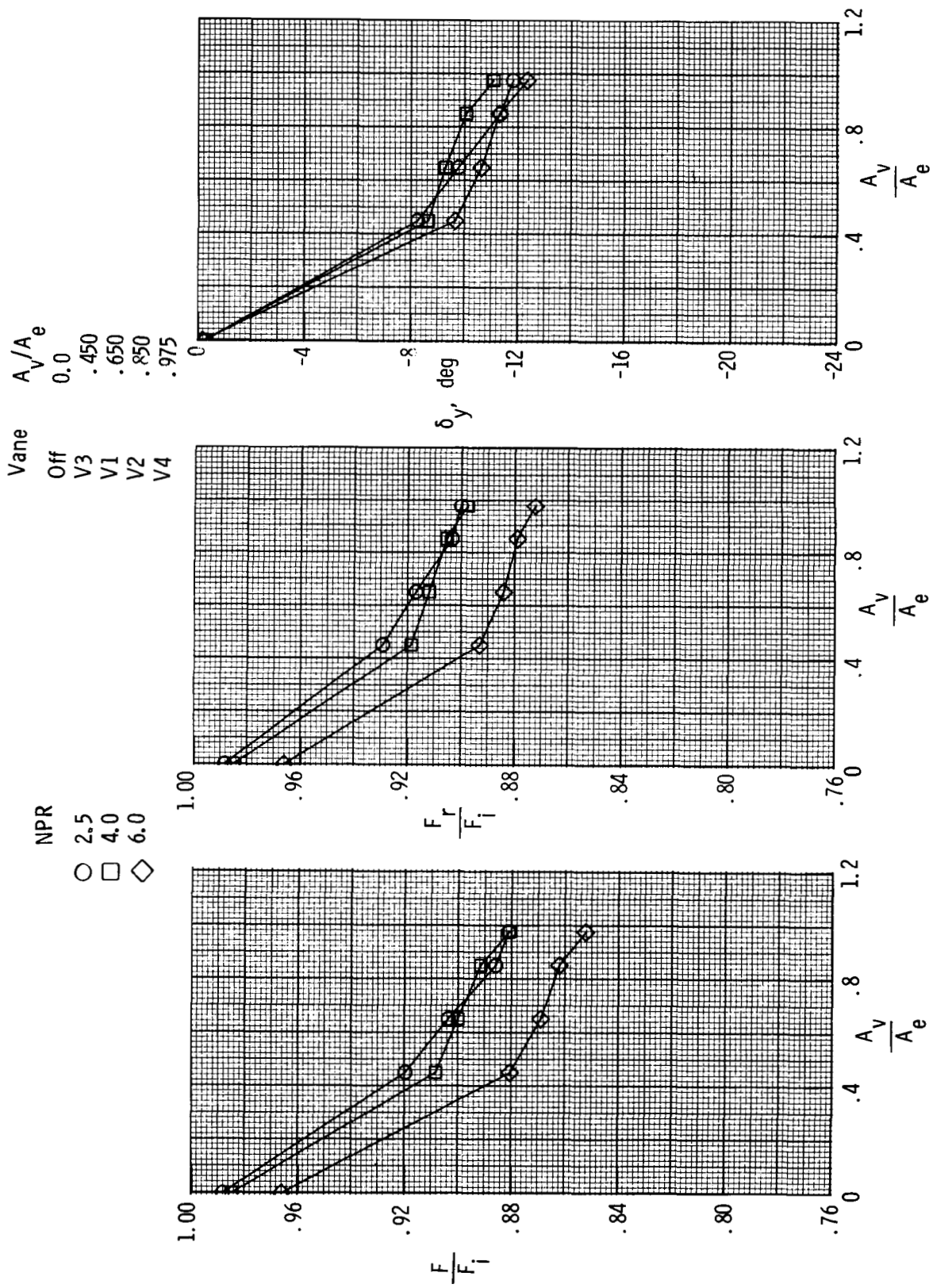
Vane A_v/A_e
 Off 0.0
 V3 .750
 V1 1.083
 V2 1.417
 V4 1.625

NPR
 ○ 2.5
 □ 4.0
 ◇ 6.0



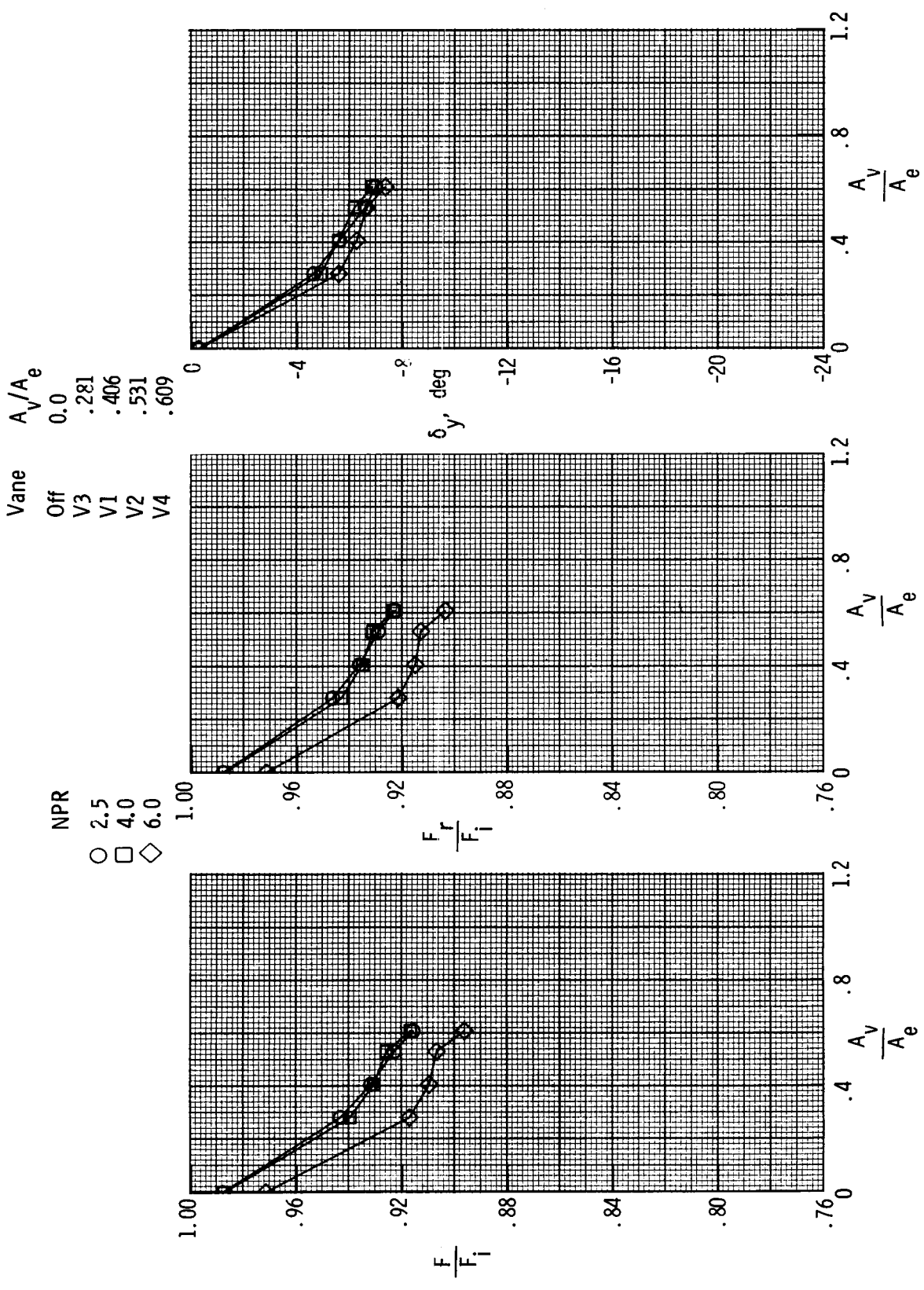
(a) AR = 1.5.

Figure 21. Effect of flat post-exit vane area on nozzle performance for 2-D C-D nozzles with $\delta_{v,p} = 0^\circ$ and $\delta_{v,y} = -30^\circ$.



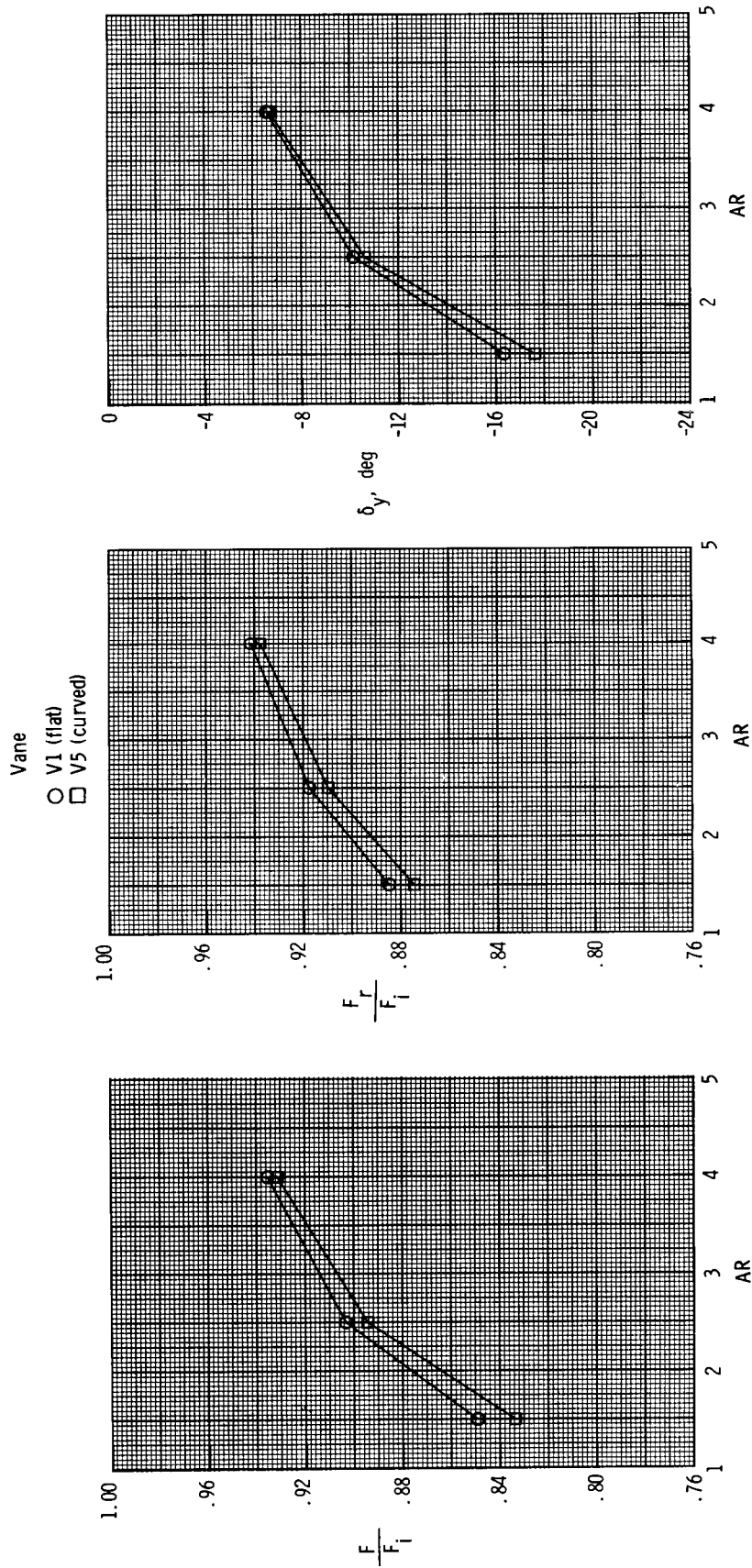
(b) AR = 2.5.

Figure 21. Continued.



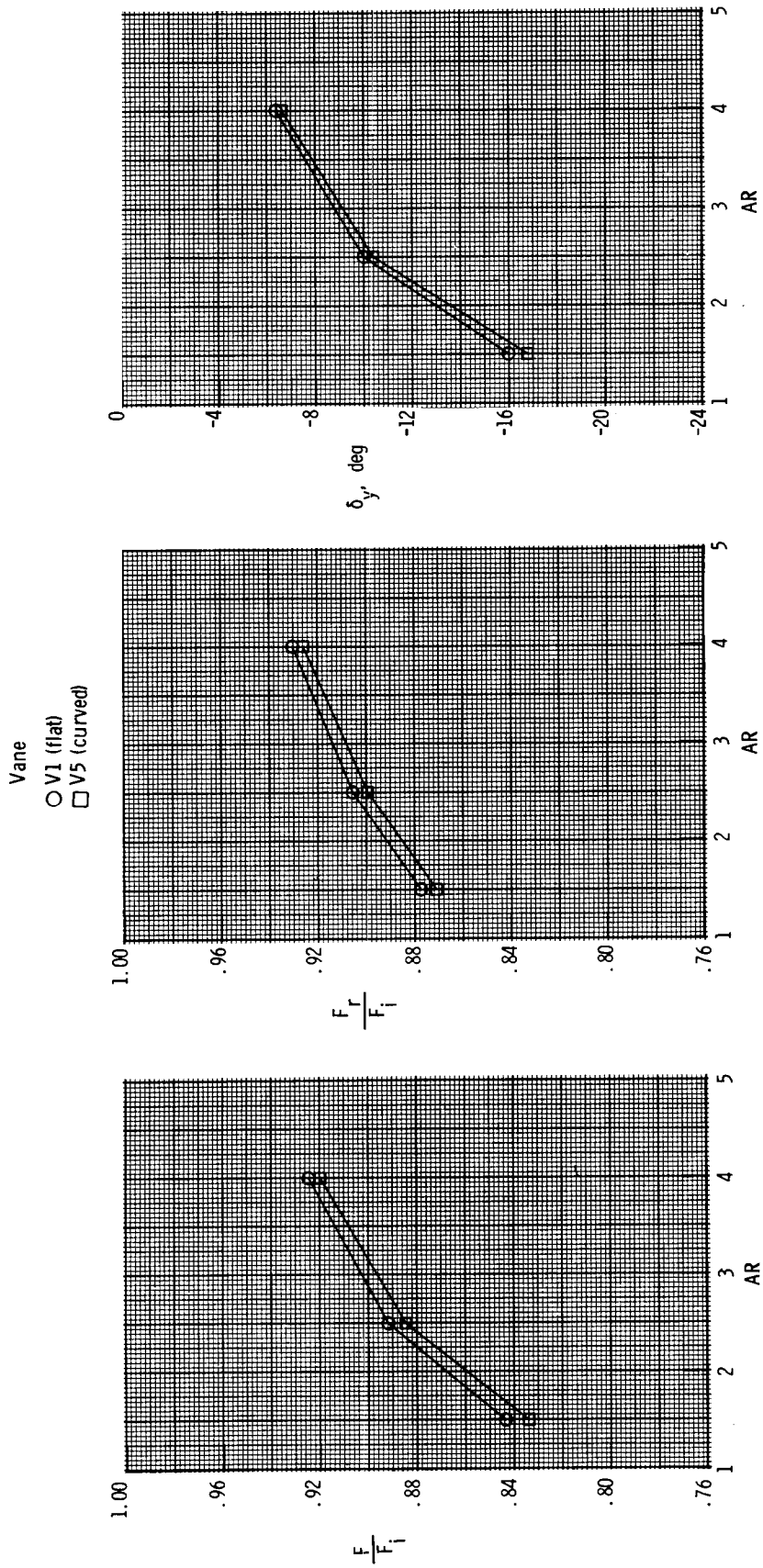
(c) AR = 4.0.

Figure 21. Concluded.



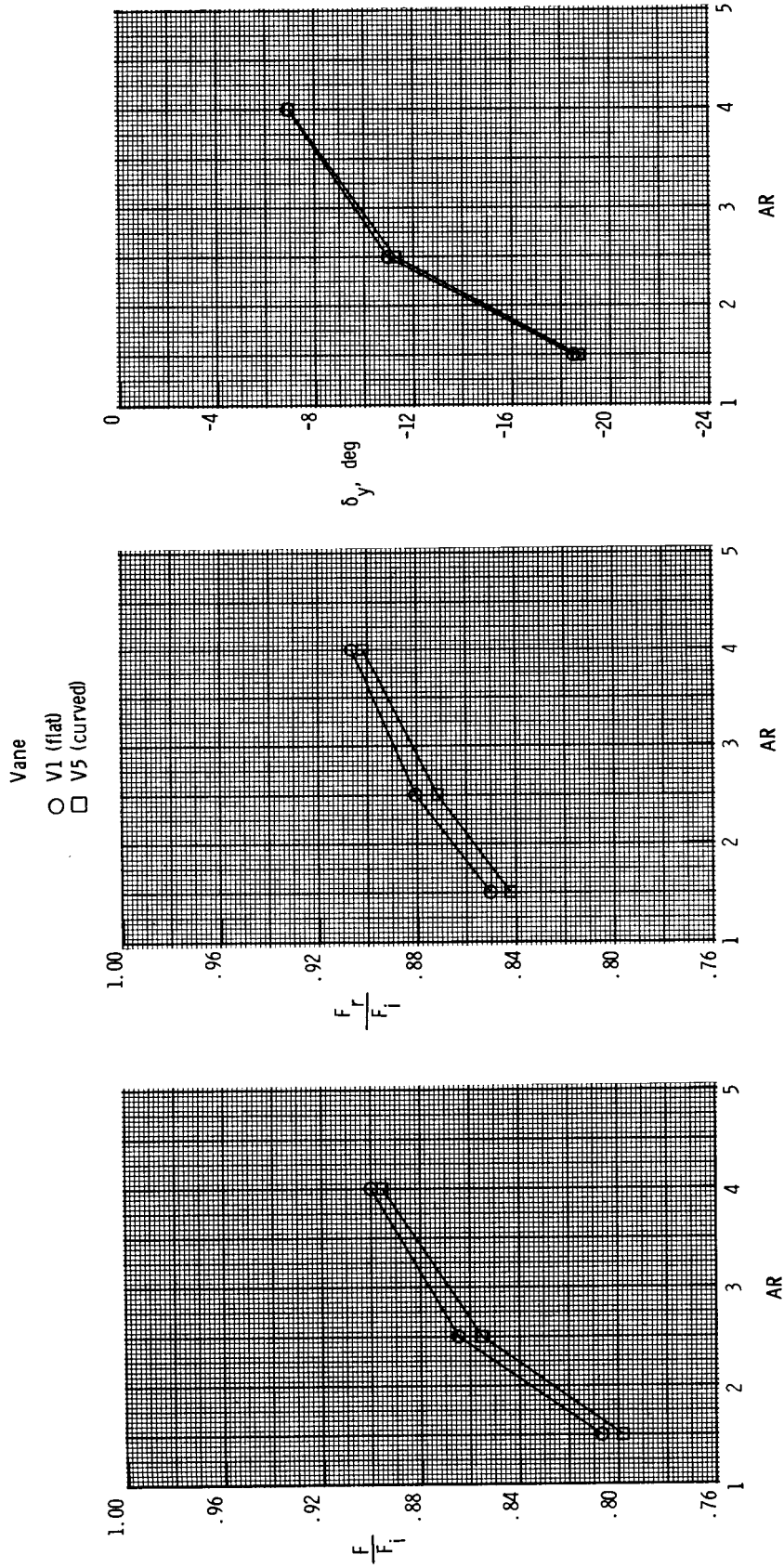
(a) NPR = 2.5.

Figure 22. Effect of post-exit vane curvature on nozzle performance for 2-D convergent nozzle with $\delta_{v,p} = 0^\circ$ and $\delta_{v,y} = -30^\circ$



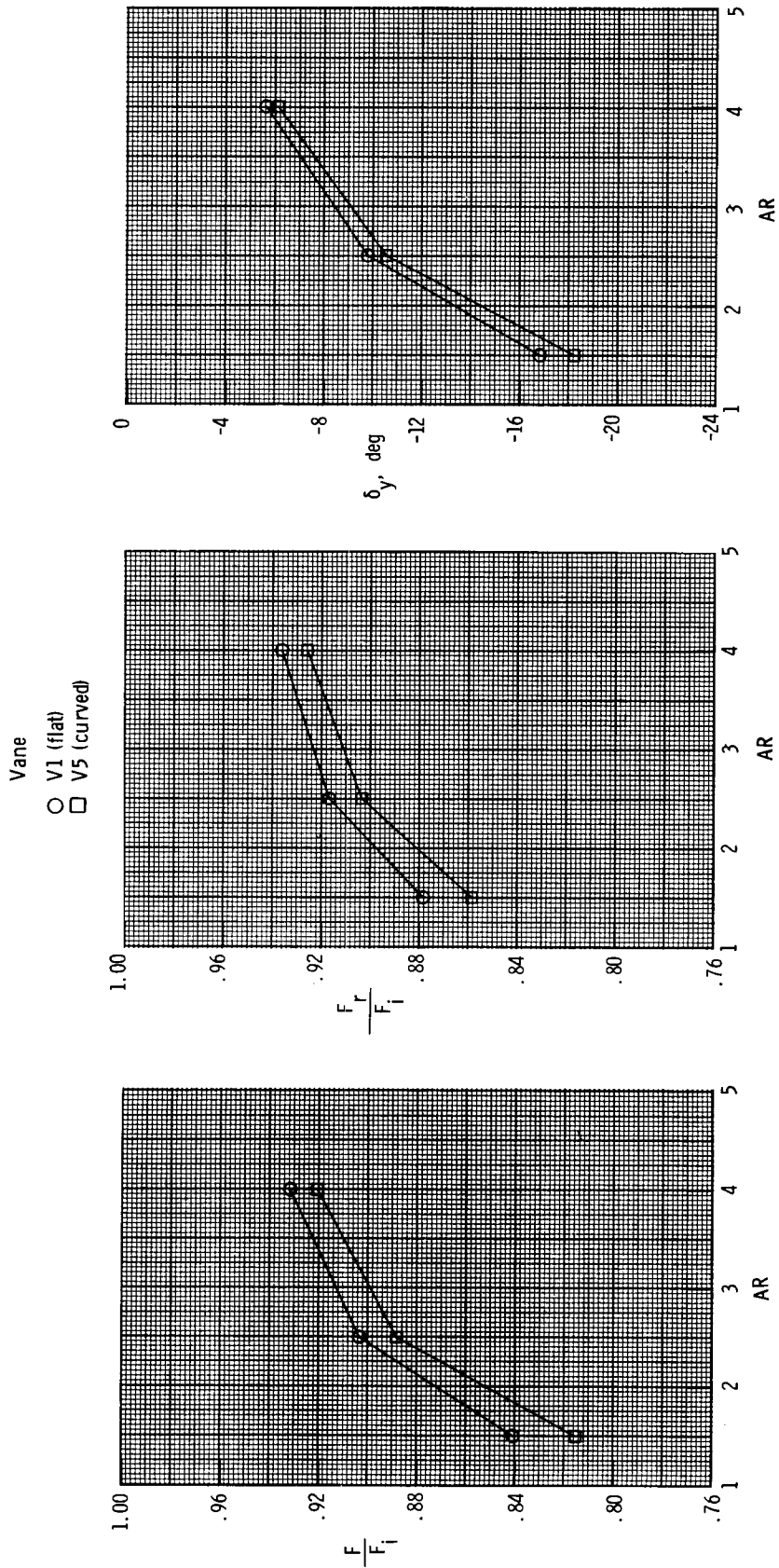
(b) NPR = 4.0.

Figure 22. Continued.



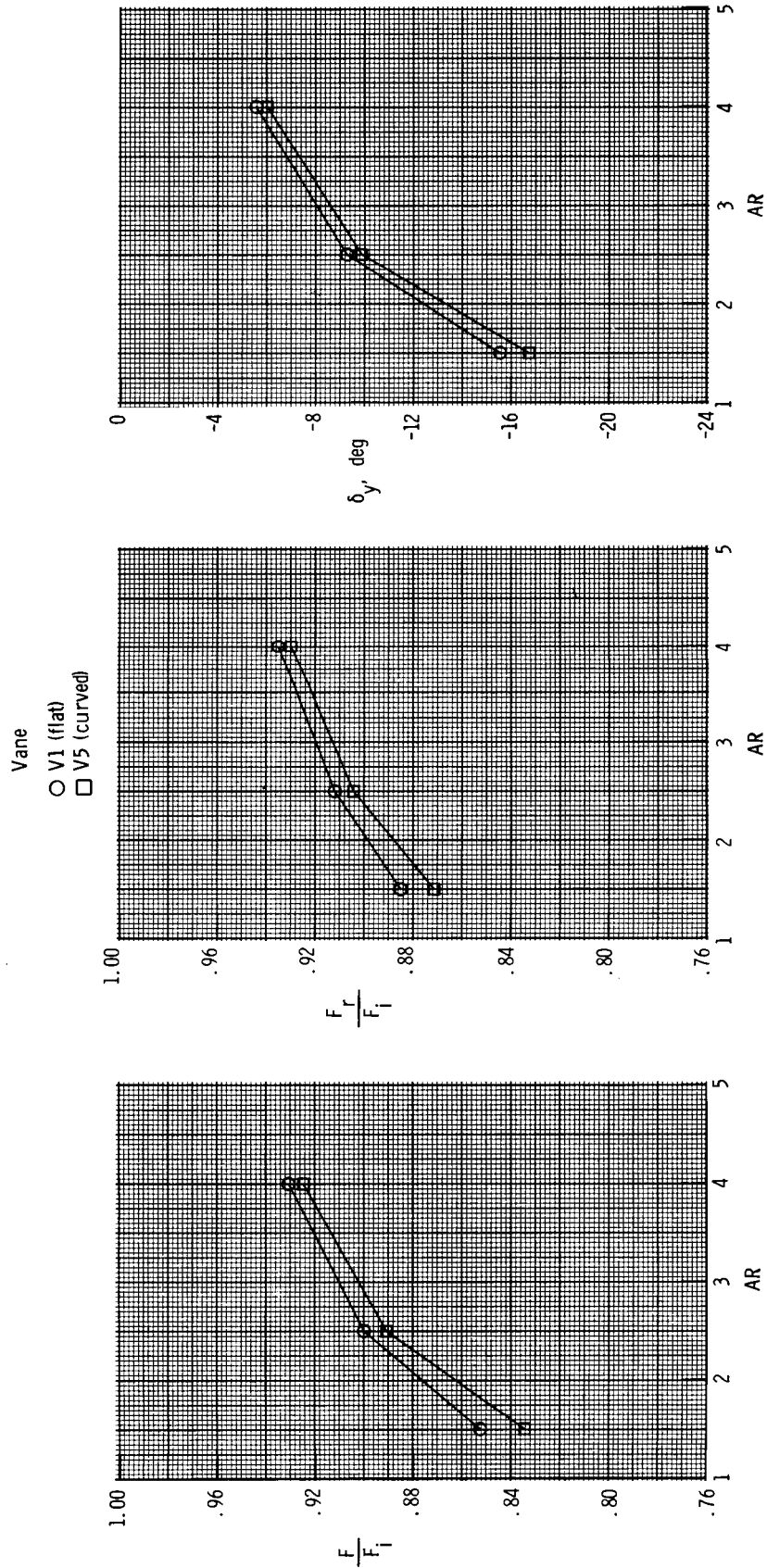
(c) NPR = 6.0.

Figure 22. Concluded.



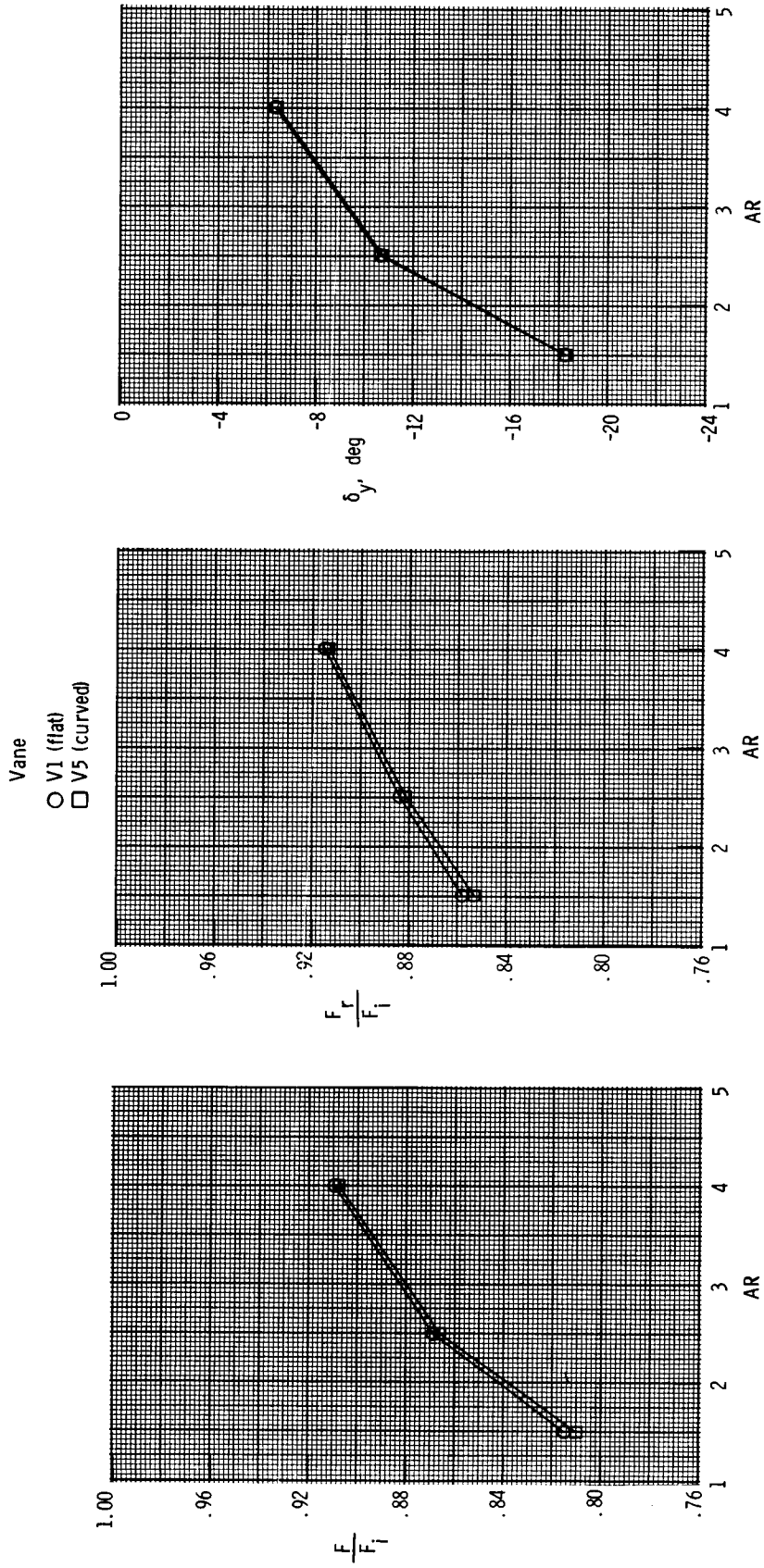
(a) NPR = 2.5.

Figure 23. Effect of post-exit vane curvature on nozzle performance for 2-D C-D nozzle with $\delta_{v,p} = 0^\circ$ and $\delta_{v,y} = -30^\circ$.



(b) NPR = 4.0.

Figure 23. Continued.



(c) NPR = 6.0.

Figure 23. Concluded.



Report Documentation Page

1. Report No. NASA TP-2813	2. Government Accession No.	3. Recipient's Catalog No.	
4. Title and Subtitle Static Performance of Nonaxisymmetric Nozzles With Yaw Thrust-Vectoring Vanes		5. Report Date May 1988	
		6. Performing Organization Code	
7. Author(s) Mary L. Mason and Bobby L. Berrier		8. Performing Organization Report No. L-16389	
		10. Work Unit No. 505-62-91-01	
9. Performing Organization Name and Address NASA Langley Research Center Hampton, VA 23665-5225		11. Contract or Grant No.	
		13. Type of Report and Period Covered Technical Paper	
12. Sponsoring Agency Name and Address National Aeronautics and Space Administration Washington, DC 20546-0001		14. Sponsoring Agency Code	
		15. Supplementary Notes	
16. Abstract A static (wind-off) test has been conducted in the static test facility of the Langley 16-Foot Transonic Tunnel to evaluate the effects of post-exit vane yaw vectoring on nonaxisymmetric nozzles. Three baseline nozzles were tested: an unvectored two-dimensional convergent nozzle, an unvectored two-dimensional convergent-divergent nozzle, and a pitch-vectoring two-dimensional convergent-divergent nozzle. Each nozzle geometry was tested with three exit aspect ratios (ratio of nozzle width to height at exit) of 1.5, 2.5, and 4.0. Two post-exit yaw vanes were externally mounted on the nozzle sidewalls at the nozzle exit to generate yaw thrust vectoring. Vane deflection angle (0° , -20° , and -30°), vane planform, and vane curvature were varied during the test. Results indicate that the post-exit vane concept produced resultant yaw vector angles which were always smaller than the geometric yaw vector angle. Losses in resultant thrust ratio increased with the magnitude of resultant yaw vector angle. The widest post-exit vane produced the largest degree of flow turning, but vane curvature had little effect on thrust vectoring. Pitch thrust vectoring was independent of yaw thrust vectoring.			
17. Key Words (Suggested by Authors(s)) Nonaxisymmetric nozzles Yaw thrust vectoring Pitch thrust vectoring Internal performance		18. Distribution Statement Unclassified—Unlimited Subject Category 02	
19. Security Classif.(of this report) Unclassified	20. Security Classif.(of this page) Unclassified	21. No. of Pages 76	22. Price A05